POLITECNICO DI MILANO

Department of Civil and Environmental Engineering

Master of Science in Civil Engineering for Risk Mitigation

Master of Science Thesis

Introducing Textile Reinforced Concrete for Retrofitting of Existing Structures: Numerical Design Prediction

Supervisor: Prof. Matteo Colombo

Candidate: Eslam Omar Soliman

Co-supervisor: Dr.Isabella Colombo

December, 2015

Abstract

The structural engineering had faced recently a quite new engineering challenge due to the necessity to figure out the optimum solution in strengthening old buildings which had experienced damage due to the failure of its structural members to stand with the acting stresses. In that sense, many strengthening techniques had been developed such as; the so called traditional techniques (RC or steel jacketing) and using of advanced cementitious composites like Fibre reinforced concrete and Textile reinforced concrete. The common problems linked to traditional techniques are mainly; the excessive increase of the element section and mass due to the added RC jacketing which reaches to 60-70 mm, while the low fire resistance of the glued steel jacketing is considered a negative aspect when steel jacketing is used.

Textile reinforced concrete was introduced as a strengthening material and it has been characterized with its excellent mechanical properties especially the pronounced pseudo-ductile behavior and tensile strength. TRC is produced by combining a very fine grained concrete with multiaxial fabric. Furthermore, adding Alkali resistant (AR) glass, Carbon, Kevlar or Aramid to the TRC matrices gives high effectiveness because they are placed in the main stresses directions. Unlike the randomly distributed short fibres such as glass fibre reinforced concrete (GRC), the advantage of al-kali-resistant (AR) glass or carbon fibres in comparison with steel reinforcements is that they are not prone to corrosion. So no need to add a concrete cover sequentially slimmer element can be obtained.

The parameters that feature the behavior of TRC are multiple. Particularly, the fabric geometry, the method that the fibres were woven and the contact surface between the added layer of TRC and the old existing element is triggering the performance of the strengthened element. In this sense, the surface treatment determines transmission of the tangential stresses through the contact surface.

This research aims to study the mechanical characterization of textile reinforced concrete by experimental investigations carried out on different TRC matrices mix design and the effect of adding the polypropylene fibres to the TRC. Moreover, a comprehensive explanation to the coupling behavior of reinforced concrete specimen retrofitted by textile reinforced concrete is explained in this thesis as well by presenting double edge wedge splitting test in two approaches; experimental and numerical. The numerical approach used the finite element software Abaqus for modeling un-retrofitted and retrofitted specimens with TRC in order to study the correspondence between the experimental and numerical approaches results. Furthermore, studying the effect of adding polypropylene to TRC was highlighted as well.

Acknowledgement

I proudly acknowledge for my glorious home country Egypt where I have grown up and earned my educational foundations which make me able to proceed further studies in one of the best Engineering schools in the world. This thesis has been accomplished in Politecnico di Milano where everyone gives support and positive energy to come over any challenge and difficulty therefore, I would like to send my thanks to everyone belongs to this great university; teaching staff, administration and students. I would like to gratefully acknowledge my supervisor Professor Matteo Colombo for his subjective guidance and motivation. Moreover, for facilitating most of the obstacles and solving many problems during this study. Special thanks to Dr. Isabella Colombo who was the key person behind this research. She didn't hesitate for one moment to orient me to the most productive path and provide me all the needed materials and scientific advices in a very friendly way. Also, I am grateful for the research staff in Department of Civil and Environmental Engineering, in Lecco campus (Polo Territoriale di Lecco) for their friendly spirit and studying advices. And I would like to thank the technician's staff whom helped me a lot in specimen's preparation.

I would like to mention that I was pretty lucky to have a very supportive colleagues and friends whom I have been living with in the beautiful city Lecco for more than two years, sharing all the hard and good times. And I can say that without my lovely group of friend I wouldn't be able to end up with success.

Finally there is no word expresses the great gratitude I owe to my mother for her continuous prayers and absolute love that she is dedicating to me. And also for being patient during my stay away from home for more than two years. And tons of thanks to my father for his supportive advises. And for my beloved siblings Eman and Ehab for being always in the place where I need them. And for every single person in my beloved family specially my nephews and my niece whom represent the joy and happiness source in my life.

Table of contents

List of figures

List of tables

Chapter 1
Introduction.

The term of retrofitting had been defined as the process of adding strengthening layers to the existing structure member in order to restore the load carrying capacity to meet the safety and the design requirements. The means of retrofitting is developing rapidly nowadays, either in the retrofitting techniques or the used strengthening materials. The development aims to reach the optimum strength and stiffness for the retrofitted member with respect to two main considerations, the first concerns on the volumetric size of the new added layer. The second consideration is economical which concerns on the cost of the retrofitting process with respect to the cost of reconstruct the structure. In case of heritage buildings the economical consideration doesn't impose a reconstruction cost.

Development of different techniques became very necessary in order to find the optimum behavior for the strengthening cementitious composite material. These advanced techniques include metallic grid reinforced surface coatings, shotcrete overlay, externally bonded fiber reinforced polymers (FRP), ultra high fiber reinforced concrete and textile reinforced concrete.

Principally, this thesis exhibits the possibility of using the textile reinforced concrete (TRC) in the strengthening process. TRC has been characterized with its excellent mechanical properties especially the pronounced pseudo-ductile behavior and tensile strength. This gives TRC great advantages in strengthening and repair of existing structures as well as it offers great possibilities with respect to its application in new construction. Furthermore, the advantage of using TRC manufactured with al-kali-resistant (AR) glass or carbon fibres in comparison with steel reinforcements is that they are not prone to corrosion. So no need to add a concrete cover sequentially slimmer element can be obtained. TRC is produced by combining a very fine grained concrete (maximum aggregate size is less than 2 mm) with multiaxial fabric. Unlike the randomly distributed short fibres such as glass fibre reinforced concrete (GRC), Using TRC made by Alkali resistant (AR) glass, Carbon, Kevlar or Aramid gives high effectiveness because they are placed in the main stresses directions. Table 1.1 gives some mechanical properties of different fibres used in thin cementitious composite.

Fiber Material	Density g/cm^3	Tensile strength MPa	Elastic Modulus GPa	Ultimate elongation %
AR Glass	2.8	1400	70-80	2
Glass E	2.5	2000-3500	70-80	3.5-4.5
Carbon, high modulus	1.85-1.9	2400-3400	390-760	0.5-0.8
Carbon, high strength	1.75	4100-5100	240-280	1.6-1.73
Aramid	1.44-1.47	3600-3800	62-180	1.9-5.5
Polymeric	1.1-1.25	40-82	2.6-3.6	1.4-5.2
Steel	7.8	up to 600	206	20-30

Table 1.1: Mechanical properties for different fibres. [A.Magri

The mechanical properties of TRC depend on the mix design which should be a best compromise between many requirements such as, bond behavior, workability and durability. The equivalent modulus of textile is different from the elastic modulus of the fibres themselves which depends on the production process of the textile. The filament fineness influences the mechanical properties of the composite material. Also, bond between the reinforcement and the matrix has effect on strength and ductility of TRC. This thesis speaks also about the durability of TRC. Some tests had been carried out to study TRC durability and the effect of the external environmental circumstances. Furthermore, the effect of the produced pressure due to the repetition of sequential freezing thawing cycles is stated. In this sense numerical model was accomplished using finite element approach to predict the behavior of a strengthened specimen with TRC with tow solutions. First solution was TRC casted without polypropylene addition while the second solution used TRC casted with polypropylene addition. The validation of this model has been performed by means of the experimental investigation results that had been carried out to determine the plastic tensile behavior of the textile reinforced concrete by performing a direct tensile test to different design mix of TRC. Moreover, the numerical model simulate the double edge wedge splitting test (DEWS)[di Prisco 2010] which the experimental result could be obtained by the test done and explained by A. Magri [Magri 2012].

1.1. Engineering problem statement.

Predominantly most of the old structures which are in necessary need of intervention by means of rehabilitation were built according to old standards which do not guarantee the safety requirement in particular when it is subjected to seismic action. Traditional techniques and material which were very common in the retrofitting process induce an excessive increase of the retrofitted element volume. It is worthy mentioned that the traditional jackets considered being effective only by adding 60-70 mm thickness of concrete. This volume increment is not acceptable in many cases as it might be an obstacle to the element functionality to accomplish its pre-desirable job. and/or keeping the aesthetics of the architecture design especially if the retrofitted structure is historical heritage where in this case the traditional techniques with its excessive increase in volume may change the original design of the building which reduces the value of the heritage itself. From the other side, the steel jackets were introduced in retrofitting of existing structures as the add thickness of steel jacket is less than concrete jackets. But the very low fire resisting capacity of the glued steel jackets remains as a weakness point to this proposal.

Alternatively, Textile reinforced concrete (TRC) is one of the recent developed cementitious composite materials which have proven a competent performance in terms of mechanical properties and workability. Unfortunately, the available studies on the application of TRC as strengthening material are scarce and they concern more on shear strengthening for beams.

1.2. Objectives of the thesis.

The main objective of this research is to study the behavior of textile reinforced concrete when it is applied to an existing structure member in order to restore its carrying capacity. In particular, this research aims to cover some points: First, addressing the plastic tensile behavior of the textile reinforced concrete. Some experimental tests were carried out in Politecnico di Milano labs to estimate the mechanical characterization of some different TRC's mix design. The specimens were subjected to direct tension stress by applying constant value of displacement step. Moreover, the workability of each mix design was tested as well using the slump test. In order to assess the tensile strength for the retrofitted concrete sample with TRC. Second studying the behavior of a retrofitted reinforced concrete specimen with TRC by introducing (Double edge wedge splitting) DEWS test as an advanced technique developed from the (Wedge splitting) WS test. Unlike the bending and Brazilian test where the compressive and tensile stresses acts on the bending and splitting plane respectively, DEWS test features the possibility of reproducing the stress distribution on the section of the notched specimen by inducing tensile stress state indirectly by applying compressive load without any crosswise compressive stresses. This test was modeled numerically with two TRC solution (with and without polypropylene addition) to give a comprehensive explanation to the influence of using polypropylene fibres in manufacturing TRC.

1.3. Thesis outlines.

The structures of this research based on 6 chapters. The introduction chapter addresses general definition to the term of retrofitting and its latest techniques and materials. More attention was given to the textile reinforced concrete as it is the used strengthening material in this thesis. The engineering problem was presented in this chapter. Then, the main objectives behind this thesis are explained as well.

The following two chapters represent the state of arts. Chapter two provides an overview for the textile reinforced concrete in particular, the different mix design characteristics and also the specification of the reinforcement fibres. Then, the tensile strength of TRC and durability behavior is stated. Finally, some examples for the fields of TRC application are given.

Chapter three explains in details the bond mechanism between the new added strengthening material layer and the existing old concrete layer. Also, the behavior of TRC when it is used for confinement is given. At the end of this chapter the behavior of a strengthened beam and column are exhibited.

In chapter four, the experimental program is introduced. The chapter starts by presenting the experimental investigation on the mechanical characterization of TRC and its results. Then DEWS technique was introduced including the test description, used devices, test preparation and surface treatment as it will be further detailed. The investigation on strengthened sample with TRC and the results for its tensile and compression test are given.

Chapter five presents the development of the numerical model using the finite element approach. DEWS technique modeled using Abaqus 6.13 where the plastic behavior in compression and tension were introduced. The obtained results were compared to the results obtained from the experimental investigation explained in chapter four.

The conclusion and the recommended remarks for future development is presented in chapter 6.

Chapter 2

State-of-the-arts of TRC

2.1. Introduction

Textile reinforced concrete is considered one of the new advanced cementitious material obtained when a very fine grained concrete combine with fabric. Because of the small maximum aggregate size used in TRC production, the matrix is closer to be a mortar therefore it may be called TRM. Using the textile reinforced concrete has many advantages. TRC has proved high effectiveness in particular, high durability and strength performance. Also, it is placed in the main stress directions unlike the randomly distributed short fibre such as glass fibre reinforced concrete (GRC). In addition TRC is very fixable for reinforcing the curved components near to the surface in different load directions and it has the possibility of forming open structures with displacement stability. Moreover, the easy and reproducible positioning of yarns in the shape of textile fabric is considered an economic profit. A lot of research projects had been done in many universities. These research centers raise some triggering points in TRC such as, the basic mechanism regarding load carrying capacity, the durability aspects and bonding characteristics. TRC has applied for many structural items under different environmental and load conditions such as, formwork, facades, tanks, containments and strengthening of existing structures.

2.2. Mix design

Obviously the mechanical properties of the matrix depend on the mix design. Not only the mechanical properties but also the bond behavior, workability during production process and the material durability are depending on the mix design. Particularly in TRC the full penetration of the paste inside the mesh should be fulfilled. For this sake, the maximum aggregate size is usually less than 2 mm thus the matrix may be classified as a mortar. to optimize all the requirements mentioned above, the mix design should be the best compromise between this requirements and the economic aspects for the industrial production. Table 2.1 exhibit different mix compositions were developed in the collaborative research center of Aachen University.

Materials		**Mineral based matrices**		
		PZ-0899-01	FA-1200-01	RP-03-2E
Cement content	kg/m^3	490	210	980
Fly ash	kg/m^3	175	455	210
Silica fume	kg/m^3	35	35	210
Binder	kg/m^3	700	700	1400
Plasticiser	% by mass of binder	1.5	0.9	2.5
Siliceous fines (0-0.125mm)	kg/m^3	500	470	118
Siliceous sand(0.2-0.6)	kg/m^3	715	670	168
w/c		0.57	1.33	0.36
w/b		0.40	0.40	0.25

Table 2.1: Examples of mix design [Magri 2012].

To obtain the needed level of the flowable consistency, small size of aggregates is used (around 0.6mm) besides adding plasticizers and high amount of binders with taking into consideration the effect of silica fume addition to the binder. Generally adding silica fume with amount more than 10% by the mass of total binder content increase the density of the matrix, therefore, it reduces the flowable consistency. On the other hand using silica fume decreases the alkalinity of the mix. Also, when it is used together with Fly ash the occurred pazzolanic reactions increases the density of the mix, decrease the calcium hydroxide in the interface zone and enhance the durability of the composite. Moreover, using Fly ash improves the viscosity which is necessary to the paste penetration into the fabric [Mobasher2005]. Contrariwise the yield strength decreases with increasing Fly ash content (figure 2.1).

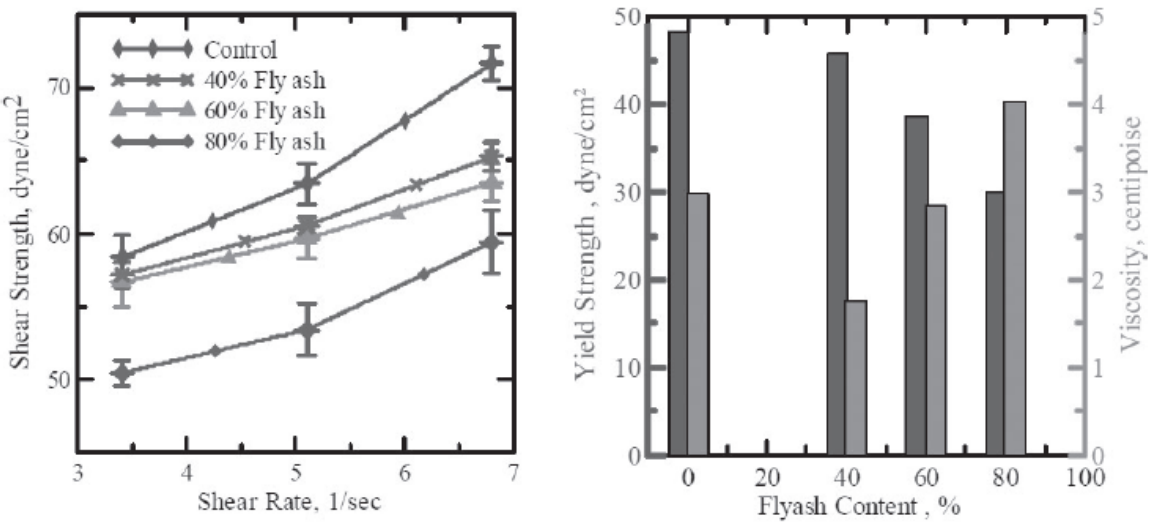

Figure 2.1: effect of Fly ash on, shear strength vs. shear rate (a), yield strength and viscosity (b) [Mobasher2005].

In order to investigate the fresh concrete properties standard flow test, flow time and rheology measurements should be performed [Brameshuber2001]. Figure 2.2a shows the slump cone test which measures the flow of the matrix through the cone on a horizontal plane. The flow time is the needed time for concrete to flow through the V shape funnel shown in Figure 2.2b. While Brookfield Rheometer (figure 2.2c) is used to determine the rheology of the matrix based on the used amount of Fly ash. The shear rate is varied during the tests from higher rpm values at the start (20) to lower value (10). The whole test finishes after 16 minutes. The rheological properties are computed starting from shear stress vs. strain diagram.

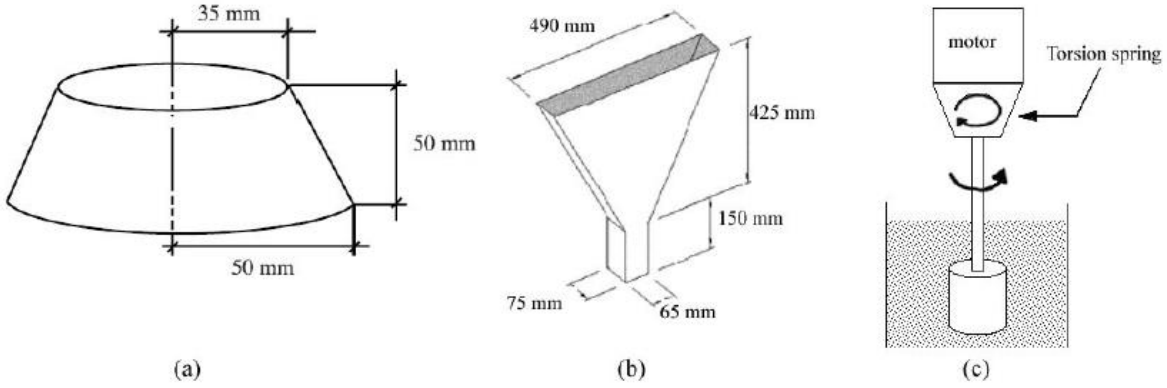

Figure 2.2: Slump cone test (a), flow time (b), Rheology test (c)

The traditional mechanical tests were performed to characterize the hardened concrete properties. These tests aimed to determine compressive and tensile strength, Young modulus and shrinkage. Table 2.2 shows some obtained results at Collaborative Research of Aachen (SFB 5532) according to German standard rules (DIN 18555-309.82, DIN 1048-5 06.91, DIN 52450 08.85) [Brockmann2001]. Knowing that, all specimens were stored at 20˚C. The compressive strength ranges from 32 to 98 MPa at 28 days while the observed shrinkage strain was between 0.56 and 1.47. Introducing the phenomena of size effect makes some difference during performing the experimental tests for quasi-brittle materials which had shown some dependence of the nominal strength at the ultimate load on the specimen size. However, in TRC applications it is important to investigate thinner structures (d=10mm). Results reported in table 1.4 shows that no significant size effect is observed.

Matrices	Compressive strength [MPa]		Flexural strength [MPa]		Young's modulus [MPa]	Shrinkage [mm/m]
	28 days	90 days	28 days	90 days	28 days	28 days
PZ-0899-01	74	89	7.6	8.1	33000	0.81
FA-1200-01	32	46	5.1	6.7	24800	0.56
RP-03-2E	98	108	8.1	9.4	26500	1.47

Table.2.2: hardened concrete mechanical properties [Brockmann2001].

Specimen dimension	slenderness	PZ-0899-01	FA-1200-01	RP-03-2E
b x d x l	l/d	σ_c	σ_c	σ_c
mm^3	-	MPa	MPa	MPa
10 x 10 10	1	93.99	42.74	146.91
20 x 20 x 20	1	94.56	43.44	150.27
40 x 40 x 40	1	101.18	44.88	152.96
10 x 10 x 20	2	98.90	47.54	156.81
20 x 20 x 40	2	95.09	39.75	153.15
40 x 40 x 80	2	89.58	37.52	154.24
10 x 10 x 40	4	77.34	43.12	135.24
20 x 20 x 80	4	89.13	38.15	127.58
40 x 40 x 160	4	87.37	36.51	143.10

Table.2.3: Compressive strength results for different specimens size [Banholzer 2006, Brameshuber 2003].

2.3. Reinforcement Fibres

The amount and the arrangement of the used fibre materials influence the properties of the textile reinforced concrete composite. To obtain high reinforcement efficiency in the composite, the fibres should have a modulus of elasticity higher than that used in concrete matrix. Also, high fibre tenacity and breaking elongation achieve high effectiveness of the reinforcement. In order to ensure a life-long reinforcing effect, the fibre material should withstand the alkaline medium without losing its characteristics. In addition, small relaxation under the permanent loads and the strong bond between the concrete and the reinforcement are from the requirements on the fibre material to produce the optimum reinforcing effect in the matrix.

The most used materials in textile reinforcement fabrication are Alkali-resistant glass fibre (AR-glass), Carbon and Aramid. Figure 2.3 shows the mechanical characteristics of these materials with different yarn fineness .

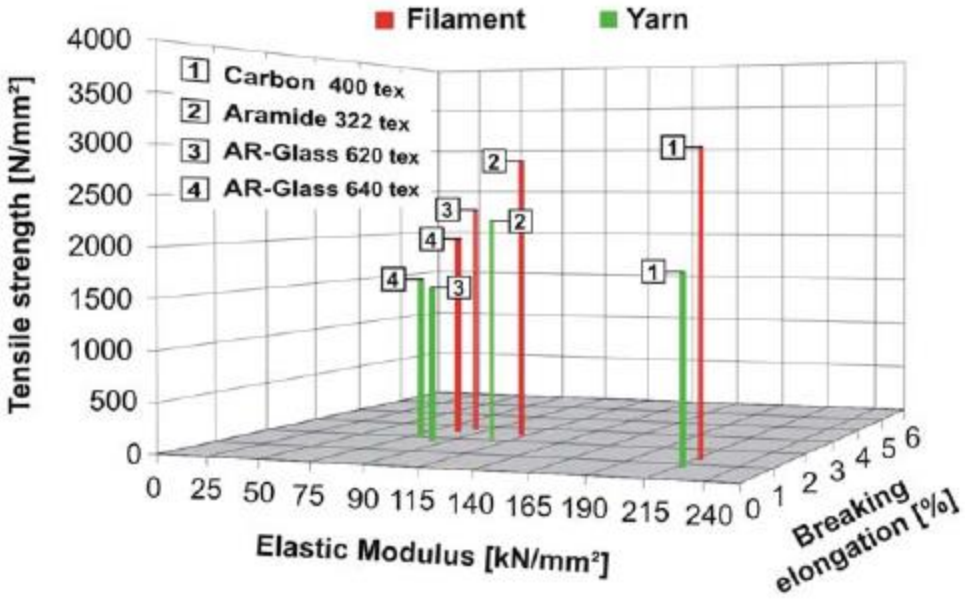

Figure 2.3: Mechanical properties of selected high performance filament yarns [ITP,TU Dresden]

In order to form the AR-glass, Carbon or Aramid, they can be made up as filament or twisted yarns. Moreover, the filament yarns have a small structural elongation which makes them better choice. One yarn consists of several hundreds to thousands of single filaments (figure2.4.) Therefore, the number of the filaments and its diameter and density are used to represent the fineness of the yarn.

The filaments in the yarn should be parallel and drawn as the locations of each single filament inside the yarn together with the interaction between the filaments themselves affect the stress-strain relationship of the filament yarn.

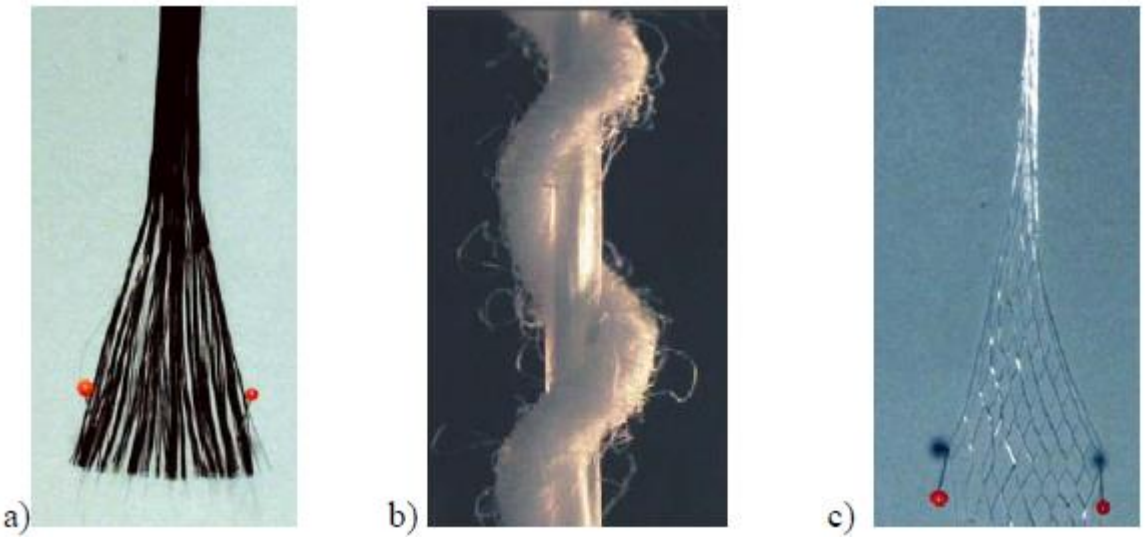

Figure 2.4: yarn construction a) filament yarn, b) bundled yarn, c) foil fibrillated tape [ITP,TU Dresden]

2.3.1. Alkali resistant (AR)-glass filament yarns.

Because of its relatively efficient behavior comparing with its cost, AR-glass reinforcement is widely used. AR-glass filament yarns are designed especially for reinforcing the concrete in order to resist the corrosive alkaline solution in the concrete. AR-glass was developed by Pilkingtons in the 1970s, based mainly on silica-soda-calcia glass and with and addition of 16% zirconia. Glass-RFC made from AR fibres was not completely immune to degradation, however developed soluble coating applied to the fibres. An AR-glass filaments diameter ranges between 9 to 27 μm. AR-glass mechanical characteristics depend on the fineness of the yarn, where the tensile strength vary up to 1400 Mpa and 2% elongation while the modulus of elasticity is 70 to 80 Gpa [Gries et al. 2006].

The most triggering criterion which makes the textile fabrication process usable for concrete reinforcement are is the possibility to produce open structures with high displacement stability. open grid structures provide a good permeability and complete envelope with the concrete. The most common fabrics are bi-axial or multi-axial wrap knits as they proved their suitability for many uses. Figure 2.5. shows different types of textile fabrics used for reinforcing concrete.

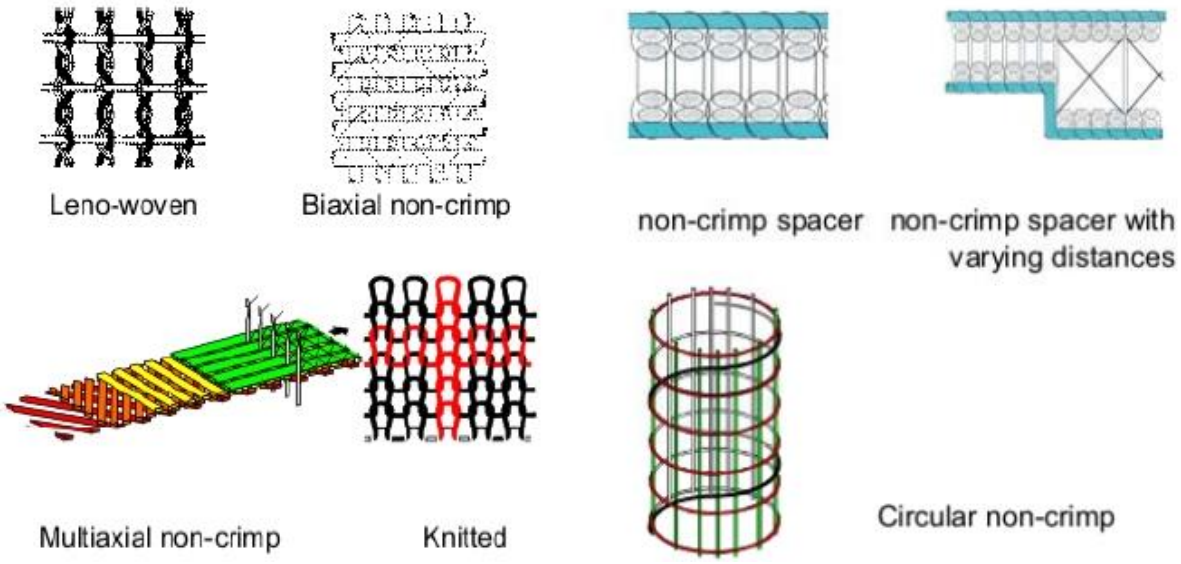

Figure 2.5: different types of textile fabrics used for reinforcing concrete [ITA, RWTH Aachen University].

The most used textile fabric in reinforcing concrete are:

- Scrims

It is produced in two forms, planer scrims and circular scrims. In the planer scrims the textile fabrics are produced by superimposing thread system with or without fixing the cross points. The highest stiffness and tenacity can be obtained if the reinforcing threads are exactly positioned and drawn in the load direction. There are two methods to form scrim, the biaxial scrim (formed by two thread system) and the multi-axial

scrim (obtained using three or more thread system). The circular scrims are produced using several bonding principles, like knitting, welding and gluing.

- Wrap knits

Similar to the Scrims with the possibility to insert a parallel and drawn weft thread according to the mesh pattern to reduce the deterioration of the reinforcing threads. It is manufactured in three different forms, plane wrap knits, three-dimensional spacer wrap knits and circular wrap knits (Figure2.6).

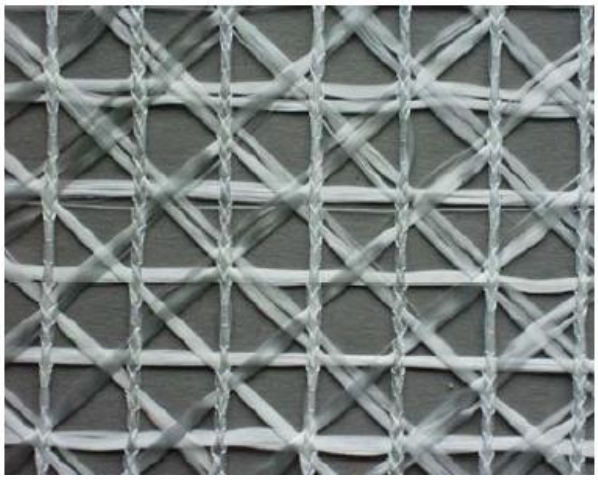

Figure2.6: Multi axial wrap knit [ITP, TU Dresden]

- Woven fabric

It is defined as a fabric manufactured by shedding two rectangular crossing thread system, wrap and weft. The weaving pattern of the fabric influences its properties. There are three basic weaving patterns, plain, twill and stain (Figure 2.7) Multi-layer woven fabric consists of several layers linked by binding wrap thread to ensure a defined space between layers.

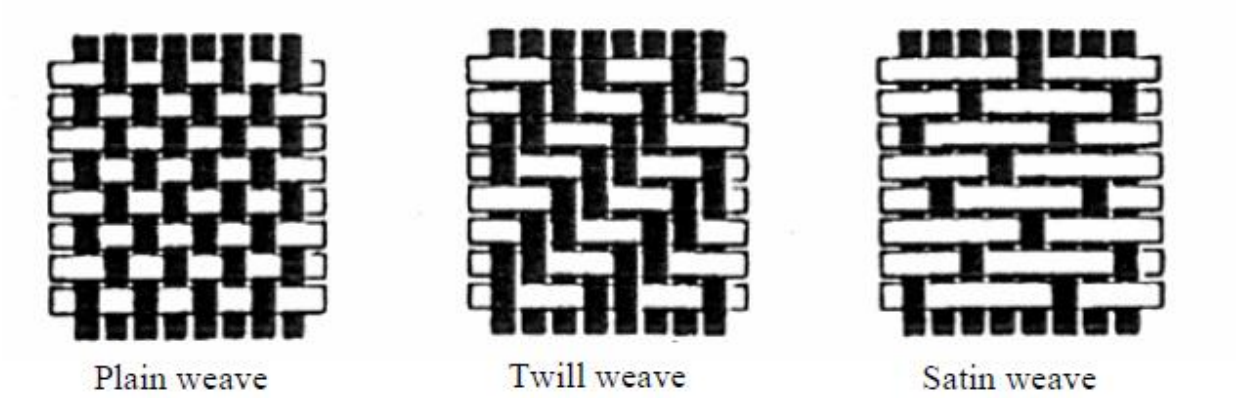

Figure 2.7: Different weaving patterns [ITA, RWTH Aachen University].

2.4. Tensile strength of TRC

The mechanical properties of the composite material are influenced by the filament fineness which can be determined according to DIN EN ISO 2060, the material density. Beside these characteristics also the bond between reinforcement and matrix has an effect on the strength and ductility of TRC. Basically, the forces inside the composite material transmit from the matrix system to the bond between matrix and filament respectively between filaments themselves. As a result to the brittleness of the AR-glass reinforcement the bond between the matrix and AR-glass influence the peak load and the ultimate strain. Unlike the steel bars in the steel reinforced concrete, TRC reinforcement fibres lack the homogeneity which makes the bond behavior in TRC different than its alternate in steel reinforced concrete. Not all filaments in TRC are in contact with the matrix, some of these filaments are anchored in the cement paste. However, the others are exposed to the slippage.

The stress-strain behavior of the single filament is measured by tensile test machine Fafegraph ME according to DIN EN ISO 5079 where the stress-strain behavior of yarns are given according the international standard ISO 3341. The modified test set-up for the determination of tensile strength and breaking strain of the yarns has been developed at the Institute of Textile and Clothing Technology (Figure 2.8).

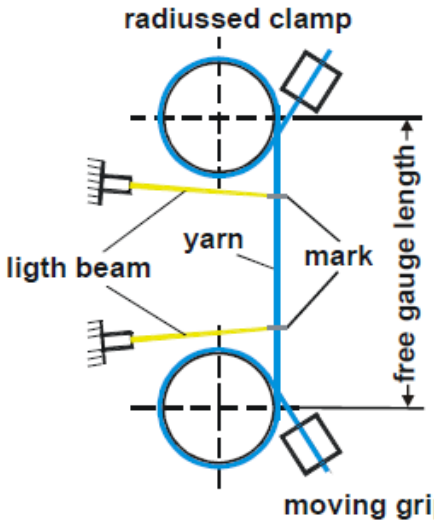

Test conditions	
- climate:	(20 ± 2) °C; (65 ± 2) % R.H.
- clamp:	wire clamp/ vulcanised flat (with cleaning)
- clamping length:	500 mm
- test speed.:	200 mm/min
- initial load:	0.5 cN/tex
- strain measuring:	optical extensiometer
- test:	20 per bobbin

Figure 2.8. Test set-up and test conditions for the determination of stress-strain behavior of yarns [ITP TU Dresden].

This test has proven high sensitivity for the results. In addition, several tests can be performed in a relatively less time and the test gives direct measurement of the strain. While, in order to obtain the effect of yarns length or waviness on the tensile strength, the load can be passed into the yarns trough two resin blocks. This method gives a very short and exactly free clamping length (Figure 2.9).

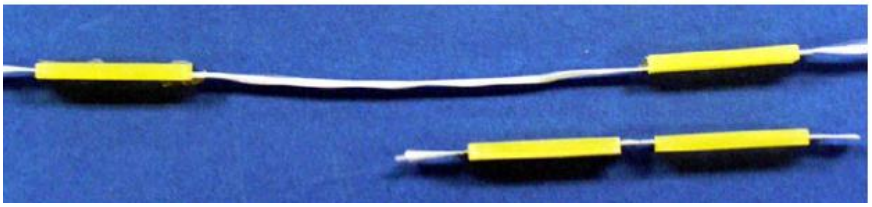

Figure 2.9: Using two epoxy resin blocks to define the clamping length [ITA, RWTH Aachen University].

Due to the unequal loading of the filaments within the yarn because of the slippage and existing material defects, the tensile strength of the filaments are distinctly not equal. The bond between the filaments affects on both results of the yarn tests and the tests performed on the composite material [Off2001]. Figure 2.10 shows some convergence between the obtained results in both cases while the tensile strength obtained from the performed test on single filament is higher.

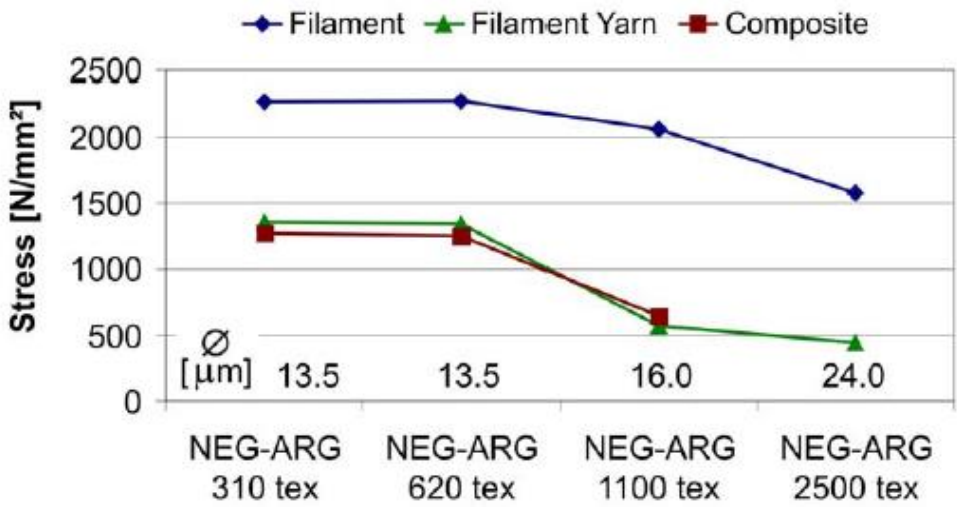

Figure 2.10: .tensile strength for different AR-glass filament diameters [ITP TU Dresden].

Yarn-Matrix-Bond theory [Banholzer 2004] gives a tension failure mechanism in the yarn based on some experimental investigation. The roving is schematized as a cylindrical structure with concentric rings (Figure 2.11a). Outer filament ring collapse first then the adjacent ring until the core filament failure (Figure 2.11b).

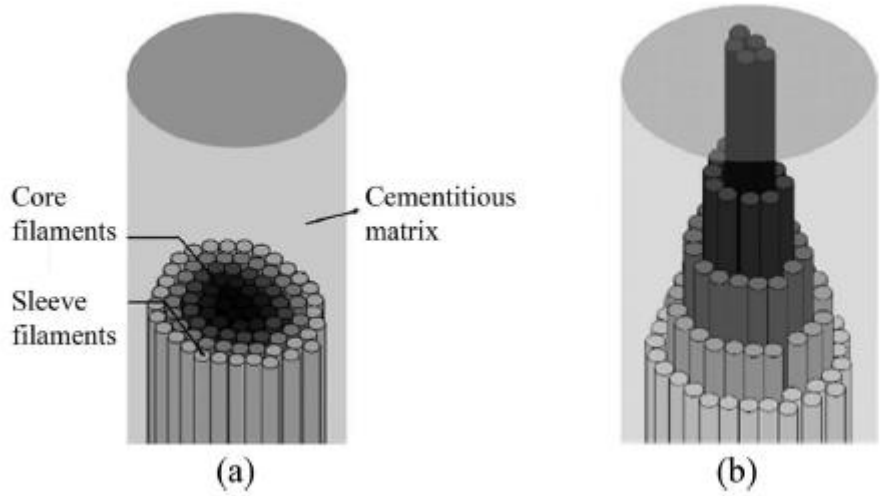

Figure 2.11: yarn failure mechanism embedded I matrix [Cohen and Peled 2010]

Beside the characteristics of the yarns, the penetration of the matrix paste in the fabric yarns is one of the factors affect the bond behavior in TRC. In particular, good penetration guarantees better bond strength due to the direct contact between the filaments and the cement paste is relatively higher [Peled et al. 2006].

Better bond strength can be obtained during the production process or even after casting during the curing stage. Regarding the production process, The pultrusion technique enhances the bond between matrix and fabric comparing with the lay-up technique [Peled et al.2006]. Curing after casting also has an effect on the bonding behavior inside TRC. Evidently the bond between the fabric and matrix increase if the matrix is fully hydrated and when applying pressure on the specimen after the casting process to allow the paste penetration in the fabric [Mobasher et al. 2006]. Moreover, using a proper detergent in treating the surface of the bundle improves the bond [Peled et al.2008]. It is worth to be mentioned that, the higher bond between matrix and fibres gives higher composite strength and lower ductility.

Tensile stress-strain curve for TRC is typically non-linear. Figure 2.12 exhibits textile reinforced concrete behavior. Also, the behavior of the fabric is included in the figure. According to Hegger et al. (2007) proposal the curve may be divided into three sections.

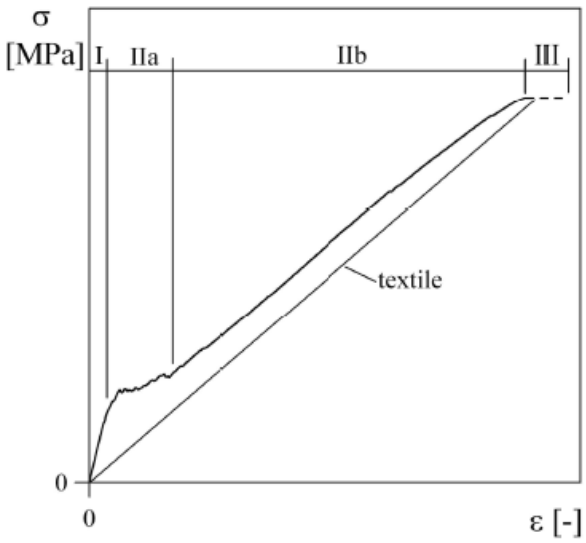

Figure 2.12: Typical stress-strain curve for TRC [Hegger et al. 2004].

First section (I) represent the un-cracked material behavior where the reinforcement contribution is negligible and apparently the linear slope represent the elastic modulus of the concrete.

Second stage (IIa) the matrix reaches its tensile strength in a specific section creating first crack, therefore the load transfers to fabric through this crack. Then, the load redistributed by the fabric according to the bond between the fabric and matrix until another section reaches the tensile strength creating another crack and so on. As a result of this repetitive process a multi-cracked pattern forms along the specimen. This branch of the curve defined by fairly constant load (IIb) where the deformation increases as well as the total equivalent strain. No more cracks in this stage and fabric strained upwards because the concrete contribution is negligible now only the fabric resists the load.

Eventually, the fabric reaches its ultimate strain (III). The failure in the AR-glass fabric is brittle failure; therefore, the final plateau was indicated by dashed line as the TRC reinforced with AR-glass fabric doesn't experience this stage. Many factors affect the position of the point where the fabric reaches the ultimate strain such as, the fabric geometry, reinforcement ratio and the bond strength.

2.5. Durability of TRC

Durability is a triggering factor to select the structural material in general. Durable material guarantees higher maintenance level for the mechanical response during the expected life time. Since TRC has been considered a structural material, hence, its durability level should be determined. The main challenges for the TRC durability are the loss of strength due to AR-glass degradation and the weather condition effect. Several researches and model have been developed in order to study the durability of TRC [Orlowsky and Raulpach 2008, Purnell and Beddows 2005]. Orlowsky and Raulpach (2008) proposed durability model that could predict the strength loss over the life time for TRC component stored outside where the predicted strength loss given by this model for TRC element stored in Aachen was 37% for 50 years. Evidently, in the early summer season when it rains more frequently and the temperature is relatively high, more strength loss rates are observed. Therefore, the matrix porosity has a great effect on TRC durability. Moreover, the alkalinity if the material affects its durability. Ordinarily, the matrix with reduced alkalinity has a good durability behavior [Butler et al. 2010].

The external environment has an effect also on durability behavior for instance, the pressure dilated due to the freezing water in the capillary pores exceeds the tensile strength of the material then causes damage in concrete [Neville 1996]. The produced pressure depends on the permeability of the cement paste where the higher the permeability the lower the pressure. Also, the repetition of sequential freezing thawing cycles leads to the development of the pressure and its consequences. The pressure dilation raises the volume of the water to 9% then the excess water expelled. In consequence the moisture content increases. Concrete ability to resist the freezing-thawing damage depends on many factors, the degree of saturation, and the permeability and water-binder ratio. Generally the lower degree of saturation makes higher material resistance to freezing and thawing. The critical degree of saturation is

the value which if it is exceeded then the material is prone to freezing-thawing damage. Many factors used to specify the value of the critical degree of saturation, the size of the body and its homogeneity and the rate of freezing. introducing the amount Air Entrained Agent (AEA) is essential during concrete production because the bubbles of air generate an additional space where the excess water can be accommodated. Subsequently, the pressure dilation development is prevented [Lomboy and Wang 2009]. On the other hand, low permeability and low water-binder ratio are the attributes of the high strength concrete (HSC) even without using the AEA (Figure 2.13.) the reason behind that can be demonstrated into two points.

- The reduced available amount of water reduces the possible water penetrated inside the concrete.
- HSC typically has very fine pores, where it is very difficult to freeze the pore water.

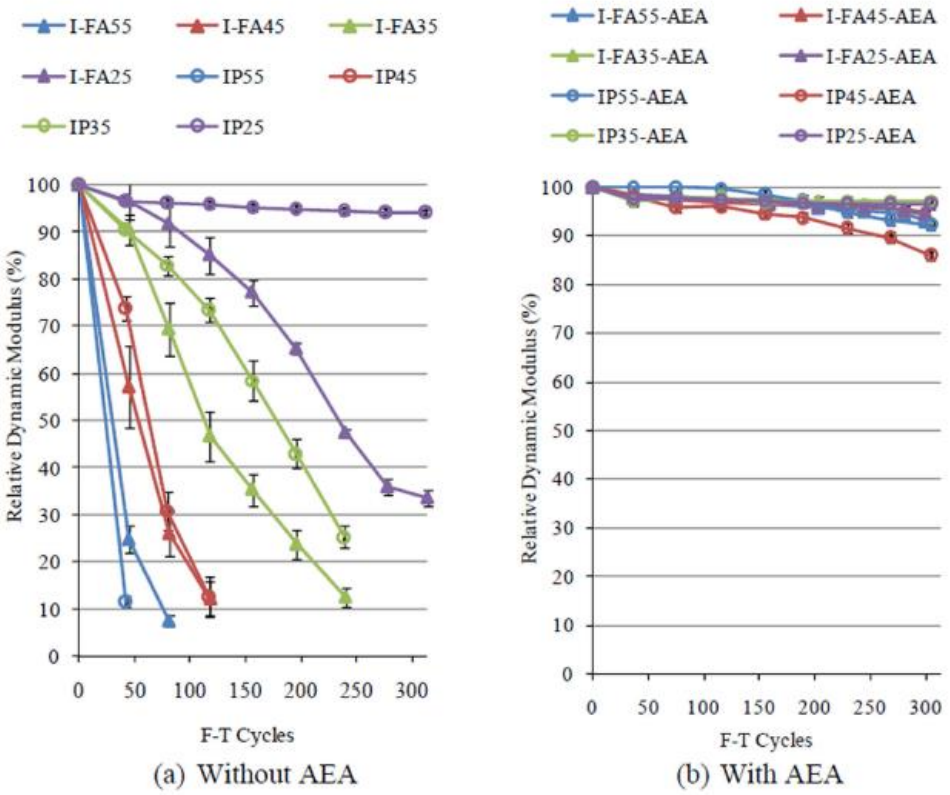

Figure 2.13: Relative dynamic modulus of concrete without (a) and with (b) AEA subjected to freezing-thawing cycles [Lomboy and Wang 2009]. I-FA and IP refers to different mix design; for each mix, different W/B ratios are considered.

Figure 2.14 Compares the behavior of HSC (0.25 W/B) ratio and conventional concrete (0.55 W/B ratio) after being exposed to freezing-thawing cycles. Considering the acting loading conditions besides the freezing –thawing effect on the same concrete member- regardless its grade- reduces the resistance of the member to the freezing-thawing damage. According to figure 2.15 the lower the grade of concrete the lower the number of cycles sustained [Sun et al.1999]

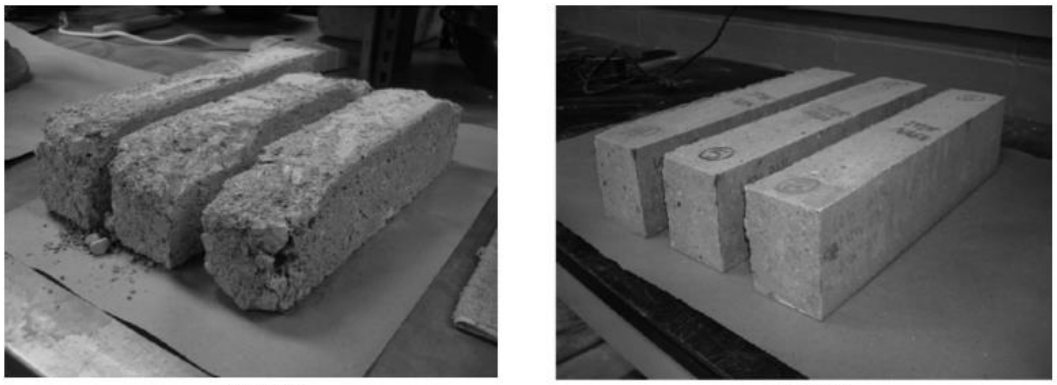

Figure 2.14: conventional concrete (a) high strength concrete(b) specimens after the exposure to 300 cycles [Wang et al 2009].

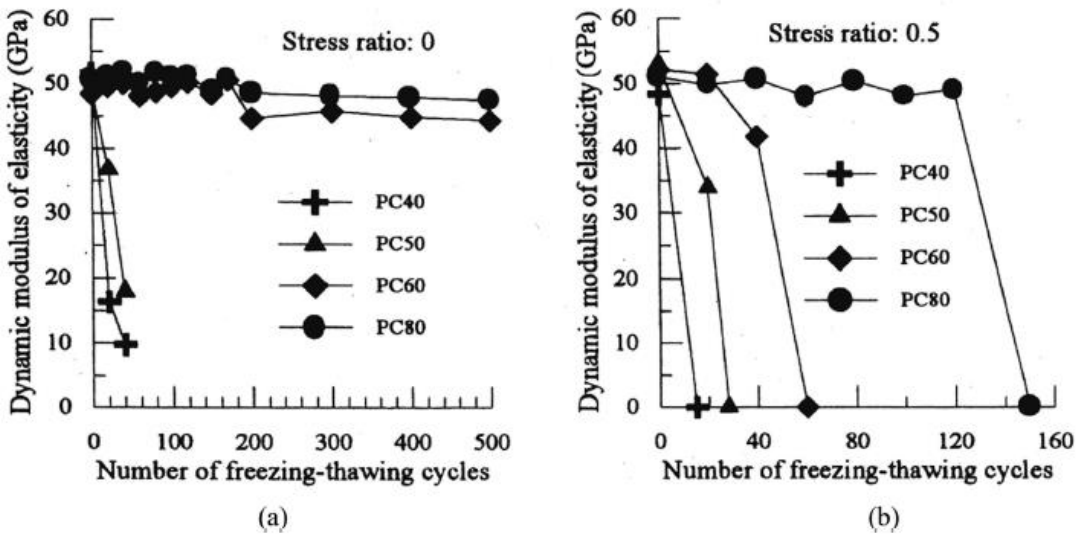

Figure 2.15: loss of dynamic modulus of elasticity of Portland cement concrete under the double action of load and freezing-thawing cycles- no stress (a), stress ration 0.5 (b). [Sun et al 1999]

Eventually, the effect of freezing and thawing on TRC is still not clear up to now as there is no enough information available for the mechanical properties behavior of TRC under freezing-thawing conditions. While, few investigations can be found for fibre reinforced concrete behavior under freezing-thawing conditions [Graybeal and Tanesi 2007, Cavdar 2014, Sun et al.1999] (figure 2.16).

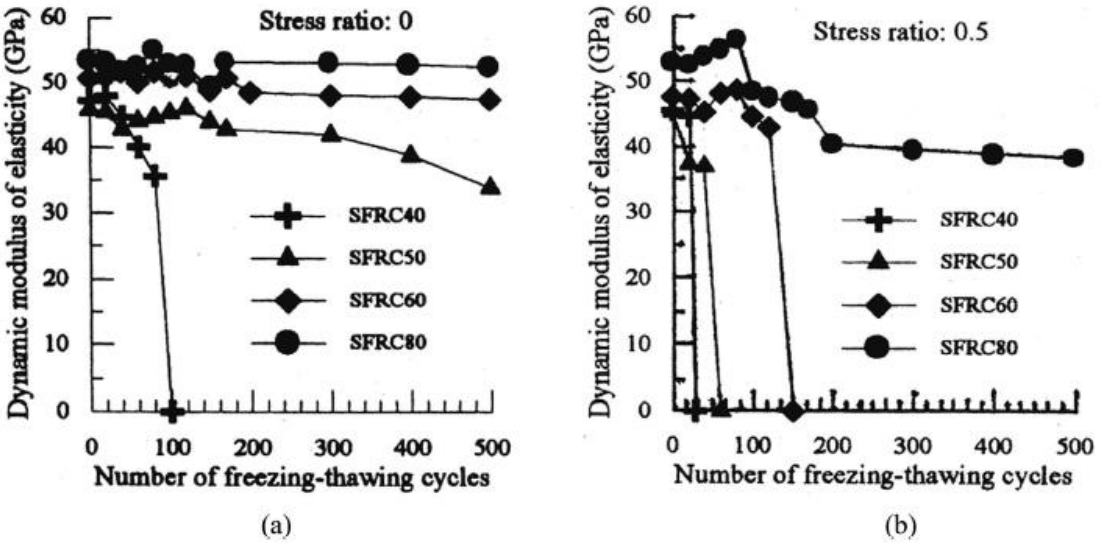

Figure 2.16: loss of dynamic modulus of elasticity of steel fibre reinforced concrete under the double action of load and freezing-thawing cycles- no stress (a), stress ration 0.5 (b). [Sun et al (1999)]

2.6. TRC Fields of application.

TRC can be applied in retrofitting of existing buildings structural members such as, roofs, columns, beams and coupling beams (figure 2.17). According to Mechtcherine [Mechtcherine 2013], adding thin layer of TRC to the structural members of an existing building has two beneficial effects; first, improve this member strength, second, TRC cracks pattern is very fine which gives the added TRC layer protective function in addition. It is worthy to be mentioned that, the most wide used fabric in reinforcing TRC is AR-glass.

Figure 2.17: Applying TRC layers to different structural items [Curbach and Sheerer 2011].

In order to study the effect of applying TRC to the structural members, R/C coupling beam was tested in Politecnico di Milano laboratory in the framework of the RELUIS (REte dei Laboratori Universtari di Ingegneria Sismica) project [Muhaxheri2014]. The importance of the coupling beam is that it is very critical element for structures subjected to seismic action. The test was performed by applying monotonic and cyclic loads on two solutions, un-strengthen and retrofitted (figure 2.18a). The coupling beam dimensions were 450mm long, 300 height and 100 mm wide with 8 mm longitudinal reinforcement diameters and 6mm for transversal reinforcement diameter distributed each 100mm. As it is shown in (figure 2.18b) applying TRC layer increased the maximum peak load to 78%. Also, slight improvement of the ductility was observed.

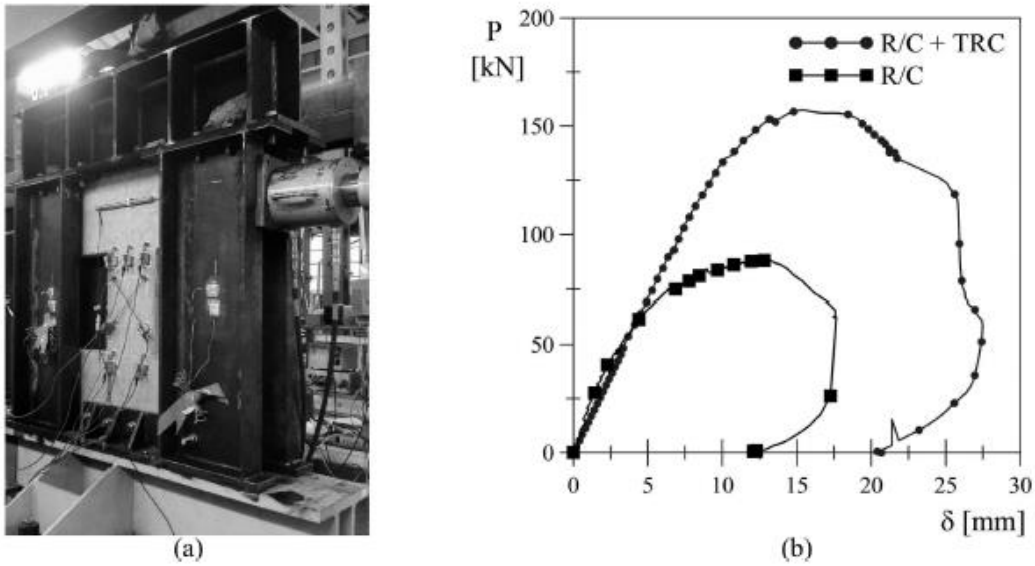

Figure 2.18. R/C coupling beam during test (a), load-stroke curve for un-strengthen and retrofitted coupling beams (b) [Muhaxheri2014].

Regarding the application of TRC in new structural elements, figure 2.19 shows some structural items constructed with TRC e.g. Façade panel, wall panels, roof elements, pre-cast roofs and tunnel linings.

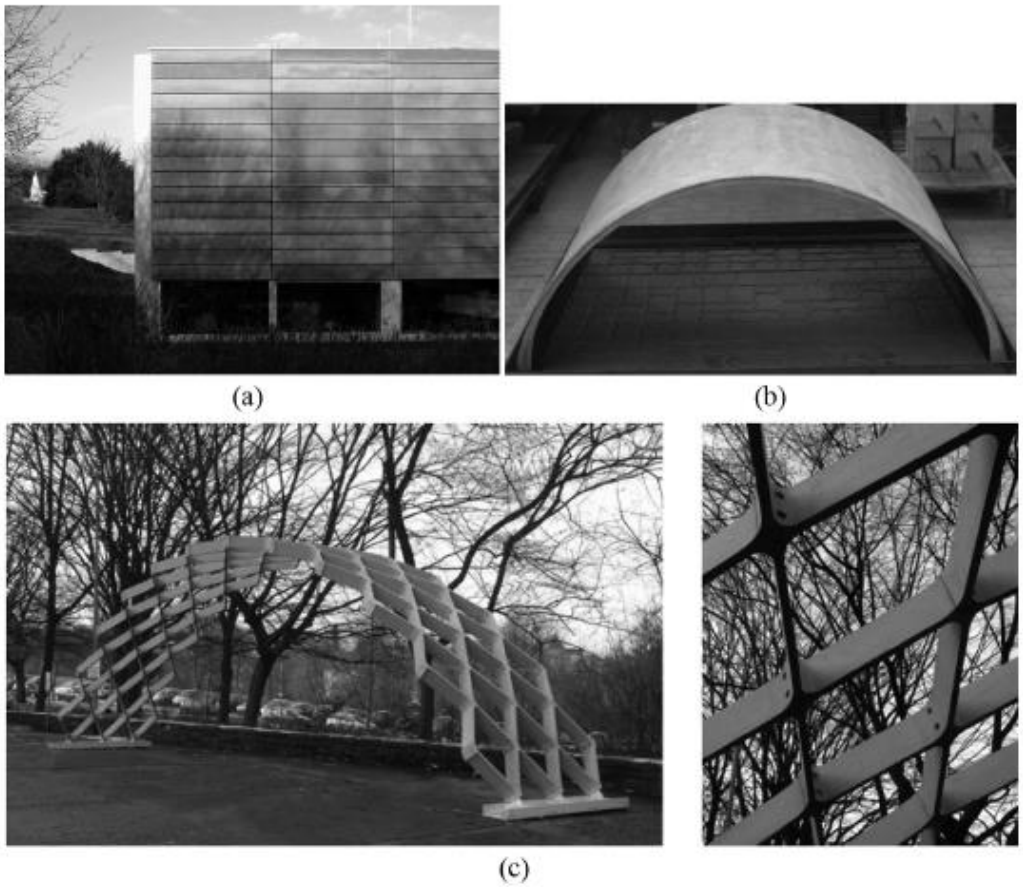

Figure 2.19 TRC Façade element constructed on the Institute of Structural Concrete at RWTH Aachen University, Germany(a), TRC shell roof (b) and TRC grid structure (c) [Hegger and Voss 2008]

Concerning TRC application in tunnel lining, the European project A.C.C.I.D.E.N.T (Advanced Cementitious Composite In DEsign and coNstruction of safe Tunnel) investigated a multilayer element made of Steel Fibre Reinforced Concrete (SFRC) and high performance Fibre Reinforced Concrete (HPFRC).TRC layer was embedded into this element at the interface to enhance the performance during exceptional loads [Di prisco et. 2013]

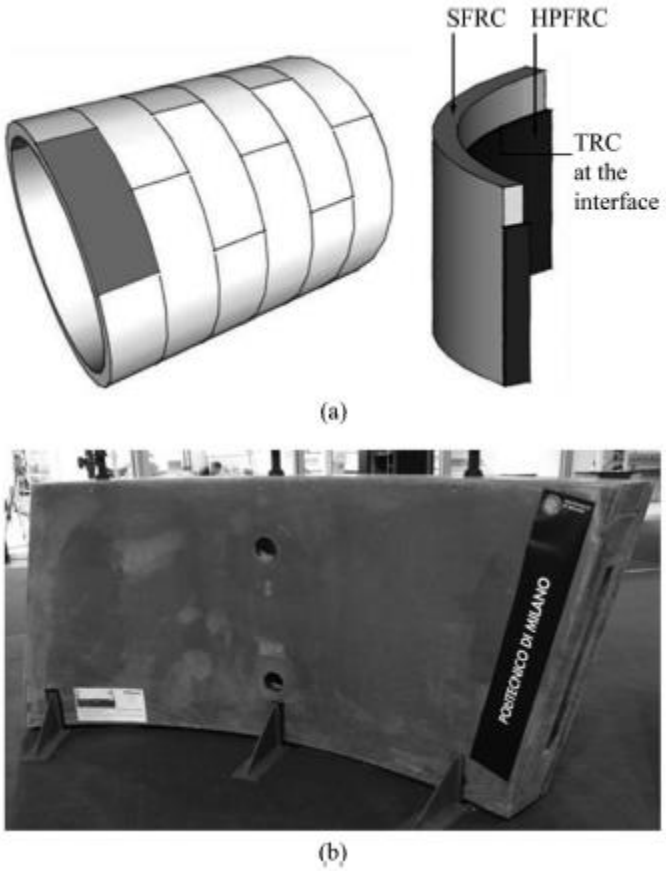

Figure 2.20: Multilayer tunnel lining: TRC layer position (a), protype exposed to the MadeExpo exhibition (b) [Di prisco et al.2013]

Chapter 3

State-of-arts of retrofitting

3.1. Introduction.

The main objective of applying the retrofitting layers to existing concrete members is to restore the load carrying capacity and stiffness. The bond between the existing member's substrate and the new added layer triggers the composite action effectiveness. In addition, surface preparation together with the repair material goodness and method of application are considered crucial issues in the retrofitting process. Evidently, using sandblasting gives a roughness about 1-2 mm which is quite enough to obtain good bond between the existing material and the new one.

It is worthy to mention that, using the traditional jackets is effective only by adding 60-70 mm thickness of concrete. To overcome this excessive thickness FRP (Fiber Reinforced Polymer) was introduced as it gives high strength and stiffness, good durability with very thin layer comparing with the traditional method. A very important limitation of using FRP is the high cost. In that sense, textile fabric had been used recently to enhance the bond between fiber and matrix. Unfortunately, the studies

about using TRM in strengthening concrete structures are few. The available studies in that issue concern on flexural or shear strengthening for beams and e bond behavior between concrete and textile.

In this chapter, using TRC in strengthening process is presented with some application with different type of loading. Also the bond behavior, bond layers and bond models had been exhibited.

3.2. Bond between the added layers of TRC and existing concrete member.

If the old concrete members strengthened by applying new TRC layer, the bond between the old and the new layers are characterizing the retrofitting goodness of this member. In order to guarantee full composite action of the strengthened concrete member, the bond forces must transfer from one layer to another through bonding joint. Separate bond test could be used to determine the force transfer mechanism between the TRC strengthening layer and the old concrete layer. This test gives some characterizing data like shear loading- deformation relationship and the transferable ultimate bond force [Ort 2003].

3.2.1. Modes of bond failure.

The kind of strengthening and the point where the bond failure begin are affecting strongly the bond failure mode. The bond failure of flexural strengthened ordinary concrete member can generally start at different points. Figure 3.1 shows different failure modes depends on the position of the starting points.

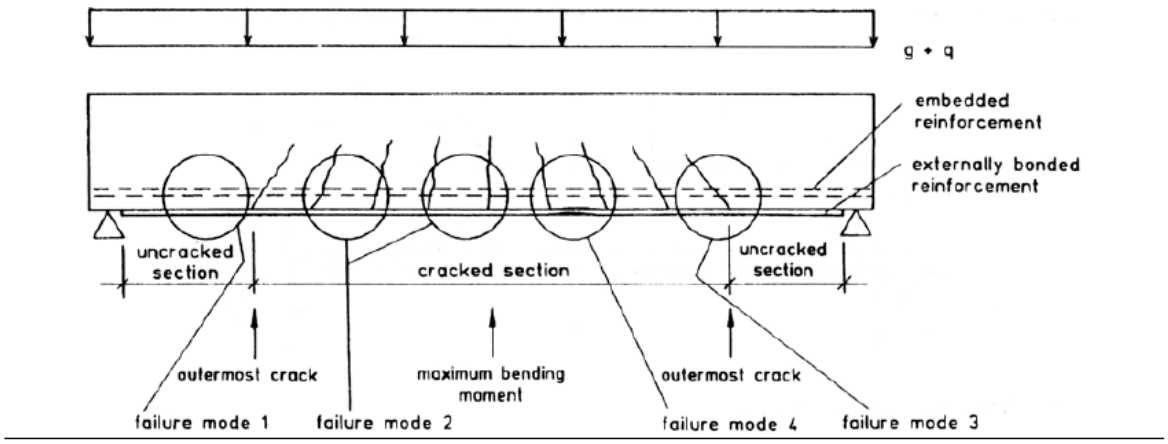

Figure 3.1: Modes of bond failure [Bla 1998]

All these failure modes must be kept in mind when developing a design model to draw the outline of the failure.

3.2.2.Layers of bond failure.

Figure 3.2 exhibit three different layers of failure that may theoretically occur between the new and old layers.

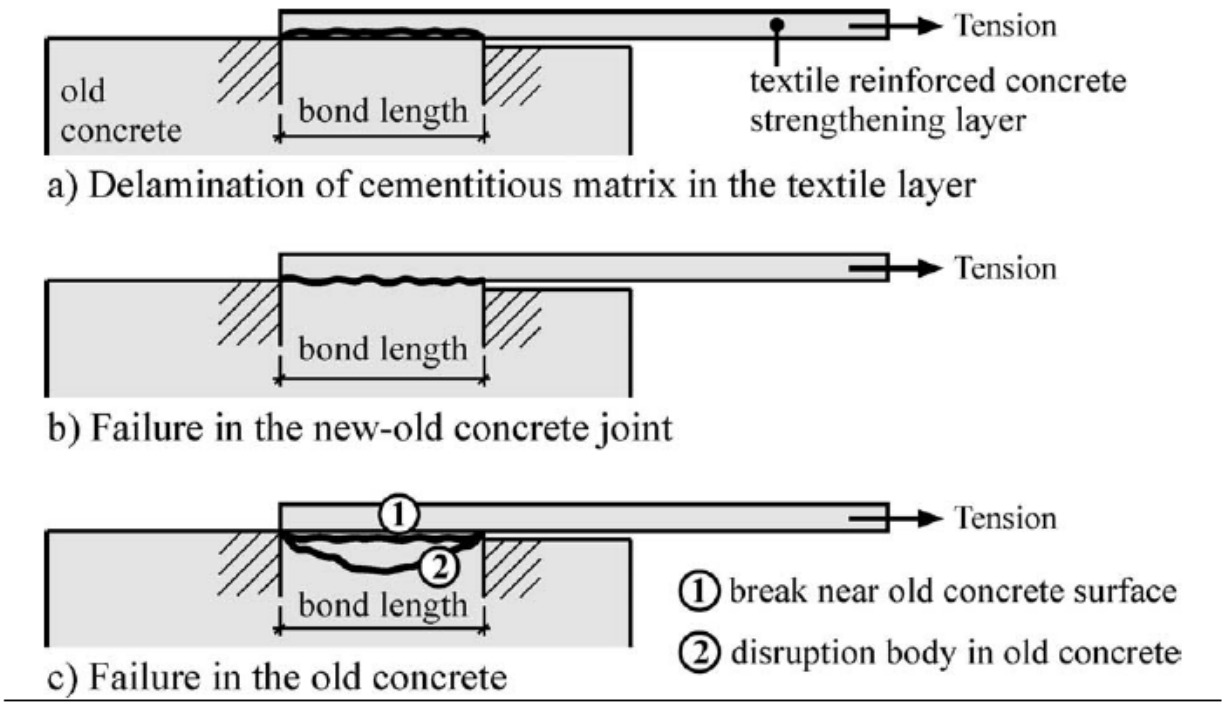

Figure 3.2: the potential failure layers between old and new concrete layers [Ort2004].

Speaking about failure layer (b), it can be avoided by strong interlocking between the existing concrete member and the strengthening layer. In that purpose, sandblasting of old concrete surface is highly recommended. In case of using fabric made of very thick multi-filaments yarns, new bond failure mode may occur at the anchorage range of TRC strengthening to the old concrete. The failure happen due to pullout of fibers from the fine grained layer Figure (3.3). The bond of these thick yarns and surrounding matrix can only be activated a relatively large fiber length.

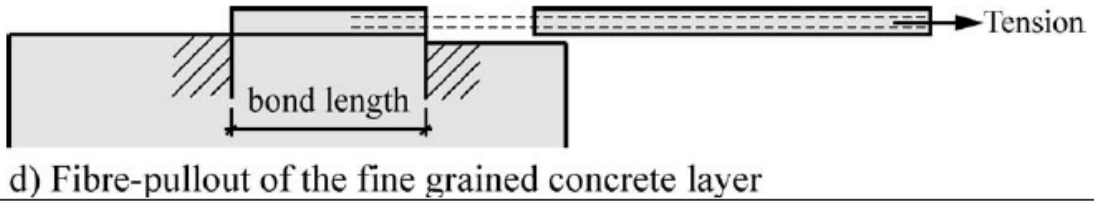

d) Fibre-pullout of the fine grained concrete layer

Figure 3.3: Inner bonding failure inside the new concrete layer [Ort2004].

3.2.3. The influence of the possible failure layers on load carrying capacity.

3.2.3.1. The influence of TRC type.

The larger the opening width between fibers leads to greater area for the distributed cementitious matrix between fibers. This is very crucial for the load carrying capacity of TRC layer as the matrix between fibers only able to carry tensional peel off forces (Figure 2.4).

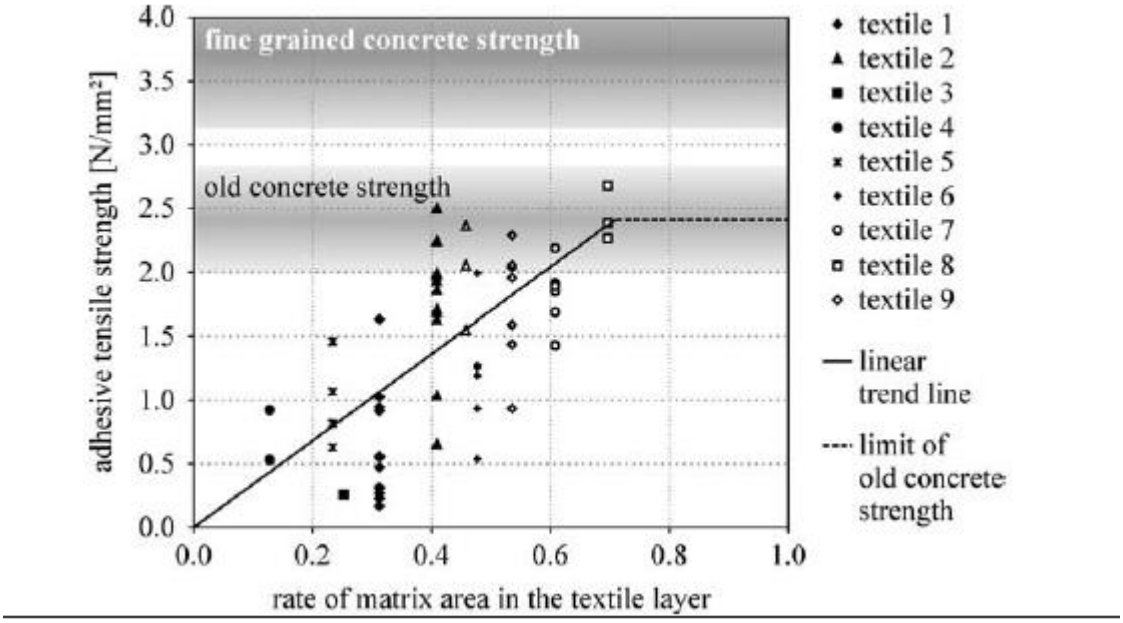

Figure 3.4: Influence of matrix area on load carrying capacity [Ort2004].

3.2.3.2. Influence of roughness of new-old concrete joint.

Apparently, rough surface of the old concrete member makes the new-old concrete joint is rough too and sequentially higher load carrying capacity of this layer. According to [RAN 1997] researches which show bond behavior in different cases of reinforcing and roughness preparing methods. The best result has been taken from high pressure water blasting followed by sandblasting the old concrete. An unprepared rough surface of concrete is less suitable and an unprepared formwork concrete surface is completely unsuitable for force transfer through the bonding joint.

3.2.3.3. Influence of the old concrete properties.

The deformability of old concrete depends on the maximum aggregate diameter [Holl 1994]. The large size of the old concrete member leads to higher interlocking effect between aggregates thus, developing bond cracks.

3.2.3.4. Deformation of the bond

The cracks inside the strengthening layers are extended to form transversal cracks with an angle between 90˚ to 30˚ in the bond region. No adhesion layer is formed between TRC and the old concrete therefore; the strengthening material doesn't form a slip interface. Figure (3.5) exhibit two case of deformation when using TRC or other material which allow to the adhesive layer to be formed.

3.2.4.Bond Models

Many investigations have already been accomplished to develop the bond model for the bonding behavior of additional adhesive bonded steel plates or CFRP strips [HOL 1994, Han1996, Neu 2000, ULa 2003]. Bond model generally describes the relationship between shear stress and slip between TRC strengthening layer and old concrete. The existing bond models for additional strengthening are basically adhesive bond laws with some assumptions that explain how the bond model is developed using some differential equations of bond slip. Also, the strain is assumed to be constant

across the thickness of the steel plates or CFRP strips therefore, the slip exist only the adhesive joint. Moreover, a simplified Strut-and-Tie model was introduced to describe the inter-relations between different forces in the bond region. Figure (3.5) shows the tension force in TRC strengthening layer (F_L) and the resulting peel off force (T_i).

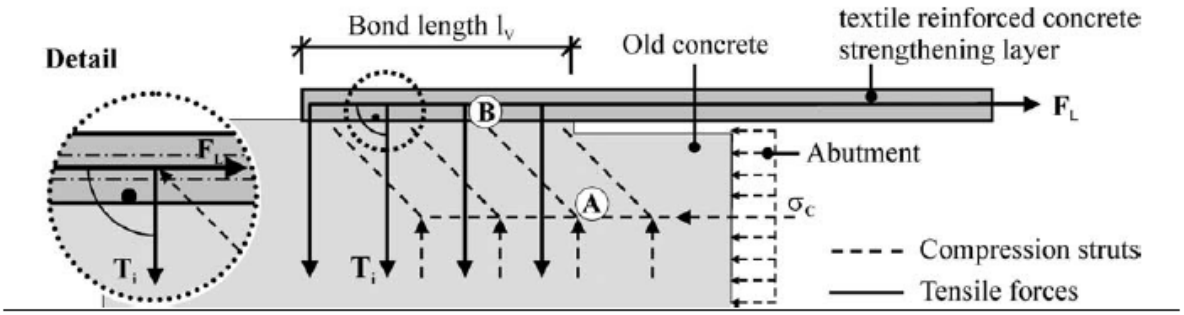

Figure 3.5: Strut-and-Tie model in the bond region [Ort 2004].

3.3. Shear frication.

According to shear friction theory, the shear strength of a concrete to concrete interface subjected simultaneously to shear and compression force ensured by friction only. A simple "saw-tooth model" is usually adopted to exemplify the basic principles of this theory, Figure 3.6. This design philosophy assumes that, due to relative slippage between old and new concrete layers, the interface crack width increases, the steel reinforcement yields in tension thus, compressing the interface and the shear forces are transmitted by friction [Santos and Júlio 2010].

The formula given in equation 2.1 is one option to compute the ultimate longitudinal shear stress at concrete to concrete interface.

$$v_u = \mu . \rho . Fy \qquad (2.1)$$

Where

μ refers to the friction coefficient equal to 1.70 for monolithic concrete, 1.4 artificial concrete and 0.8-1 concrete to steel.

ρ refers to reinforcement ratio.

Fy refers to the yield strength.

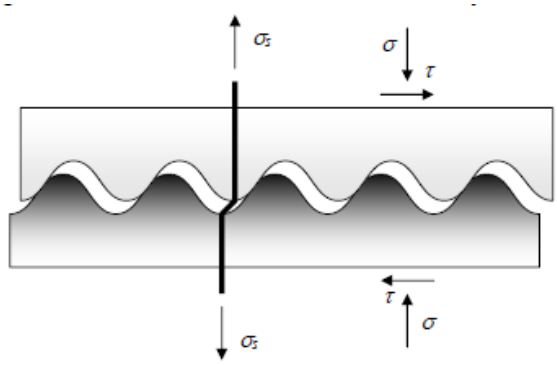

Figure 3.6: Shear friction [Santos and Júlio 2010].

3.4. Confinement

Evidently confinement is used to improve the carrying capacity for compression members. Moreover, it prevents slippage and buckling of the longitudinal reinforcement. Also, it increases the ductility of the compression members subjected to seismic actions. The technique of applying the confinement in this case based on introducing confinement pressure in either the potential plastic hinge zone or over the whole member. The traditional confinement techniques depend on using steel jackets, steel hoops or FRP (Fiber Reinforced Polymers) for upgrading. The present studies concern in using TRC produced by fine aggregates (TRM) where some experimental done on concrete [TRI 2006a, TRI 2006b] confirmed that TRM could be an alternative to RFP. TRC jacketing together with fibers in the hoops direction, just like FRP, has a very close behavior to elasticity up to failure and so the confining action is almost consumed under the axial load. At the same moment when the steel reaches yielding TRC starts to exert a continuously increasing confining action. This action value depends on the concrete lateral dilation which is affected by confining pressure; this behavior should be always taken in consideration when addressing the equation of the ultimate strength and strain of TRC-confined concrete. Figure 3.7 shows a plot for axial stress-strain for concrete confined with different number of layers with reference to the unconfined concrete curve. The first ascending branch is more or less the same like unconfined concrete while the posterior branch moves linearly until the jacket fractures due to hoop stresses which are represented clearly in the plot with a sudden drop.

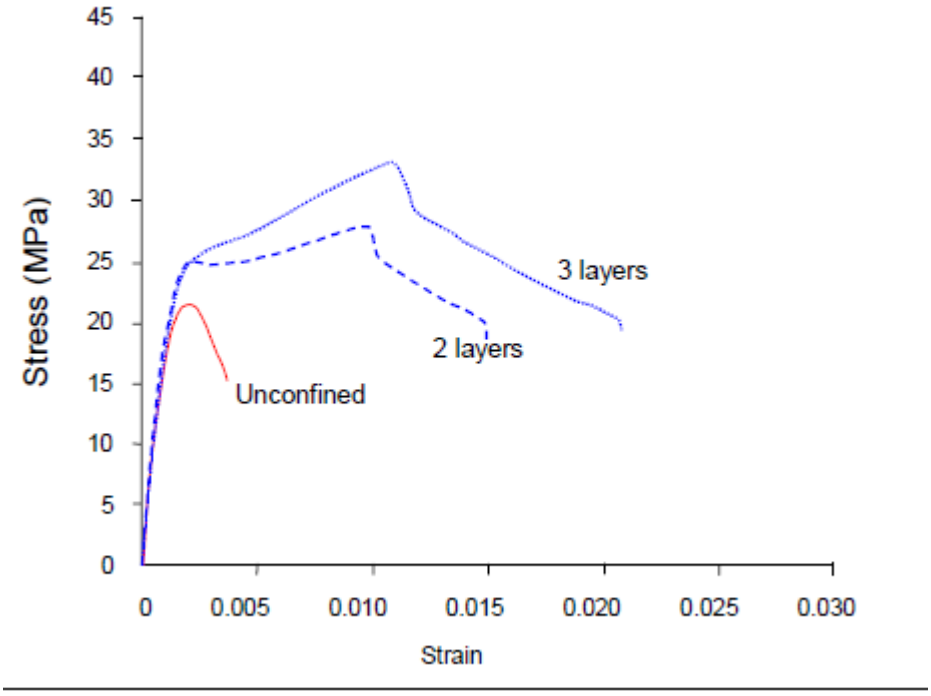

Figure 3.7: stress strain curves for concrete cylinders (150X300 mm) confined with TRC. Each layer of textile comprised a bi-directional carbon fiber grid with carbon fibers in each direction at nominal thickness equal to 0.047 mm [Ald 2005].

Expressing the confined strength f_{cc} and ultimate strain ε_{ccu} assumed to be dependent on the confining stress at failure σ_{cu} [Tri 2006a, Tri 2006b] as shown in these equations.

$$\frac{f_{cc}}{f_{co}} = 1 + K_1 \left(\frac{\sigma_{lu}}{f_{co}}\right)^m \qquad (3.1)$$

$$\varepsilon_{ccu} = \varepsilon_{co} + K_2 \left(\frac{\sigma_{lu}}{f_{co}}\right)^n \qquad (3.2)$$

Obtaining the confining stress σ_l by this equation.

$$\sigma_l = \left(\frac{\sigma_{l,h}+\sigma_{l,b}}{2}\right) = \frac{1}{2} K_e \left(\frac{2t_j}{h} E_j \varepsilon_j + \frac{2t_j}{b} E_j \varepsilon_j\right) = K_e \left(\frac{h+b}{bh}\right) t_j E_j \varepsilon_j \qquad (3.3)$$

where;

K_1, K_2, m and n are empirical constants.

b and h are the cross section dimensions.

E_j Refers to Young modulus of the jacket in lateral direction.

ε_j Refers to elastic strain of the jacket in lateral direction.

t_j is the jacket thickness

K_e effectiveness coefficient defined as the ratio of effectively confined area (Ae) to the gross area (Ag) figure (3.8). it can be obtained using equation (3.4)

$$K_e = 1 - K_2 \left(\frac{b'^2+h'^2}{3A_g}\right)^n \qquad (3.4)$$

So, by replacing E_j , ε_j by the effective jacket strength in circumferential direction F_{je}, σ_{lu} (ultimate confinement strength) can be obtained according to the equation (2.5)

$$\sigma_{lu} = K_e \left(\frac{b+h}{bh}\right) t_j f_{je} \qquad (3.5)$$

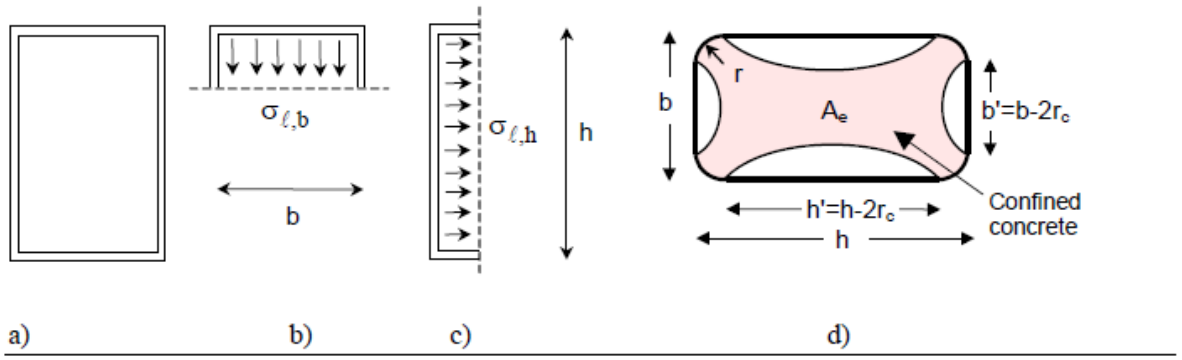

Figure 3.8: (a) Column with rectangular cross section (bXh) and (b)-(c) the approximate average of confining stresses and (d) the effectively confined area [Tri 2006a, Tri 2006b].

Some experimental tests were done on cylindrical and rectangular concrete specimens with assuming that the confined strength and ultimate strain are linearly increase with confining pressure. [Tri 2006a, Tri 2006b] gives the values of the equations empirical constants K_1, K_2=1.9, 0.047 respectively, these values indicate that TRC jackets are slightly inferior to FRP jackets but it is quite effective in increasing strength and deformability.

3.5. Behavior of a retrofitted beam.

3.5.1. Bending behavior.

According to Papanicolaou studies on using both TRM and FRP for flexural strengthening beam, the tests were done on beams with cross section 150X250 mm with 2φ12 longitudinal reinforcements on top and bottom, transversal hoops were placed in 100 mm spacing with 8mm diameter. The used concrete characterized with compressive strength equal to 34MPa. The specimens were reinforced with four layer of textile bonded in one case with cement based matrix [M4_FL], and the second case with epoxy resin based matrix [R4_FL] with a monotonically applied load. The test was performed at four points bending tests the displacement were measured at mid-span and the results were reported by load displacement curves in figure (3.9) in the plot, the curves C-FL refers to the reference specimen which represents typical response of reinforced beam (R4_FL) specimen gives double the strength and higher stiffness: the failure was associated to tensile fracture of the externally bonded layer in mid-span zone. Same response was observed for the TRM specimen [M4_FL] but with more ductile behavior and lower ultimate load due to debonding at the end of anchorage. Generally, TRM is 38% less strength effectiveness than FRP specimens.

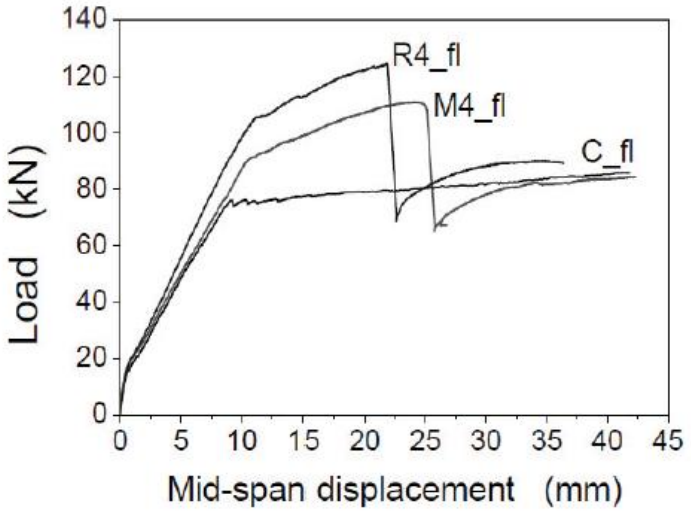

Figure 3.9: The load displacement results [Magri 2012].

3.5.2. Shear behavior.

Studies were done by Triantafillou to compare the response of shear strengthening reinforcement materials in particular TRM and FRP. The investigated beam) is subjected to four points bending test in figure (3.10). The cross section of the beam is 300X150 mm and the clear length is 2.60 m. The shear reinforcement was arranged in a quite large spacing. The used concrete compressive strength is equal to 30.5 MPa and the used textile is made of high strength carbon fiber with 168 g/m^2 and a layer thickness equal to 0.047. Two different bonding agents were applied (mortar or epoxy resin). Also, different number of layers or conventional or spiral wrapping applied textile. Based on four different combinations between different situations, the investigations were carried out on four beams formed according to this order; C refers to control specimen, M_2 refers to two textile layers of mortar, R_2 refers to two layers of epoxy resin and $M_{2\text{-}s}$ refers to two layers of mortar applied spirally.

The results were given in terms of load vs. mid-span displacement. Figure (3.11) shows that the control had the shear collapse with ultimate load of 116.5 KN with an observed diagonal cracks. Meanwhile, the failure in other specimens was due to bending with cracks in the region with constant bending moment. The maximum loads for all retrofitting solution were reported in table (3.1).

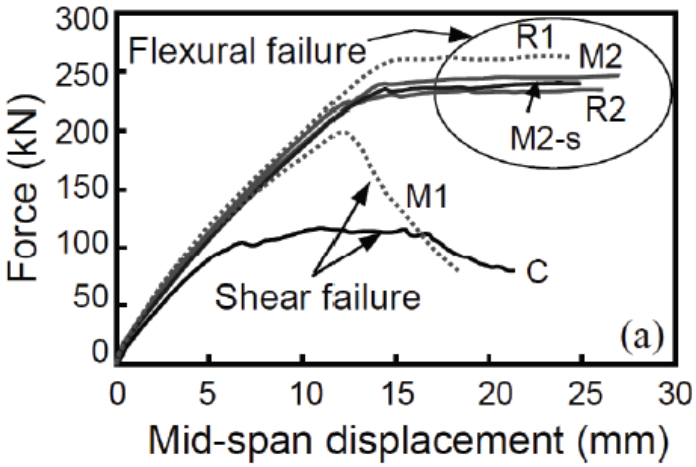

Figure 3.11: Force-mid span displacement [Magri 2012].

specimen	maximum load [kN]
R2	233.4
M2	243.8
M2-s	237.7

Table 3.1. Values for specimens ultimate loads [Magri 2012].

From the curves it can be noticed that, specimen M_1 had reached the shear failure at 200 KN with 78% shear capacity more than the control specimen. While, specimen R_1 had a flexural failure load greater than the two layer specimen R_2 and– according to the author- this was due to larger concrete cover used at the top of each beam compared to the one in the bottom. Generally, the increasing in shear resistance for all solution with two layers was distinctly observed.

3.5.3. Experimental study of the cracking behavior for TRC strengthened beam.

Some further studies had been done by Svetlana Verbruggen, where some investigations were carried out to study the influence of adding TRC to a steel reinforced concrete beam under the bending and analyzes the beam's load bearing behavior and crack pattern evolution. Three kind of specimens were tested, first specimen NE-NPC is un-retrofitted un-cracked specimen, second specimen E-NPC-TRC is retrofitted un-cracked specimen, while the third specimen is retrofitted pre-cracked specimen as it is detailed in table 3.2. All tested specimens have a total length of 650 mm and cross section dimensions equal to 100X100 mm. two longitudinal reinforcement bars with 8 mm diameter were introduced to the beam. And the shear reinforcement was overdimensioned in order to assure final failure in bending in the zone of constant moment. The used hoops have 6 mm n diameter. TRC strengthening patch were reinforced with eight randomly in-plane oriented glass fibres textiles. For the pre-cracked specimens the beam is pre-loaded in four points bending with third point loading up to a load of 18 KN.

Reference	# of specimens	Ext. reinforcement	# of precracks		# of cracks	
			#	Average	#	Average
NE-NPC	3	–	–	–	4	4
			–		4	
			–		5	
E-NPC-TRC	4	TRC	–	–	7	7
			–		7	
			–		7	
			–		8	
E-PC-TRC	4	TRC	3	4	7	7–8
			4		8	
			5		8	
			4		7	

Table 3.2: the number and type of the tested specimens during the test [Verbruggen 2014].

The loading is a displacement controlled with a displacement rate of 0.20 mm/min (Figure 3.12). LVDT was placed at the mid span of the beam in order to monitor the deflection. Also, the crack pattern evolution was detected using the digital image correlation (DIC) technique. The compressive strength of the used concrete is equal to 33.90 MPa, a Young modulus 33.8GPa and modulus of rupture of 4.8 MPa. For TRC matrix inorganic Phosphate Cement (IPC) is used.

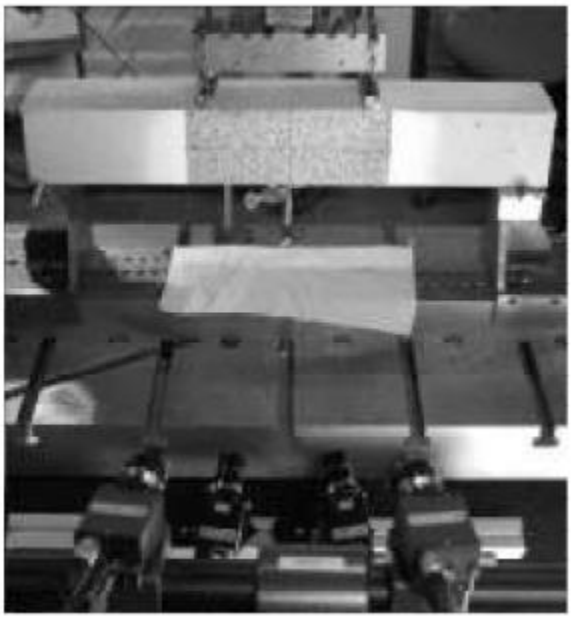

Figure 3.12: the test set-up [Verbruggen 2014].

The results were given in terms of load-deflection curves for all types of specimens (figure 3.13). Apparently, the curves show that the initial un-cracked high stiffness of the retrofitted beams is retained much longer than the un-retrofitted beams. The retention of the un-cracked stiffness is linked with the high fibre volume fraction used in TRC matrix. Beside this also, the post-cracking stiffness of the retrofitted beams is higher than the one of the un-retrofitted ones which explained by the presence of greater total amount of reinforcement.

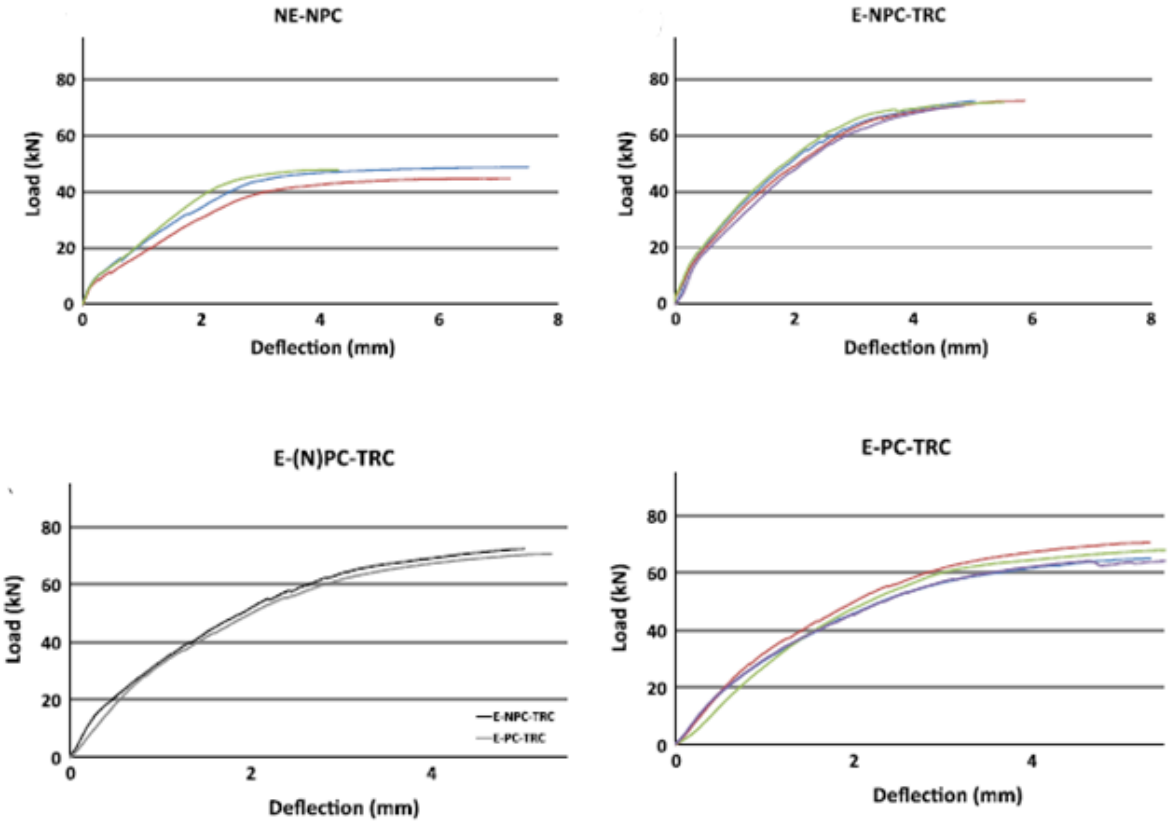

Figure 3.13: Load –deflection relationship for (a) un-retrofitted un-cracked specimen, (b) retrofitted un-cracked specimen, (c) retrofitted pre-cracked specimen, (d) comparison between un-cracked and pre-cracked retrofitted specimens [Verbruggen 2014].

During this study, the crack was defined as a difference in horizontal displacement larger than 0.02 mm at the maximum load over a horizontal interval of 5 mm, which is not adjacent to another crack interval. These values are chosen to physically indicate a crack and study the crack development. However, no links with a serviceability limit state of crack opening is made in this regard. The curve were obtained by extracting the DIC data as close as possible to the TRC but still in the concrete.

The added strengthening TRC layer to the reinforced concrete beam increases significantly the numbers of cracks formed during loading. Where four cracks were detected in the un-retrofitted specimen meanwhile, seven cracks existed in the retrofitted specimen as it is detailed in figure 3.14. From the other side, the total horizontal displacement is much higher for the un-retrofitted beam than the retrofitted one at the same loading conditions.

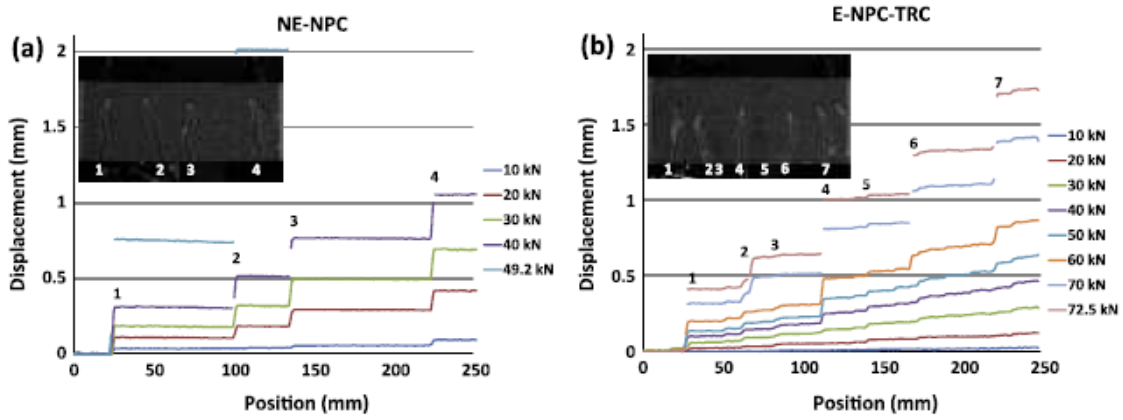

Figure 3.14: Crack width evolution regarding the position and width at different loading levels for (a) un-retrofitted specimen, (b) TRC retrofitted specimen [Verbruggen 2014].

The evolution of the cracks width is given in figure 3.15. With taking in consideration that, the cracks had been marked with the same numbers that used in figure 3.14. The main purpose of this correlation is to analyze the influence of TRC as a strengthening material on the initiation and growth of the cracks.

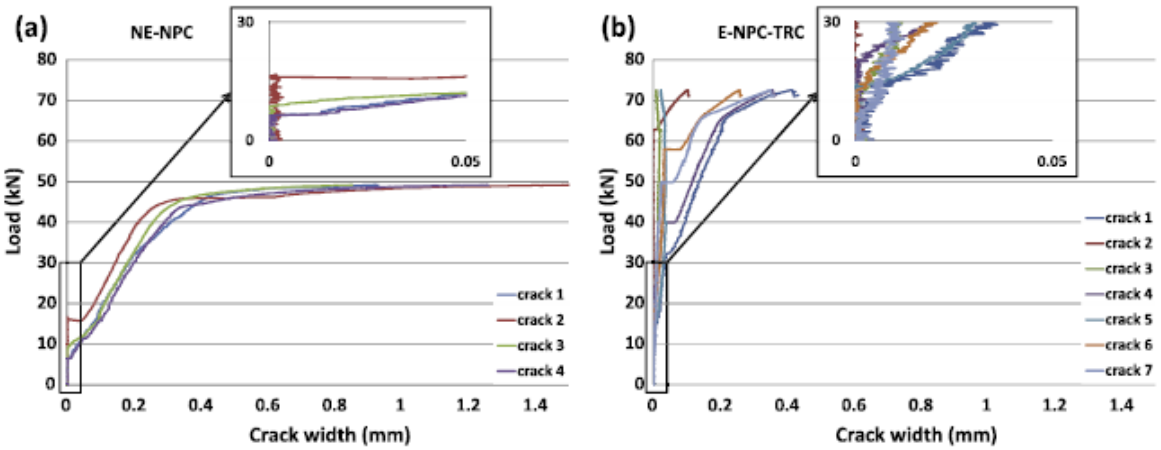

Figure 3.15: Crack width evolution for (a) un-retrofitted specimen, (b) TRC retrofitted specimen [Verbruggen 2014].

3.6. The behavior of retrofitted column.

Addressing TRM and FRP jackets effect on RC members is included in experimental program carried out by Papanicolau by introducing the confinement pressure of the jackets to the axially loaded concrete specimen with considering unreinforced specimen as a reference. Two types of specimens were investigated, one is cylindrical specimen with diameter equal to 150 mm and 300 mm height (A,B) and the second one is rectangular specimen with cross section dimensions equal to 250X250 mm and 700 mm height (C). The specimen's reinforcement has reinforcement as well as the reinforcement used in the beam tests.

All the specimens were reinforced with textile sheets of high strength carbon fibers (168 g/m^2) with 0.047 mm in thickness and using both mortar and epoxy resin as a bonding agents. The test was carried out by applying monotonically uniaxial compression load to the specimens. The notation given to each specimen were in form Y-XN where Y refers to the specimen type (A,B or C), X refers to the jacket type (C is the control specimen, MI is mortar specimen, MII is mortar specimen with higher strength and R is the resin based jacket) while N refers to the number of textile layers either 1 or 2. Results were expressed in peak load and ultimate strain and were normalized to the reference specimen's results (table 3.3).

Specimen	f_{cc}/f_{co}	$\epsilon_{cc}/\epsilon co$
A_C	1.00	1.00
A_MI2	1.36	4.80
A_MII2	1.57	5.40
A_MI3	1.74	5.65
A_MII3	1.77	6.10
B_C	1.00	1.00
B_R2	1.53	8.35
B_MII2	1.25	4.90
B_R3	1.92	12.75
B_MII3	1.49	5.40
C_C	1.00	1.00
C_R2	1.29	6.20
C_MII2	1.40	5.90
C_R4	1.47	10.15
C_MII4	1.51	8.80

Table 3.3. Strength and deformability results normalized to reference specimen's results [A.Magri 2012].

Comparing between FRP and TRM results, TRM was less effective in both strength and durability despite of TRM reached significant increase in compressive strength and deformability depends on the number of mortar layers. From another aspect, the failure of mortar specimens was less surprising than FRP. This was due to the slowly progressing fracture of fibers while in FRP explosive failure was observed due to the release of a large amount of strain energy.

3.7. Practical application.

TRC was applied as a strengthening layer during the retrofitting process carried out in 2006 for RC roof shell at the University of Applied Science in Schweinfurt, Germany [Mechtcherine 2011]. This project were carried out with the technical support of the collaborative research centre SFB528" Textile reinforcement for structural strengthening and retrofitting" of the TU Dresden. Figure 3.16 shows the RC shell needed strengthening. With 80 mm in thickness, 27 m side length and approximate span of 39 m. the shell's cantilever wings have experienced deformation up to 200 mm. the strengthening intervention was necessary after exceeding the ultimate tensile strength in the upper steel reinforcement layer of the roof. A TRC layer of 15 mm thickness containing three layers of textile sheets made of carbon fibre was applied to these particular areas in order to increase the load carrying capacity and to come over further deformations.

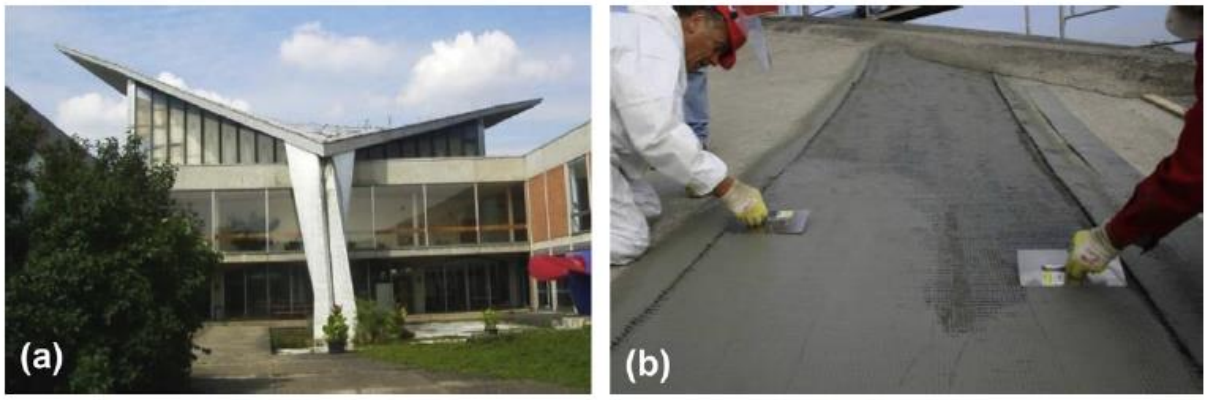

Figure 3.16: (a) Damage hypar-shell at the FH Schweinfurt (Germany), (b) strengthening with TRC process [Mechtcherine 2011].

Chapter 4

Experimental program

4.1. Introduction

Textile reinforced concrete has been a good choice that allows architect and engineers to design thin and light weight structures without losing the high load bearing capacity. In addition the high level of durability is so far guaranteed since no cover against corrosion is needed. Also, bi-dimensionality of the fabric gives the advantage for Textile Reinforced Concrete to resist bi-axial loads.

As it is known for any composite material and TRC as well, TRC depends on the bond behavior between the reinforcement and the matrix. Bond may be affected by many factors such as, curing conditions and pressure applied after laminate casting, fabrication technique, fibre type and treatment of fibre surface. In this chapter the mechanical characterization of TRC is presented according to some experimental tests have been carried out on different design mix. Moreover, the behavior of retrofitted concrete specimens is explained as well in this chapter with reference to the experimental program carried out in Politecnico Di Milano by A. Magri [Magri 2012].

4.2. Experimental investigation on Mechanical characterization of TRC.

4.2.1. Concrete matrix composites.

The test was carried out on three different matrix compositions with different Polypropylene fibre amount (P.P) and fixed water-binder ratio and fixed amount of superplasticizer. The matrices design mix is reported in table 4.1. Three specimens for each mix design were casted. The specimen dimensions are 400X70X6 mm, and network of textile F3 was put as a middle layer.

MIX M1	**A/(C+L)=0.19**				
UHPC	1	0.0015	m^3		
Cement 5.25	600	0.9	kg	900	g
Sand	957.03	1.435547084	kg	1435.5	g
Water	209	0.3135	Liter	313.5	g
Admixtures	44	0.066	Liter	66	g
Slag pozzolan	500	0.75	Liter	750	g

(a) First mix(F3+ NO P.P).

MIX M2	A/(C+L)=0.19				
UHPC	1	0.0015	m^3		
Cement 5.25	600	0.9	kg	900	g
Sand	957.03	1.435547084	kg	1435.5	g
Water	209	0.3135	Liter	313.5	g
Admixtures	44	0.066	Liter	66	g
Slag pozzolan	500	0.75	kg	750	g
P.P fibre	4.75	0.007125	kg	7.13	g

(b)Second mix (F3+ P.P1).

MIX M3	A/(C+L)=0.19				
UHPC	1	0.0015	m^3		
Cement 5.25	600	0.9	kg	900	g
Sand	957.03	1.435547084	kg	1435.5	g
Water	209	0.3135	Liter	313.5	g
Admixtures	44	0.066	Liter	66	g
Slag pozzolan	500	0.75	kg	750	g
P.P fibre	9.5	0.01425	kg	14.25	g

(c)Third mix (F3+ P.P2).

Table 4.1: Matrices design mix.

4.2.2.Production technique.

The hand lay-up technique was used to perform the specimens for test. This technique is characterized by the exertion of a negligible pressure during production [Colombo 2013]. Moreover, it is known as the most common technique for producing fibre reinforced composite due to the simple production procedure and its low cost, in addition this technique gives more flexibility to produce complex shaped specimens. A suitable amount of matrix was spread over the formwork using a roller to reduce the air bubbles inside the matrix. Steel rails were placed on the formwork to fix the fabric which was tightened at the edge of the formwork covered with another layer of matrix spread using the roller again. After casting process the specimens were cured for one day in climatic chamber.

4.2.3.Workability

In order to determine the fresh state properties of concrete, the slump test was done. Where the fresh concrete was poured in a slump cone and then the flow was measured on a horizontally aligned glass plate. The slump test results are reported in table 4.2. Note that, first mix was excluded from slump test because it is too viscose to perform the slump test.

Shots	Diameter [mm]
0	200
5	220
10	230
15	250
20	265
25	270

(a) Second mix.

Shots	Diameter [mm]
0	135
5	150
10	160
15	170
20	180
25	185/190
30	190/195
35	200
40	205
45	210/215
50	215

(b) Third mix.

Table 4.2: Slump test results.

4.2.4.The test.

As mentioned before three different matrix compositions were produced to study the role played by the poly propylene fibre in the concrete compositions. The casted specimens have dimensions of 400X70X6 mm and three specimens for each matrix composition were tested. Two steel plates with dimensions 55X70 mm were glued at the two ends of each specimen to guarantee homogeneous load distribution to avoid any tensional and bending moment due to misalignment of the constraints. The tests were done by introducing constant displacement rate of 0.02 mm/sec. (Figure 4.1)

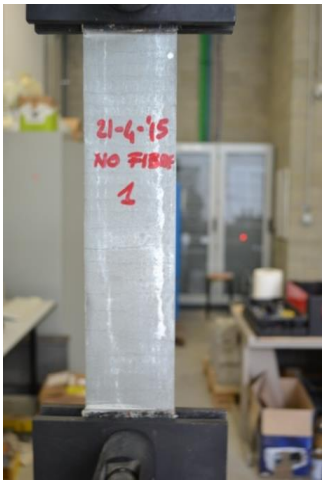

(a) (b)

(c)

Figure 4.1: test setup.

4.2.5.Results.

The specimen's dimensions after 28 days are reported in table 4.3. After performing the tensile test for the specimens, the results are shown in terms of stress [σ] vs. normalized displacement [δ/l] curve. The nominal stress was obtained by dividing the applied load by the specimen cross section. The normalized displacement was computed as the ratio between the stroke displacement and the initial length between the clamping edges. For each matrix compositions three curves were obtained. Figure 4.2 shows the average curve of the three identical specimens stress-strain curves is shown together with the range between the maximum and minimum curves, while the typical cracking pattern are displayed on the right. It worth noting that, in all graphs each average curve was interrupted when the first of the three nominally identical specimens reaches the ultimate normalized displacement.

The specimens dimensions 21/04/2015					
specimen	Width (mm)	Thikness(mm)	Length (mm)	υ (mm/s)	P (bar)
NO PP-1	70.30	6.25	286	0.02	3
NO PP-2	71.10	6.83	287	0.02	3
NO PP-3	70.13	6.55	287	0.02	3
PP1-1	70.40	6.70	286	0.02	3
PP1-2	71.00	6.73	288	0.02	3
PP1-3	70.00	6.36	288	0.02	3
PP2-1	70.50	7.25	285	0.02	3
PP2-2	71.60	7.40	284	0.02	3
PP2-3	70.00	7.70	285	0.02	3

Table 4.3: the specimens dimensions after 28 day.

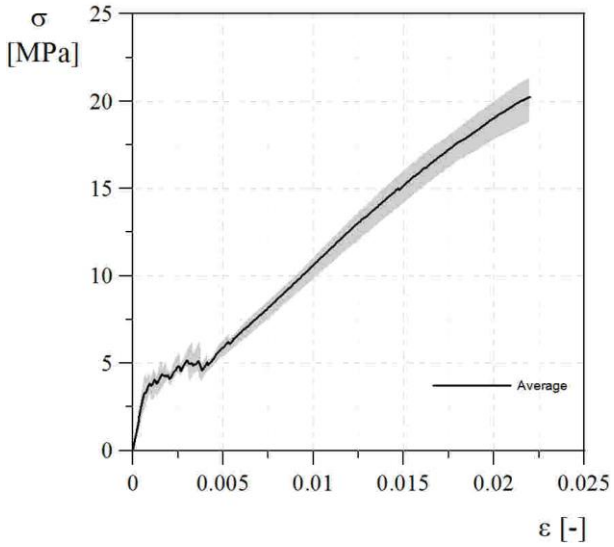

Figure 4.2(a):

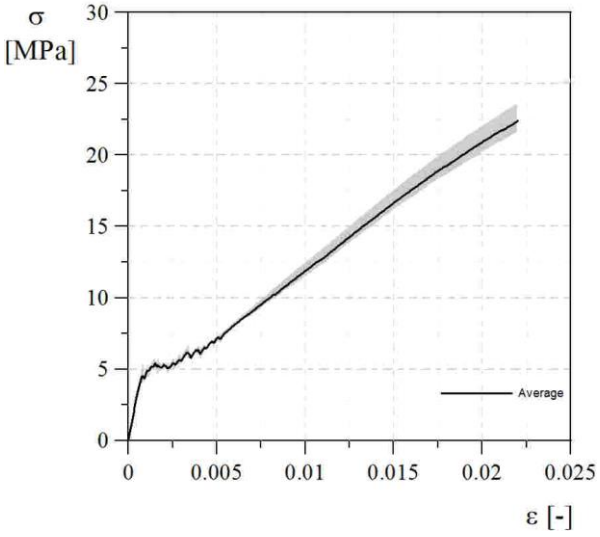

Figure 4.2(b):

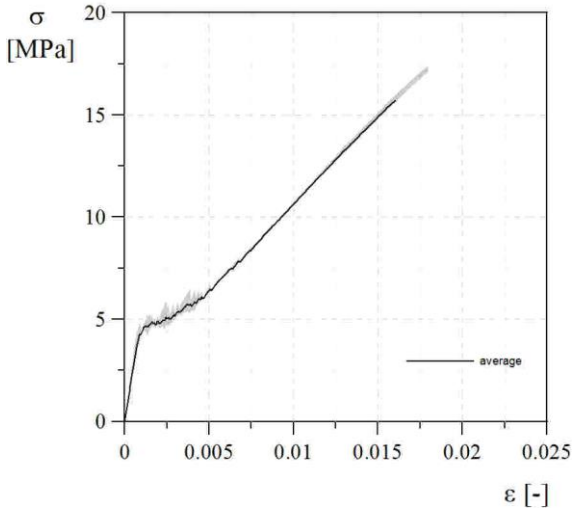

Figure 4.2(c):

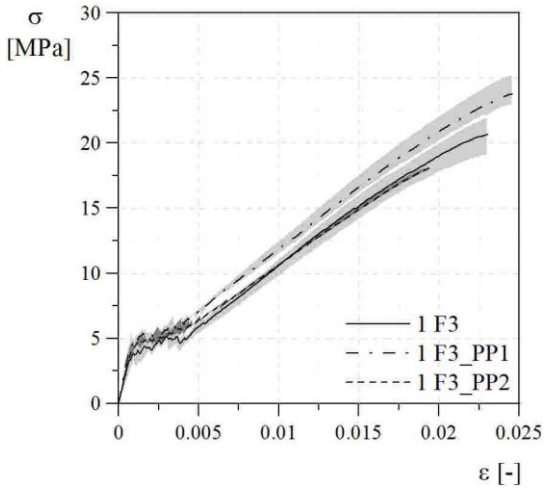

Figure 4.2(d):

Figure 4.2: TRC stress strain curves (a) F3+ no fibre, (b) F3+ 4.75 kg/ m3 fibre, (c) F3+ 9.5 kg/ m3 fibre, (d) comparison between the three mix designs.

The graphs show, that adding the poly propylene fibres to the matrix raise the tensile strength of the matrix in general and precisely the position where the first crack branch start from. Regarding to the cracking pattern, the first matrix (without PP fibres) shows some spalling failure in the cracked specimen. In the other side the other two specimens (with PP fibres) have a smaller crack width. The second matrix (F3+PP1) had proven better workability during the casting process comparing with the third matrix (F3+PP2) which has very low workability influenced the bond between the mortar and the fabric.

4.3. Investigation on strengthened samples with TRM

4.3.1. Tensile Test.

4.3.1.1. DEWS technique.

DEWS is an abbreviation for Double Edge Wedge Splitting test [di Prisco 2010] which is considered as developed technique from Wedge Splitting test (WS) [Brahwiler 1990] (figure 4.3). Unlike the bending and Brazilian test where the compressive and tensile stresses acts on the bending and splitting plane respectively, DEWS is an indirect tensile test which aims to reproduce the stress distribution on the section of the notched specimen loaded in pure tension without any crosswise compressive stresses. Figure 4.4 shows the distribution of stresses in both Brazilian and DEWS test.

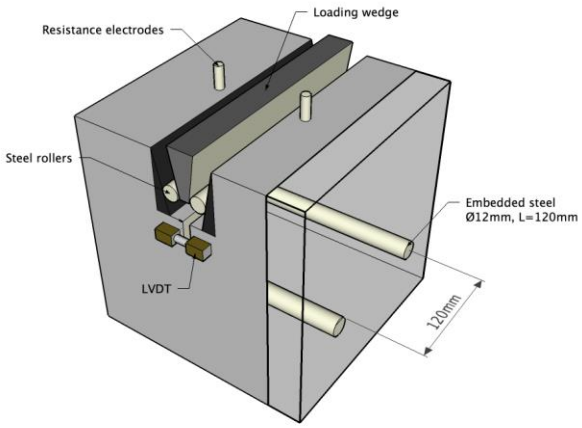

Figure 4.3: Wedge splitting test.

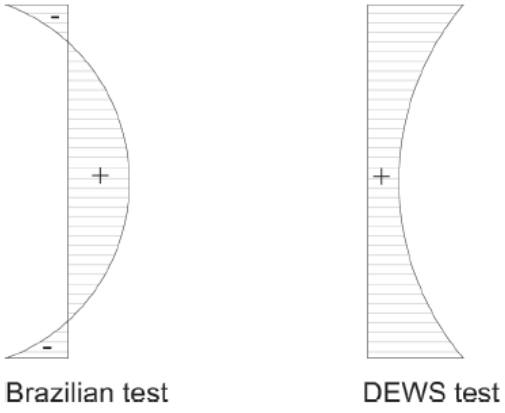

Figure 4.4: comparison between Brazilian and DEWS tests [Magri 2012].

Figure 4.5 shows how the specimens used in DEWS were developed to have two triangles opposite grooves with 45° inclination with attached steel plates to minimize sliding friction between the notches and the steel cylinder which had been accommodated into the grooves to apply the load by pushing these steel cylinders by machine platens. Cutting the two grooves starting from the grooves vertices was done to the specimen in order to avoid the cracks propagation in the highly stressed load application zone. Introducing the load in this way gives possibility to avoid the typical problems of direct tensile load application where DEWS test is carried out by applying compressive load only. In addition, one of the advantages of using DEWS is to overcome the highly localized stresses in case of ductile material where plastic deformation can take place. This can be noticed clearly in the comparison between the elastic tensile stress distribution for both Brazilian and DEWS in figure 4.4.

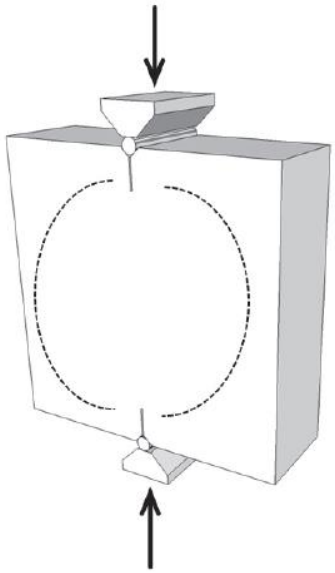

Figure 4.5: DEWS technique [Magri 2012].

Figure 4.6 explains the directions of the compressive vectors in the plate. Compression arch is starting from the loading point connected to another one started from the bottom point by straight vertical vector parallel to the smallest principal stress vector in the central region. This means that the mid span section is subjected to uniaxial tensile stresses and the strength should be very close to the tensile strength measured in uniaxial tensile test. The tests were carried out using electromechanical DMG machine with maximum capacity of 100 KN and precision class of 0.5. The details of the loading device are given in figure 4.7. Also, the cylinder used as load knife is shown in figure 4.8 and its technical specification according to DIN 6325 are stated in table 4.4

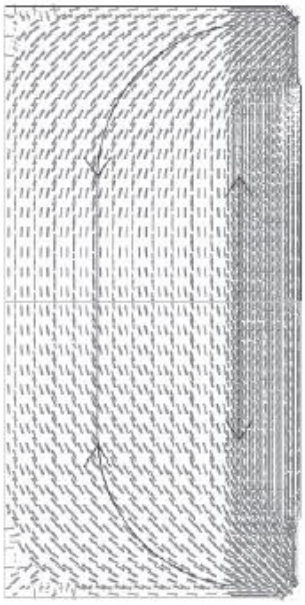

Figure 4.6: the direction of the compression stresses vectors inside the plate [Magri 2012].

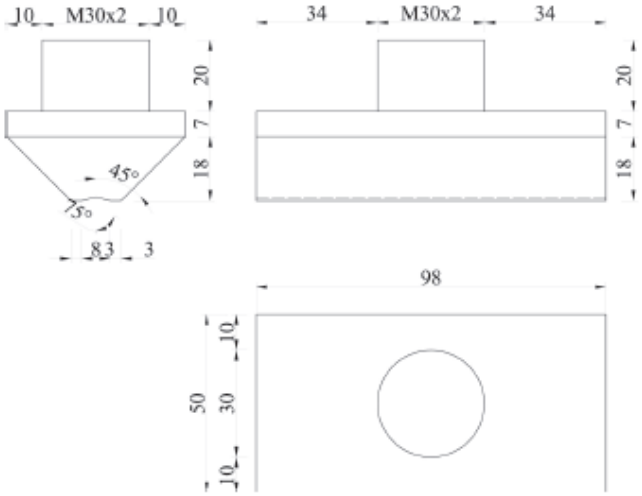

Figure 4.7: DEWS setup [Magri 2012].

Figure 4.8 Dowel pins DIN6325.

Material	100Cr6
hardness	Hrc 60 ± 2
Length	100 mm
diameter	10 mm

Table 4.4: Dowel pins specifications.

The two steel plates that had been attached to the internal face of the V- notches are mainly aiming to make better uniform distribution to the applied load through the cylinder. As a result of placing these two steel elements in attach under load application, the passive friction force is generated. This friction decreases the applied load effect on the specimens and introduces a tangential component on the sliding surface. Some experiments results obtained from tests conducted by di Prisco [di Prisco 2010]. These results were done to give a value for the coefficient of friction. In particular, many metal coupling and lubricants were confronted to estimate the friction reduction between cylinders and metal sliding area. A particular test device was made for simulating the acting loads on the sample by measuring the transmitted tensile force to the fracture area. Friction coefficient was given equal to 0.89 after using steel plates and graphite as lubricant (named Molykote U-n). The splitting force (figure 4.9) was computed according to the equation 4.1

$$F_{sp} = \mu.\frac{P}{2} \qquad 4.1.$$

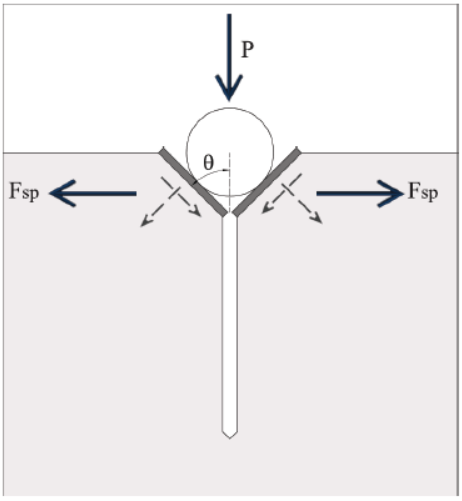

Figure 4.9: Splitting force direction with respect to the compressive force (θ=45°) [Magri 2012].

Three LVDT transducers (figure 4.10) were fixed on each side to the specimen to measure the potential crack opening. The three transducers were placed exactly at the tip of both notches and one in the middle of ligament. Another LVDT transducer was applied perpendicularly to the specimen plane as it is shown also in figure 4.11 in order to detect any detachment between the different material layers.

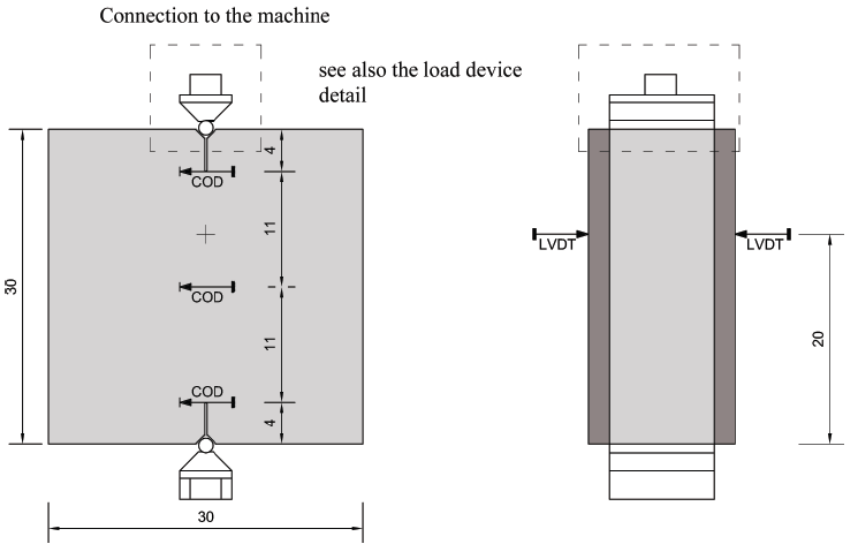

Figure 4.10: the position of the used transducers in DEWS tests [Magri 2012].

The characterization of the used transducers (full bridge HBMWA10) is reported in table 4.5. Furthermore, detailed information about the electronic measurement system that used in the whole tests was stated table 4.6.

	unit	WA10
Bridge type		full bridge
Nominal displacement	mm	10
Nominal sensitivity	mV/V	80
Characteristic tolerance	%	±0.2
Linearity deviation	%	±0.2

Table 4.5: transducer's characterizations

Figure 4.11 LVDT and SPIDER8

	unit	value
Accuracy class		0.1
Digital resolution	digit	±25000
Measured value buffer	Meas.	< 20000
Sampling rate per channel	1/s	19600
Transducer eccitation voltage	V_{rms}	2.5
Carrier frequency	Hz	4800

Table 4.6: Specifications of the electronic measurement system SPIDER8.

4.3.1.2. Test Preparation.

As it is known that during the retrofitting process, surface treatment is very triggering factor to enhance the bond between old and new materials. Principally, in order to increase the surface roughness to the specimens, the specimen's surfaces were treated by a disk of an angle grinder. Retrofitting material was applied to both sides of the substrate.

The V notches were closed using hot glue to avoid that the matrix fills the notches figure 4.1a. TRM was casted horizontally and spread on the specimen's surface after placing the AR glass fabric. In order to compact the matrix the roller was used over the matrix figure 4.12.

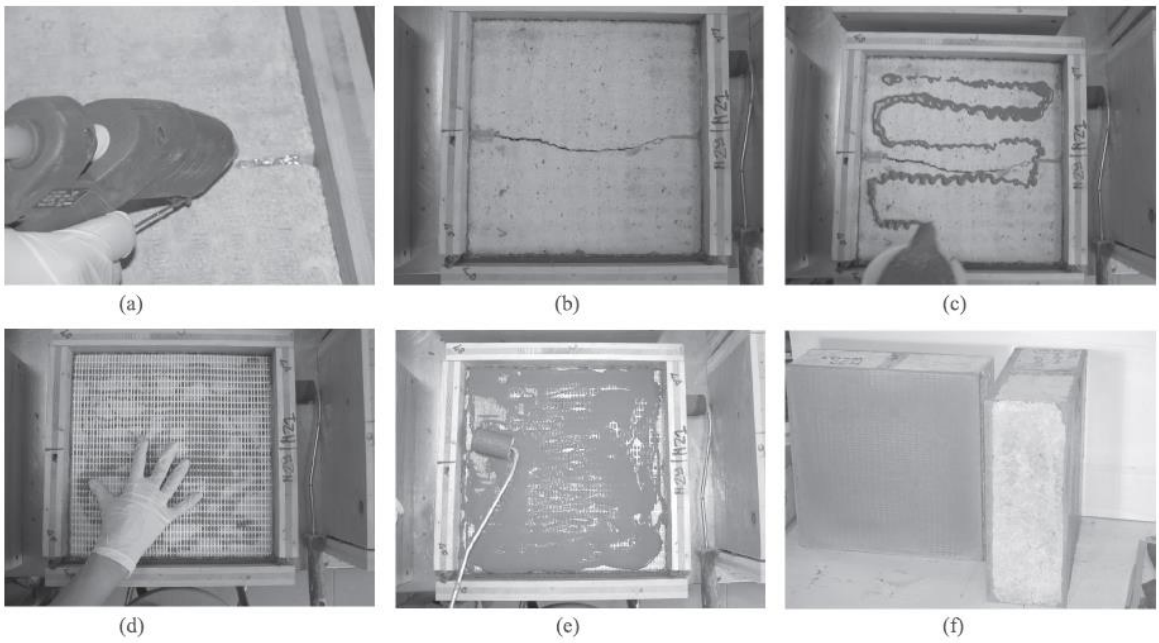

Figure 4.12: Casting process of TRM [Magri 2012].

Mix design and its mechanical properties had been already mentioned before in chapter 2. The specimens curing started directly after concrete reach its hardening. The curing takes place in a climate chamber at 98% RH for 28 days. Six specimens for each crack width were prepared to be used for compression and tension tests.

Table 4.7 shows the numbers of specimens for each crack width and each test. Also, three undamaged concrete plates and 2 for each damage level were used as a reference specimen.

Damage level (crack width)	Un-retrofitted specimens	Retrofitted specimens	tests
0 mm	3 2	3 3	DEWS Compression
0.3 mm	- 2	3 3	DEWS Compression
3 mm	- 2	3 3	DEWS Compression

Table 4.7: Number of tested specimens for DEWS and Compression tests [Magri 2012].

4.3.1.3. Mechanical characterizations for the used material

4.3.1.3.1. Concrete

The used concrete was limited to some standard characterizations that had been assigned according to standard tests. Table 4.2 exhibit the used mix design where the maximum aggregate size was 14 mm. For the mechanical properties, standard compressive test was carried out on cubic specimen [150.150.150 mm^3]. The results of ten tested samples are shown in table 4.3 [Magri 2012].

Component	Content [kg]
Cement 42.5	340
Water	170
Dracril 1100	3.4
Sand	1490
Sand sieved	379
Density [kg/m^3]	2382

Table 4.8: Concrete mix design [Magri 2012].

Specimen 150x150x150 mm^3	R_c [MPa]
1	37.51
2	33.06
3	32.76
4	31.14
5	32.98
6	32.57
7	32.53
8	33.06
9	35.09
10	37.78
R_{cm}	34
ST.D	2.21 %
R_{ck}	30.40 MPa

Table 4.9: The compressive resistance of concrete [Magri 2012].

4.3.1.3.2. Steel

In order to determine the tensile behavior for the steel bars inside the specimens, direct tensile test was done with 100 KN maximum load capacity and constant stroke rate of 0.05 mm/sec [Magri2012]. The vertical displacement was measured using transducers then the strain was computed by dividing the displacement over the gauge length. Figure 4.13 shows the obtained stress-displacement. The behavior followed three stages, first it moved linearly in the elastic stage until it reached the yield, after it went in the hardening behavior and finally the depressing phase started and continued until failure.

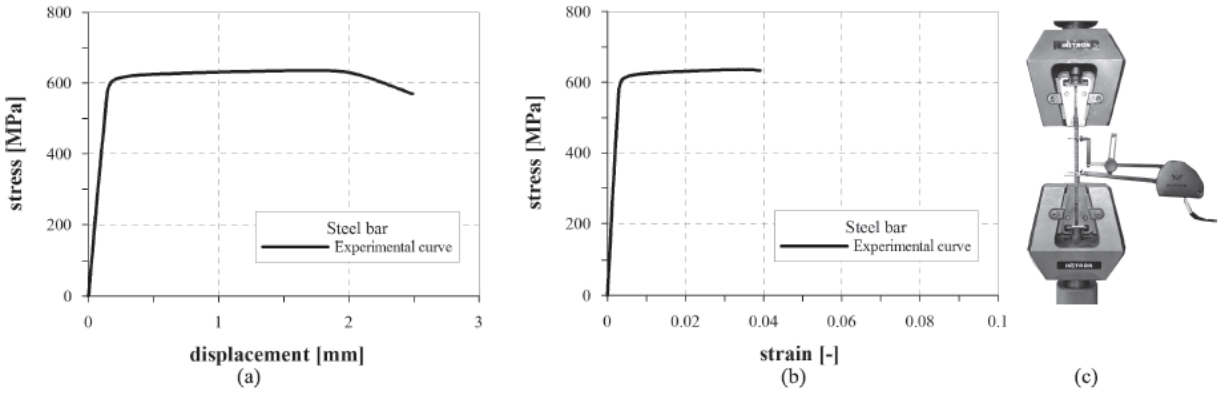

Figure 4.13: constitutive law (a) stress vs. displacement, (b) stress vs. strain. (c) The test setup [Magri2012].

4.3.1.3.3. DEWS tests results

The results for DEWS test on the retrofitted specimens are given by referring to the average behavior for each crack opening considered. The crack opening displacements were measured by the transducers placed in the middle of the section and the results were reported in terms of load vs. vertical displacement and splitting force vs. the crack opening width. Figure 4.14 shows that the linear branch of elastic behavior stopped when the cracking strength of concrete was reached where the splitting force is equal to 30 KN. After the first linear branch the steel bars starts to be loaded until they yield and fails. An average curve for the three curves was plotted in thicker font where it stopped at the first end of the three curves. Reference specimen was casted without strengthening layer and tested.

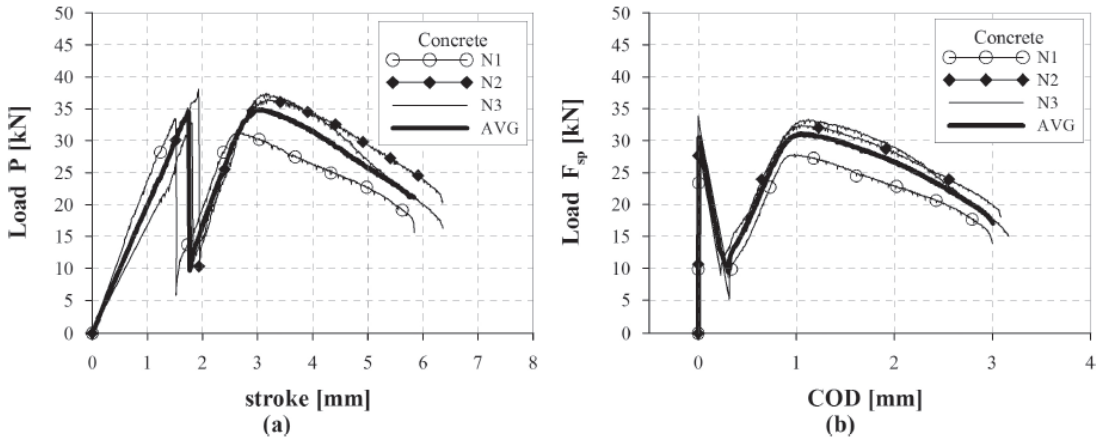

Figure 4.14: (a) vertical load Vs. vertical displacement (b) splitting force Vs. COD average [Magri 2012].

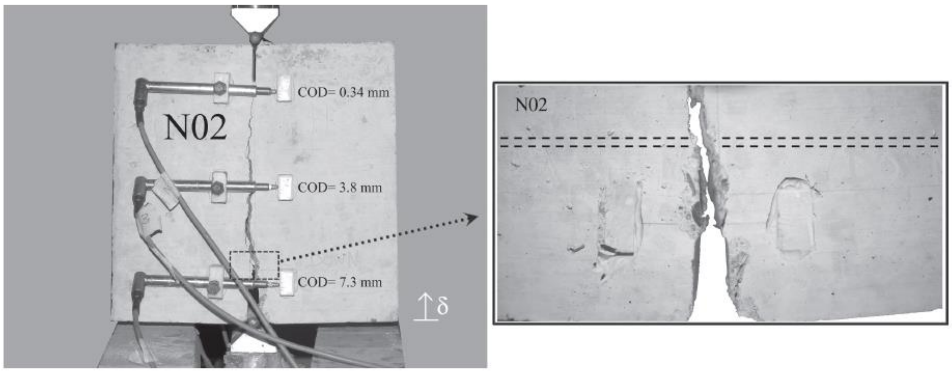

Figure 4.15 shows the crack opening pattern [Magri 2012].

Figure 4.16 shows the crack opening development with respect to vertical displacement in both specimens' sides. Unsymmetrical crack opening was observed and in most cases it start from the bottom side due to movement of press machine from that side. In figure 4.17 the development of the rotation was shown in both specimens' sides, rear and front, and they were calculated according to equation 4.2.

$$\text{Rotation} = \frac{(COD_{up} - COD_{down})}{l} \qquad 4.2$$

Where L is equal to the ligament length equal to 220 mm.

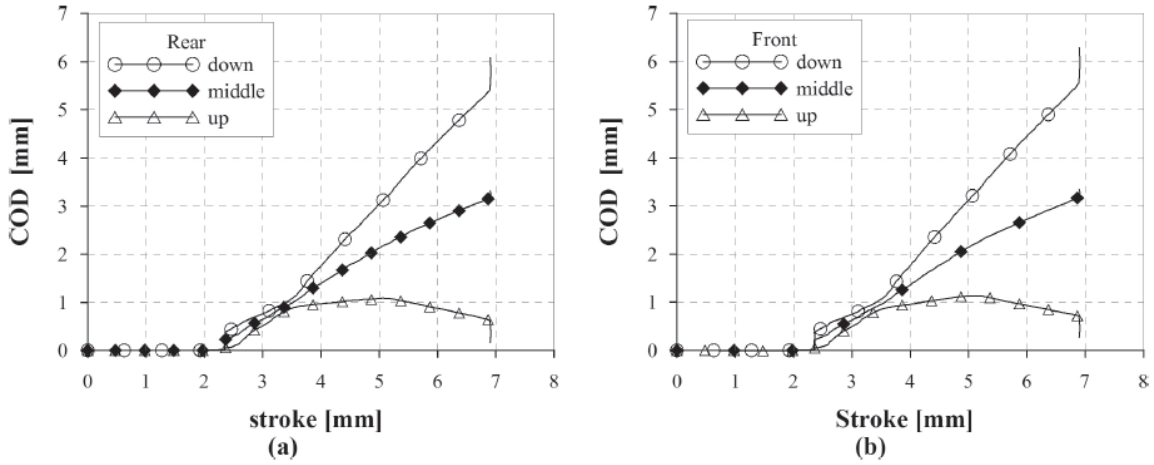

Figure 4.16: COD vs. vertical displacement (a) rear, (b) front [Magri 2012].

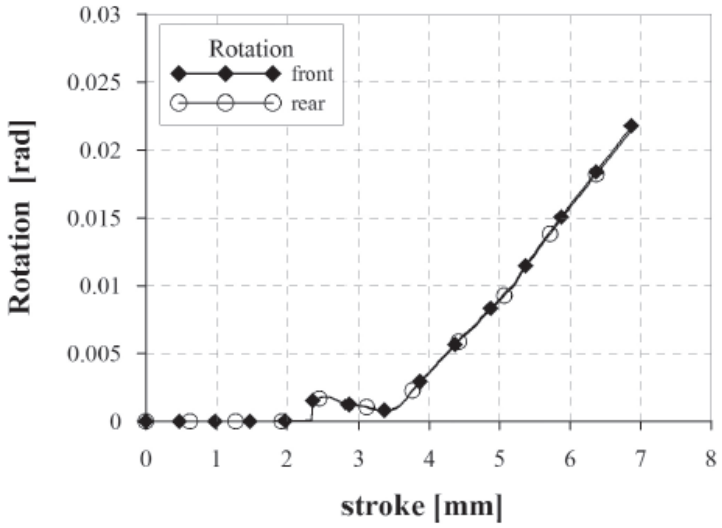

Figure 4.17: rotation vs. vertical displacement, front and rear sides [Magri 2012].

At stroke value equal to 2.3 mm, the rotation started to increase for a very small range before it decreased until stroke value equal to 3.4 mm after this value the rotation increases uniformly. Figure 4.18 describes the cracks evolution compared to rotation. The decrease of rotation is justified by the fact that the cracks opens symmetrically and then the crack propagation along the ligament tends to make uniform crack opening value. While the increase after stroke 3.4 mm is due to the unperfected symmetrical behavior of the bars that maybe caused by random defect in both steel and bond surface.

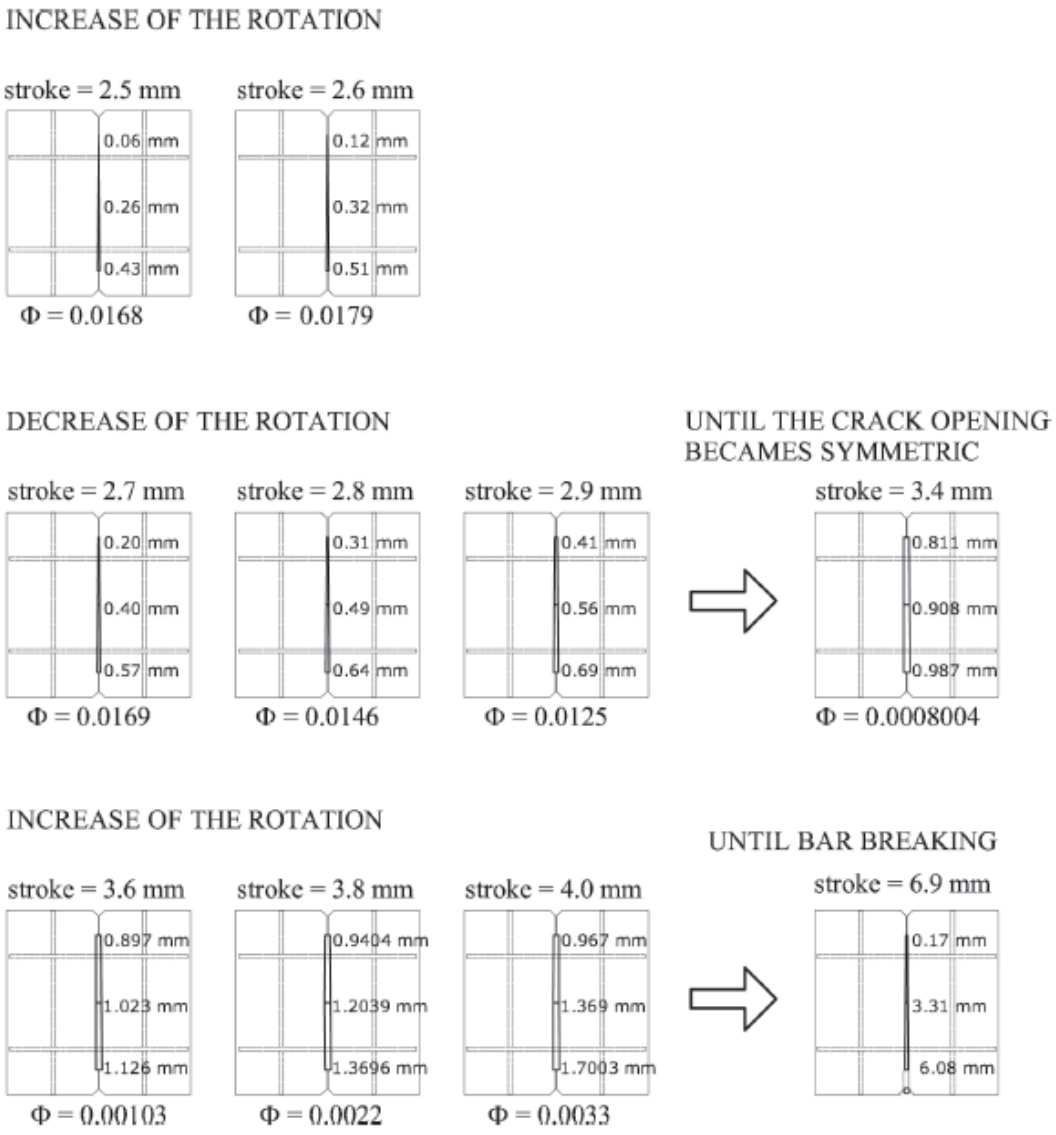

Figure 4.18: the cracks evolution comparing with rotation[Magri 2012].

4.3.1.4. Failure in the strengthening layers.

The applied load on the substrate concrete relies on the bond at the interface surfaces to transfer to the retrofitting material. TRM experienced a delamination in the central section for a length of 50 to 70 mm and sequentially multi-cracking starts. Moreover, the tangential stresses acting on the interface plane takes place in conjunction with the transferred tensile force in the middle plane of TRC layer (Figure 4.19). Due to the eccentricity between the two mentioned planes, local crushing occurs and therefore, some region of TRC matrix may detach from the original support.

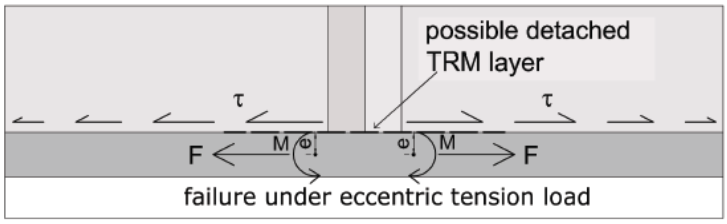

Figure 4.19: acting stresses and forces on the TRM strengthening layer [Magri 2012].

Figure 4.20a shows the results of undamaged concrete plates (w=0 mm) which were retrofitted with two layer of TRM. The results were given in terms of vertical loads vs. vertical displacement. The matrix crack strength was reached at P=65 KN and stroke displacement= 2.9 mm after the first linear branch. Figure 4.20b shows the development of the crack opening (COD) with the splitting force where the crack opening width was detected in the central position for both sides at the three position where the transducers were attached. TRM layer started multi-cracking in the central area over a length of 50 mm. All the COD measurements were stopped before the end of the test due to the TRC detachment where the instrument was glued.

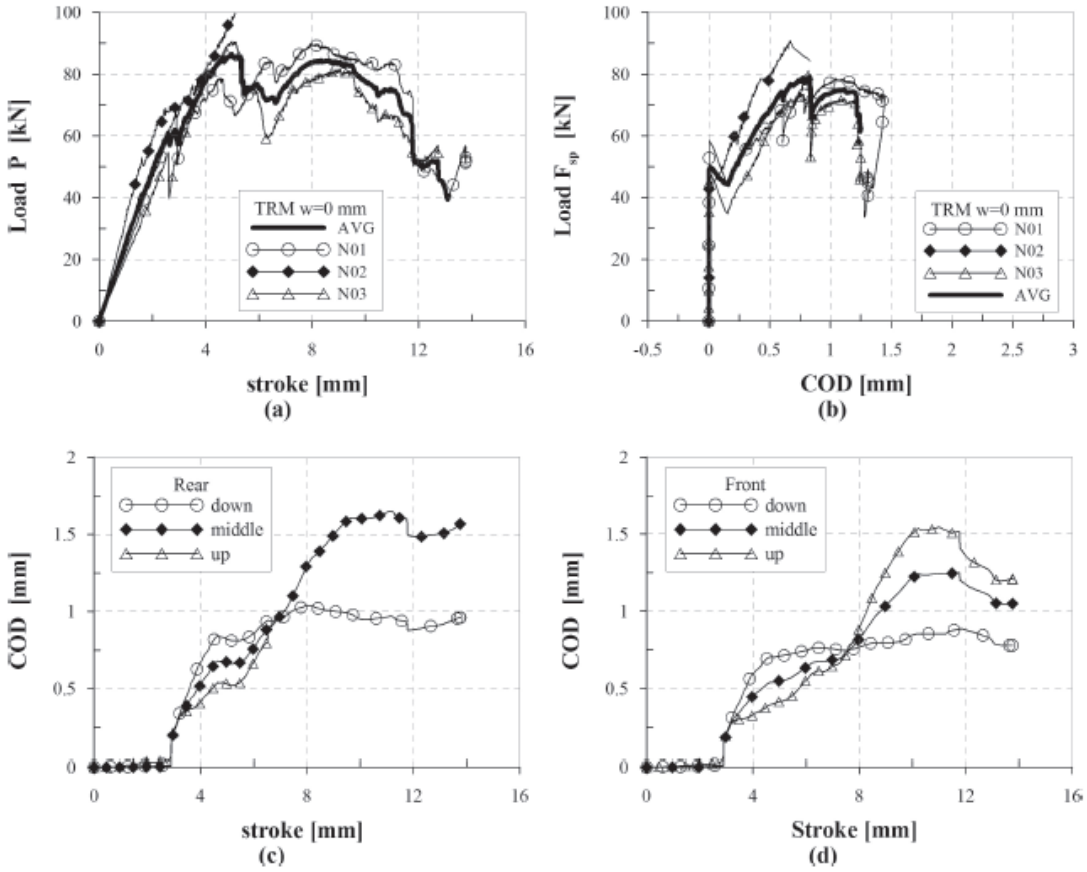

Figure 4.20: Un-cracked specimen N01, (a) Load vs. stroke, (b) Load vs. COD, (C) Displacement vs. COD for rear side, (d) Displacement vs. COD for front side [Magri 2012].

The behavior of the pre-cracked sample at 0.3 mm and 3 mm are shown in the figure 4.21 a,b. While, in figure 4.21c there is a comparison between all crack opening levels. For the un-cracked sample and pre-cracked samples with 0.3 mm, the same peak load was reached for both. Meanwhile, for pre-cracked level with w=3 mm TRC was able to restore and increase the initial strength of the reference conditions with maximum load equal to 40 KN [Magri 2012].

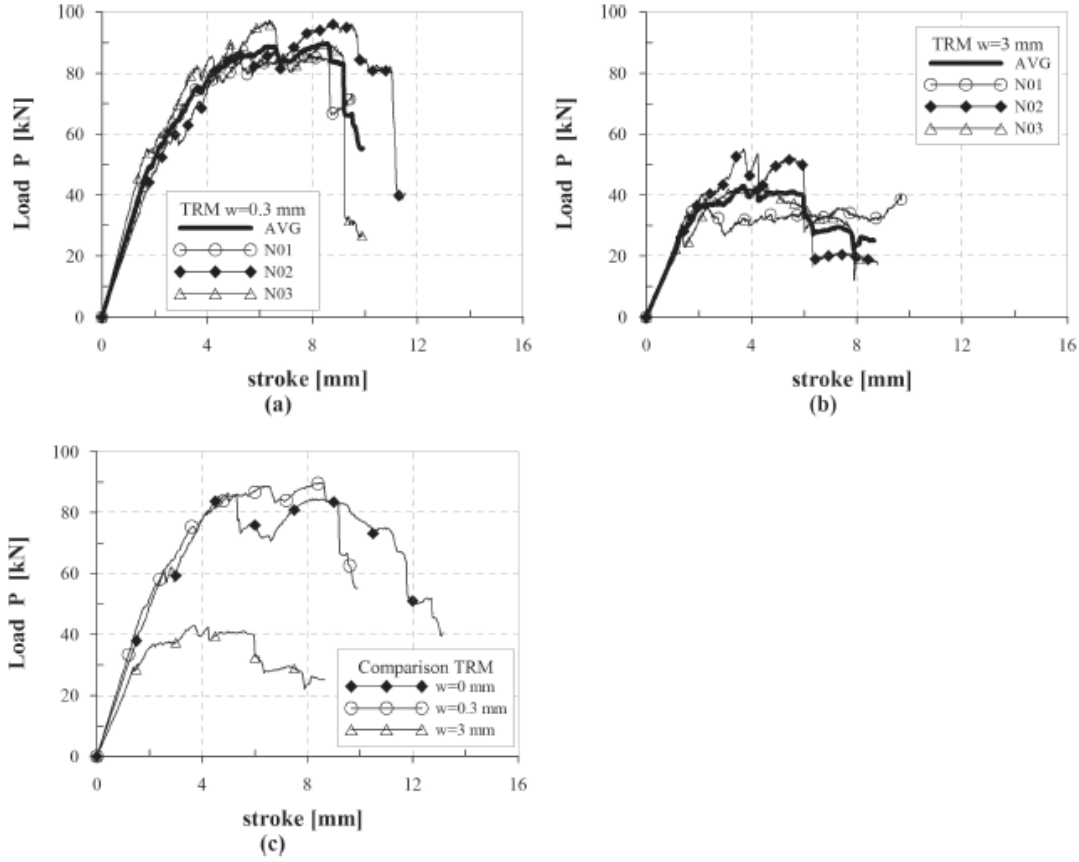

Figure 4.21: Load vs. vertical displacement, (a) pre-cracked with w=0.30 mm, (b) pre-cracked with w=3 mm, (c) comparison between the 3 cracks levels [Magri 2012].

4.3.2.Compression tests.

4.3.2.1. Test preparations and technique.

In order to carry out the compression test [Magri 2012], first, the specimens should be rotated by 90° as the crack will be perpendicular to the applied compressive load direction. The specimens' surface that supposed to be exposed to compressive load was coated with a layer of mortar before the test start to make the plane more smoothly so the possible localized failure where defects appears is mitigated (figure 4.22).

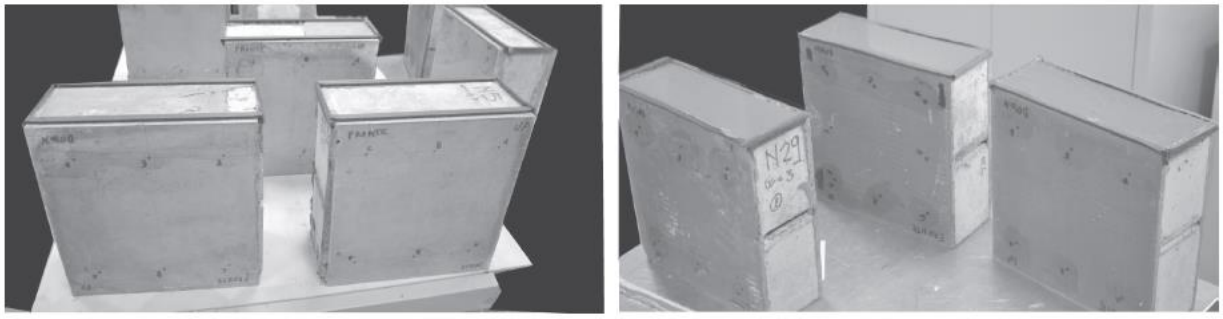

Figure 4.22: Coating process [Magri 2012].

Two 10 mm thick steel plates were placed on the upper and lower sides to the specimens as it is shown in figure 4.23. The transferred load to the retrofitting material was guaranteed by bond on the interface surface.

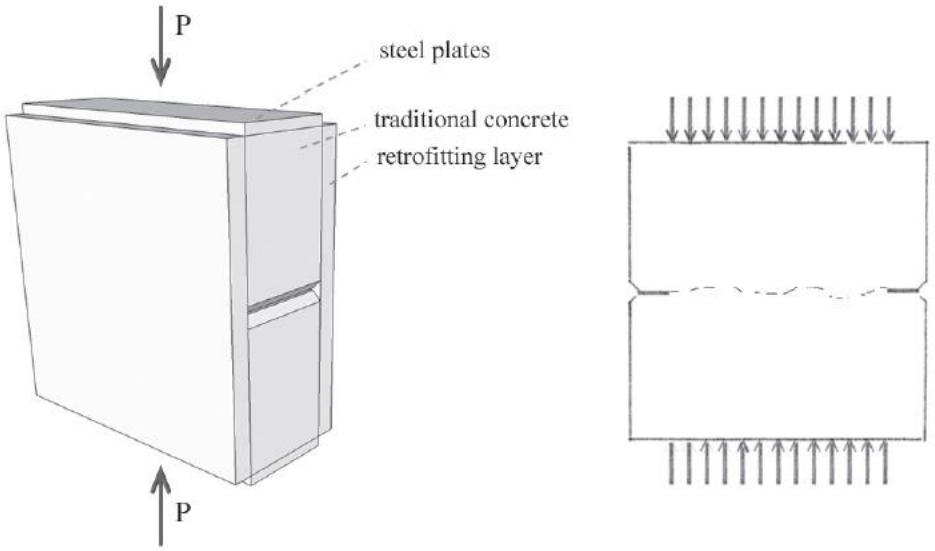

Figure 4.23: Compression test preparations [Magri 2012].

The test was carried out by a hydraulic press Controls Advantest with maximum load of 3000 KN by imposing constant stroke rate 0.05 mm/sec on specimens with and without strengthening layers for all damage levels. Three LVDT transducers were fixed on both sides perpendicular to specimen plane to measure the detachment of the strengthening layer. In addition, another two transducers were placed in the lower plane to measure the stroke vertical displacement. (Figure 4.24).

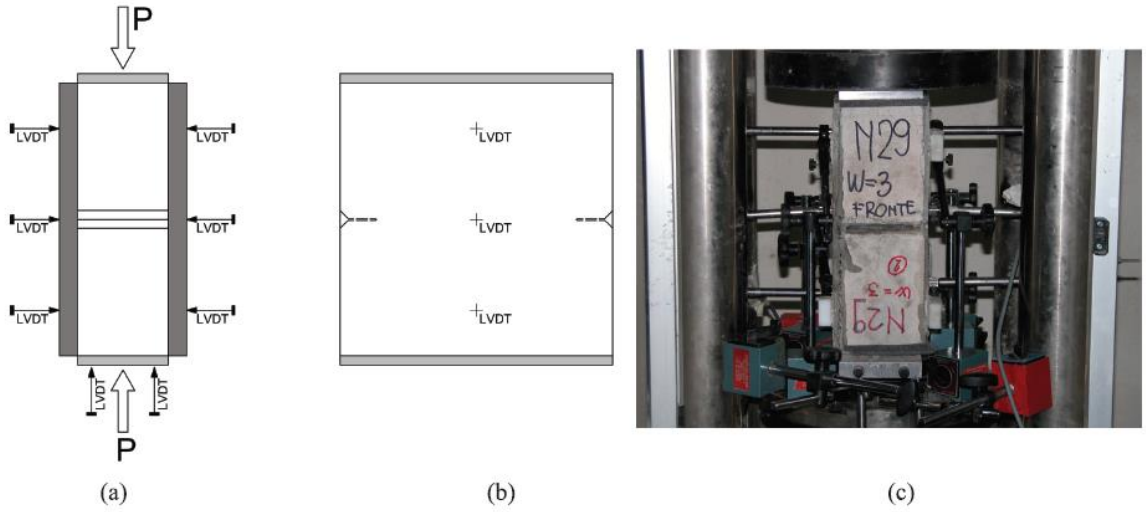

Figure 4.24: compressive test set up [Magri 2012].

4.3.2.2. Results of the compression test.

The compressive strength of plain concrete was determined according to test carried out for ten cubic specimens [150 mm edge length] and the obtained average compressive strength was 34 Mpa. Thus, the maximum compressive load could be estimated using equation 4.4.

$$P_{max}^{exp} = 34.A_{net} \qquad 4.4$$

Where A_{net} refers to the area where the load is applied. In this case it is the area between the notches which can be computed as follow.

$A_{net} = 220.100 = 22000\, mm^2$

Therefore, $P_{max}^{exp} = 748\, KN$.

Un-cracked sample (W=0).

Figure 4.25 shows elastic behavior just after the brittle collapse where the specimens reached the peak compressive load. The obtained average of the peak load of two completed tests is equal to 901 KN. This value of compressive load is higher than the pre-calculated theoretical value (748 KN). The author explains the reason behind this which might be due to the confinement effect favored by friction on the longest bases. This was due to the absence of stearic acid between steel plates and specimen during the test. The load was increased by 17% due to the confinement effect offered by the friction.

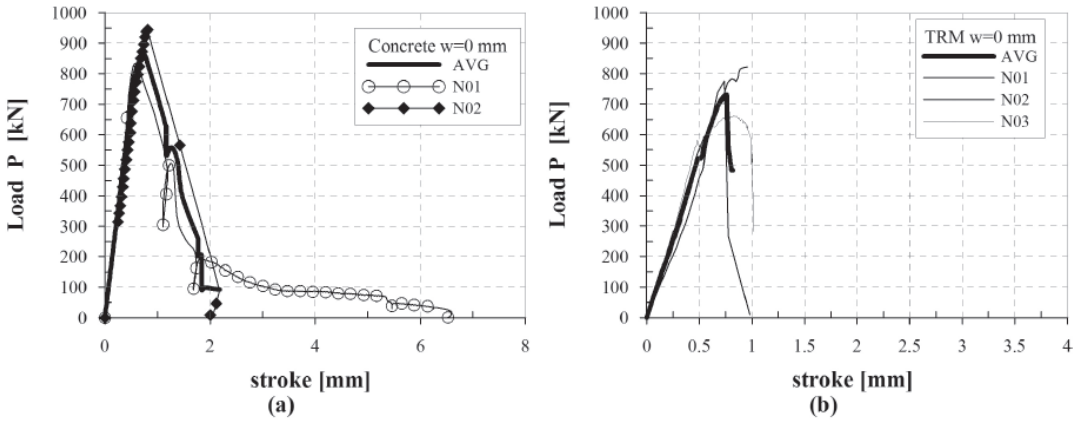

Figure 4.25: the results obtained from compressive test for un-cracked sample for both (a) concrete reference samples, (b) TRM strengthened sample [Magri 2012]..

The reason of this reduction of peak load between the value obtained from the test and the one obtained from the reference concrete plate has to be found in the complex stress transfer that is different for two section planes as it is explained in figure 4.26.

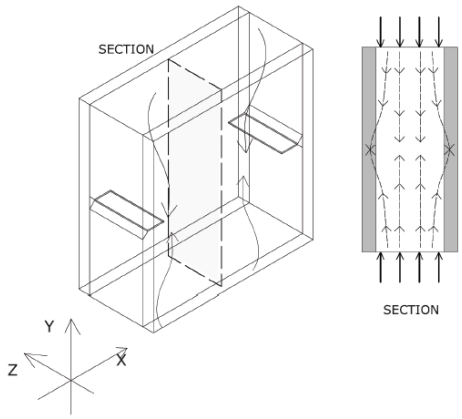

Figure 4.26: stress transfer in the TRM strengthen sample [Magri 2012].

The stress transfer was quite complex through the retrofitting layer due to the geometry of the specimen and the equilibrium mechanism (figure 4.27).

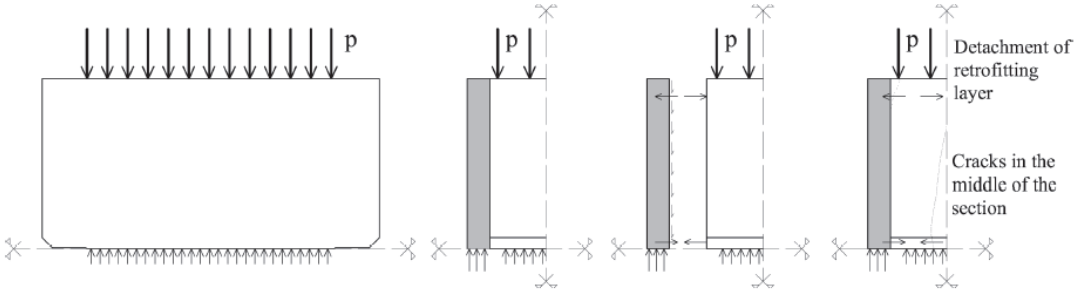

Figure 4.27: Failure mechanism [Magri 2012].

Meanwhile, TRC compressive strength layers only can be determined using according to equation 4.5.

$$F_{TRM} = F_c - \ area = 100.12.300 = 360KN \qquad 4.5$$

After the test completed, detachment of the upper layer of TRC and crack propagation in the central section were observed. This is due to the eccentricity of the vertical load with the strengthening layer. In XY plane the stresses are confined in the section ligament and they transferred to TRC layer in the section where the notches are absent. While in the transverse plane there are two sections considered the first section exist exactly at the notch level where the transmission of stress from concrete plate to strengthening layers was negligible. And the second section exists in the central section of the specimen where the stresses were transmitted partly to the reinforcement and concrete plates.

4.3.2.3. Pre-cracked sample (W=0.30 mm).

Two behaviors were observed in this case the first one is elastic until the peak load which is around 844 KN. The second behavior characterizes the failure which starts after the peak load goes lower than 592 KN then softening branch starts (figure 4.28). Two specimens were tested N01 and N02. Evidently the collapse mechanism was affected with the pre-crack initial phase. Table 4.7 explains that the pre-crack in N01 was quite symmetric in both front and rear sides. While in N02 the cracks show different behavior.

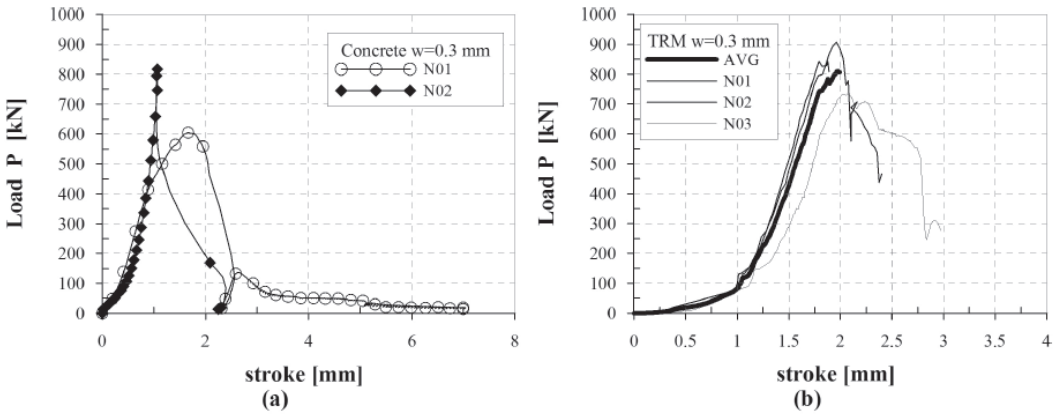

Figure 4.28: the results obtained from compressive test for pre-cracked sample (W=0.30) for both (a) concrete reference samples, (b) TRM strengthened sample [Magri 2012].

specimen	rear side [mm]	front side [mm]
N01	0.29	0.21
N02	0.4	0.031

Table 4.10: pre-cracks values (W=0.30) [Magri 2012].

4.3.2.4. Pre-cracked sample (W=3 mm).

As such previous test level crack, in this case two specimens were tested as well. Table 4.8 exhibits different pre-cracks values for both sides with 32.8% decrease in the results comparing with the retrofitting specimens. The pre-crack in this case was so high that the complete reclosure of the cracks was impossible considering the interlocked effect that can be occurred.

specimen	rear side [mm]	front side [mm]
N01	3.01	2.8
N02	3.01	1.57

Table 4.11: pre-cracks values (W=3) [Magri 2012].

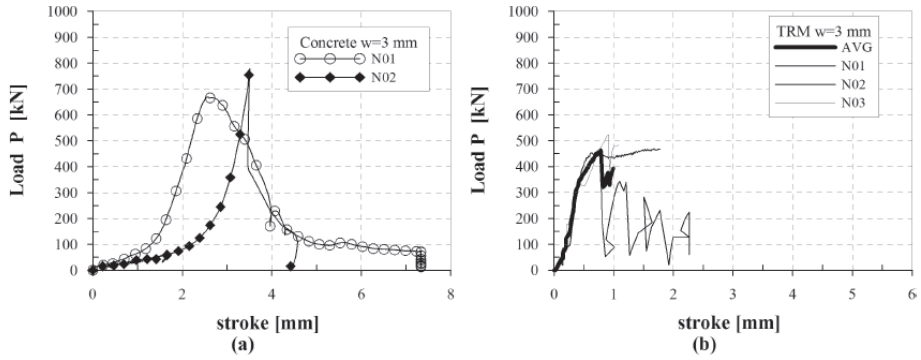

Figure 4.29: the results obtained from compressive test for pre-cracked sample (W=3mm) for both (a) concrete reference samples, (b) TRM strengthened sample [Magri 2012]

Stress transfer mechanism is shown in figure 4.29 where the compressive stresses could be transmitted only in the retrofitting layers.

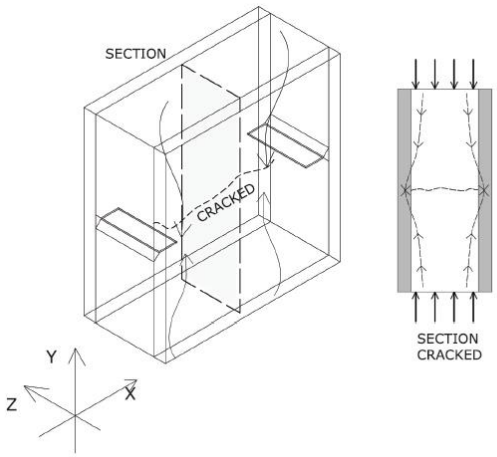

Figure 4.29: stresses transfer mechanism [Magri 2012].

Chapter 5

Finite element approach

5.1. Introduction.

Finite element approach was introduced to simulate 3D numerical model for a retrofitted reinforced concrete specimen with a layer of textile reinforced concrete. In particular two models were presented in this chapter, the first one was modeled with plain matrix of TRC and the second model used TRC matrix with added Polypropylene fibres (P.P). The models had been developed using Abaqus/ standard 6.13. The prediction capabilities used in the models are represented in this chapter in details.

5.2. Constitutive law.

5.2.1. Reinforced Concrete.

In order to estimate the elastic phase, two main parameters were defined. These two parameters are Young's modulus and Poisson ratio.

- Young modulus was obtained according to table 5.1.7 in Model code 2010 [MC2010]. As the concrete class is C25 therefore, the corresponding Young modulus equal to 32.0 GPa.

- Poisson ration was also obtained from Modal code 2010 referring to section 5.1.7.3 where υ_c=0.20 meets the required accuracy.

In order to define the plasticity behavior, the concrete damaged plasticity approach was introduced to the model. The concrete damaged plasticity model in Abaqus/ Standards consists of the combination of non associated multi-hardening plasticity and isotropic damaged elasticity to describe the irreversible damage that occurs during the fracturing process [Simulia 2011]. It uses concepts of isotropic damaged elasticity in combination with isotropic tensile and compressive plasticity to represent the inelastic behavior of concrete In addition; it gives the possibility of using rebars to model concrete reinforcement. The following parameters had been defined and introduced to the model:

- Dilation Angle: it refers to the dilation angle measured in the *p*–*q* plane at high confining pressure.
- Eccentricity: The flow potential eccentricity, ϵ, The eccentricity is a small positive number that defines the rate at which the hyperbolic flow potential approaches its asymptote. The default is$\epsilon = 0.10$.
- fb0/fc0: It is the ratio of initial equibiaxial compressive yield stress to initial uniaxial compressive yield stress σ_{bo}/σ_{co}. The default value is equal to1.16.
- *K*: It is the ratio of the second stress invariant on the tensile meridian, *q*(TM), to that on the compressive meridian, *q*(CM), at initial yield for any given value of the pressure invariant P such that the maximum principal stress is negative, $\sigma_{max} < 0$. It must satisfy the condition 0.5<K_c ≤1.0. The default value is 2/3.
- Viscosity Parameter, μ,: used for the visco-plastic regularization of the concrete constitutive equations in Abaqus/Standard analyses. This parameter is ignored in Abaqus/Explicit. The default value is equal to Zero.

The used values of the pre-mentioned parameters are given in table 5.

Dilation angel	Eccentricity	fb0/fc0	K	Viscosity Parameter
38	0.10	1.16	0.66667	0

Table5.1: the values of the parameters introduced to Abaqus.

The hardening variables ε_t^{Pl} and ε_c^{Pl} refer to the tensile and the compressive equivalent plastic strain respectively are addressing the failure mechanisms under tension and compression loading. The concrete damaged plasticity model assumes that the tension and compression behavior are uniaxial. During uniaxial tension the stress-strain response follows a linear elastic relationship until the value of the failure stress, σ_{t0}, is reached. The failure stress corresponds to the initiaion of micro-cracking in the concrete material. Beyond the failure stress the formation of micro-cracks is represented macroscopically with a softening stress-strain response, which induces strain localization in the concrete structure. While, Under uniaxial compression the response is linear until the value of initial yield, σ_{c0}. In the plastic behavior the response is typically characterized by stress hardening followed by strain softening beyond the ultimate stress, σ_{cu}. Abaqus converts automatically the stress-strain curve into stress-plastic strain one with reference to the provided stress-inelastic strain data.

According to figure 5.1, during the unloading branch started from any point on the strain softening branch, the degradation of the elastic stiffens of the material takes place. This degradation is characterized by two damage variables,d_t and d_c, which depnds on some variables such as the equivalent plastic tension and compression strains, θ refers to the temperature and f_i refers to the field variable . Then, the stress-strain relationship could be addressed using the equations number. 5.1 and 5.2 [Simulia 2011].

$$\sigma_t = (1 - d_t)\, E_0(\varepsilon_t - \tilde{\varepsilon_t^{Pl}}) \qquad 5.1$$

$$\sigma_c = (1 - d_c)\, E_0(\varepsilon_c - \tilde{\varepsilon_c^{Pl}}) \qquad 5.2$$

In the model the effective tensile and compressive cohesion stresses which are used to determine the size of the yield surface, can be obtained with the following equations.

$$\bar{\sigma}_t = \sigma_t/(1-d_t) = E_0(\varepsilon_t - \tilde{\varepsilon_t^{Pl}}) \quad 5.3$$

$$\bar{\sigma}_c = \sigma_c/(1-d_c) = E_0(\varepsilon_c - \tilde{\varepsilon_c^{Pl}}) \quad 5.4$$

Where, ε_t^{Pl}andε_c^{Pl} are the equivalent plastic tension and compression strains, $\tilde{\varepsilon_t^{Pl}}$and $\tilde{\varepsilon_c^{Pl}}$ are the equivalent plastic strain rates, E_0 refers to the elastic modulus of the material.

The stress-strain relations for the general three-dimensional multiaxial condition are given by the scalar damage elasticity equation.

$$\sigma = (1-d)D_0^{el}:(\varepsilon - \varepsilon^{pl}) \quad 5.5$$

Where D_0^{el} is the initial (undamaged) elasticity matrix. And the effective stress in this case is defined as:

$$\bar{\sigma} = D_0^{el}:(\varepsilon_t - \tilde{\varepsilon_t^{Pl}}) \quad 5.6$$

To define plastic flow potential function and the yield surface, two stress invariants of the effective stress tensor ($\bar{\sigma}$) are used. These invariants are; the hydrostatic pressure stress and the Mises equivalent effective stress and they can be obtained respectively by the following equations:

$$\bar{p} = -\frac{1}{3} trace(\bar{\sigma}) \qquad 5.7$$

$$\bar{q} = \sqrt{\frac{3}{2}(\bar{S}:\bar{S})} \qquad 5.8$$

Where, $\bar{S} = \bar{\sigma} - \bar{p}I$ 5.9

Drucker-Prager hyperbolic function (equation 5.10) is used to express the non-associated potential plastic flow in the concrete damaged plasticity model.

$$G = \sqrt{(\epsilon\sigma_{t0} + tan\psi)^2 + \bar{q}^2} - \bar{p}.tan\psi \qquad 5.10$$

Knowing that,

ψ refers to the dilation angle, σ_{t0} is the uniaxial tensile stress at failure and ϵ is a parameter refers to the eccentricity.

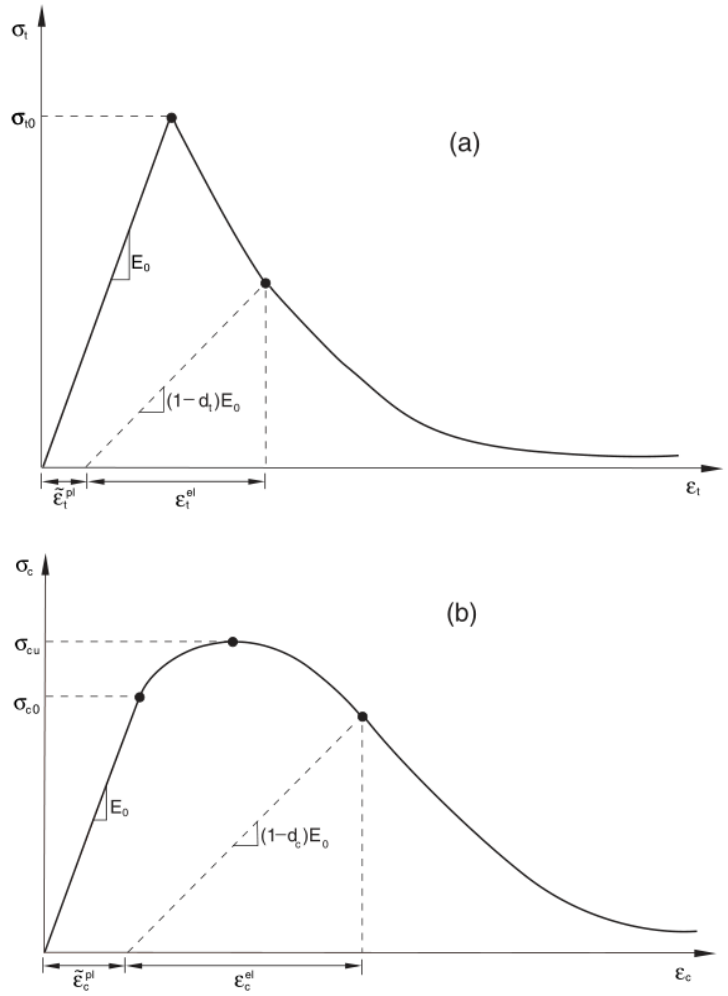

Figure 5.1: The concrete response under the uniaxial loading in (a) tension, (b) compression [Simulia 2011].

The compressive behavior was assumed to be elastic-perfectly-plastic, with a yield stress equal to 33Mpa. This value is the corresponding to the characteristic strength value (f_{ck}) obtained by the model code [MC2010] with reference to the used grade of concrete (C25). By adding the value of Δf which equals 8 Mpa, then the compressive strength is expressed in the form of the mean value where,

$$f_{cm} = f_{ck} + \Delta f. \qquad 5.11$$

The plastic tensile behavior was estimated from the characteristic compressive strength(f_{ck}). Applying the proposed equation by model code [MC2010] (equation 5.12), the obtained yield stress equal to 2.56 Mpa

$$f_{ctm} = 0.30.(f_{ck})^{\frac{2}{3}} \qquad \text{For concrete grade} \leq \text{C50} \qquad 5.12$$

In case of the absence of reinforcement in significant regions of the model, the fracture energy cracking criterion had been proposed by Hillerborg's (1976) is used to avoid the influence of unreasonable mesh sensitivity in the results. The fracture energy (G_f) represents the energy required to propagate a tensile crack of unit area [MC2010]. G_f was introduced to the model as a material parameter and it was obtained by equation 5.13.

$$G_f = 73.f_{cm}^{0.18} \qquad 5.13$$

With this approach the concrete's brittle behavior is characterized by the stress-displacement response instead of stress-strain response. In this case according to Abaqus user's manual [Simulia 2011], the post-peak behavior is assumed to be linear if G_f specified directly as material parameter (figure 5.2).

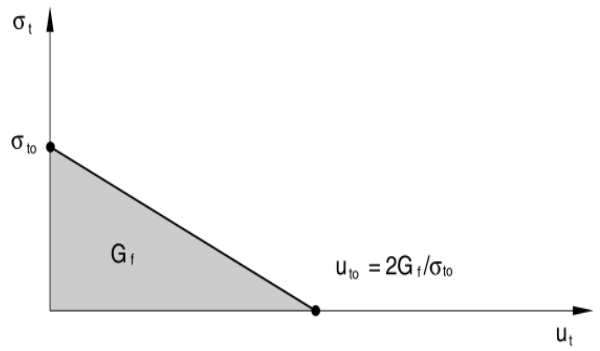

Figure 5.2: Fracture energy as assumed in concrete damaged plasticity model. [Simulia 2011].

Meanwhile, the crosponding approach proposed by the model code concerns only on the area under the first branch of the concrete tensile stress σ_{ct}- crack opening width w curve (figure 5.3) [MC2010].

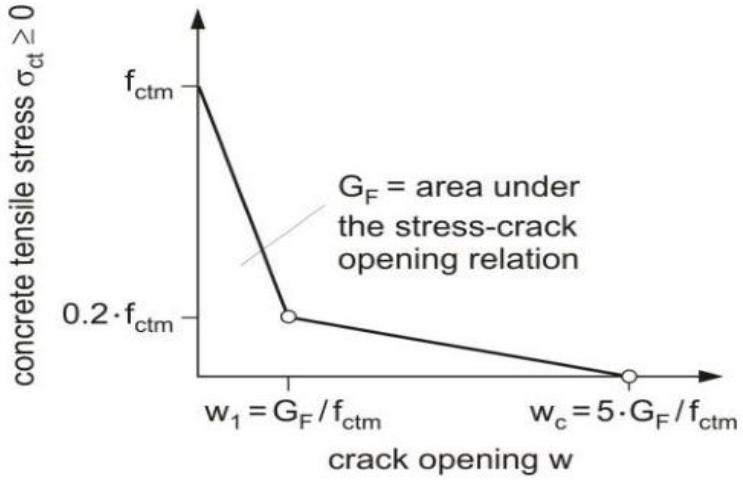

Figure 5.3: the proposed approach by the model code to estimate the fracture energy [MC2010].

5.2.2.Reinforcement steel bars.

The reinforcement steel rebars were modeled as on dimensional rods embedded into the concrete. The steel constituting rebars are assumed to follow the elastic-perfect-plastic behavior with Young modulus equal to 200000 MPa and Poisson ratio equal to 0.30 (figure 5.4). The yield stress equal to 620 MPa.

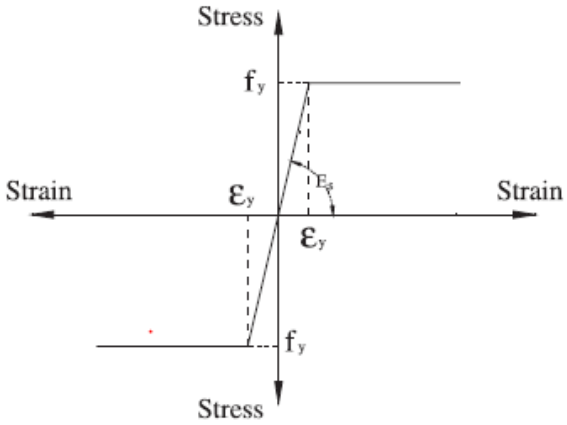

Figure 5.4: Idealized stress-strain relationship.

5.2.3.Steel plate.

Steel plates were placed in the area where the load is applied in order to avoid stress concentration. The steel plates have the same characteristics of reinforcement steel bars. (Young's modulus equal to 200000 Mpa and Poisson ration equal to 0.30).

5.2.4.Textile reinforced concrete (TRC).

The elastic behavior of TRC was characterized by Young's modulus equal to 33980 Mpa and Poisson ratio equal to 0.20.While the plastic behavior was introduced to the software through concrete damage plasticity features. Where, the default plasticity parameters (defined before in section 5.2.1) were given as follow.

Dilation angel	Eccentricity	fb0/fc0	K	Viscosity Parameter
30	0.10	1.16	0.66667	0

Table5.2: the values of the parameters introduced to Abaqus.

The compressive behavior was assumed to be elastic- perfectly plastic with yield stress equal to 83 MPa and the plastic tensile behavior was defined with two different constitutive curves according to two experimental investigation results for two different matrices of TRC; the first matrix was casted without any addition of polypropylene while the Polypropylene was added to the second mix design (4.75 Kg/m^3) the mix design is explained in section 4.2.1 of this thesis. Figure 5.5 shows the two constitutive curves used in defining TRC plastic tensile behavior. These two curves were introduced to Abaqus in terms of yield stress and inelastic strain where the introduced values for TRC matrices material without and with polypropylene fibres addition were stated in table 5.3 and 5.4 respectively.

Yield stress	Cracking strain
7	0
10	0.0086
25.56	0.020174

Table 5.3: post-peak tensile behavior for TRC for plain matrix without Polypropylene

Yield stress	Cracking strain
5.161653	0
7.491482	0.003566
22.01444	0.015964

Table 5.4: post-peak tensile behavior for TRC with Polypropylene (4.75 Kg/m^3)

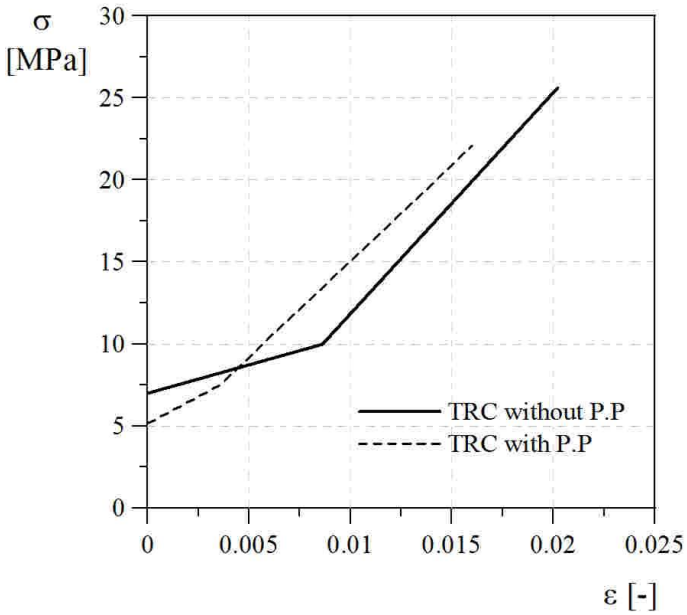

Figure 5.5: Comparison between the constitutive curves of the two used TRC matrices

5.3. Model description.

The main objective of carrying out the numerical simulation is to study the effect of adding TRC as strengthening layer to the specimen that had been tested according to the DEWS test [di Prisco 2010] which was explained in details in chapter 3 of this thesis.

Since the specimen dimensions (300.300.100 mm) were symmetric vertically and horizontally, so one quarter of the specimen only was modeled in order to minimize the computational effort of the model (figure 5.6).

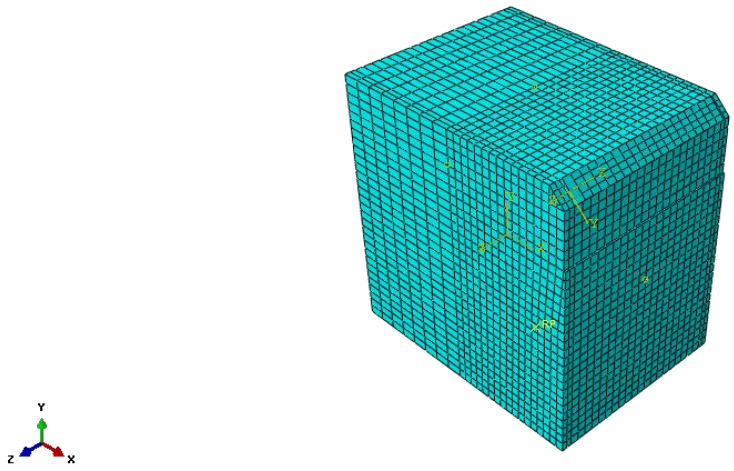

Figure 5.6: the 3d model for DEWS test.

The model was divided into four instances; concrete, TRC, steel reinforcement and steel plate. Each part represents specified material properties. (Figure 5.7) Concrete, TRC and steel plate were assigned as solid homogenous sections while the steel reinforcement was assigned as an embedded truss element these different parts were assembled together in one assembly.

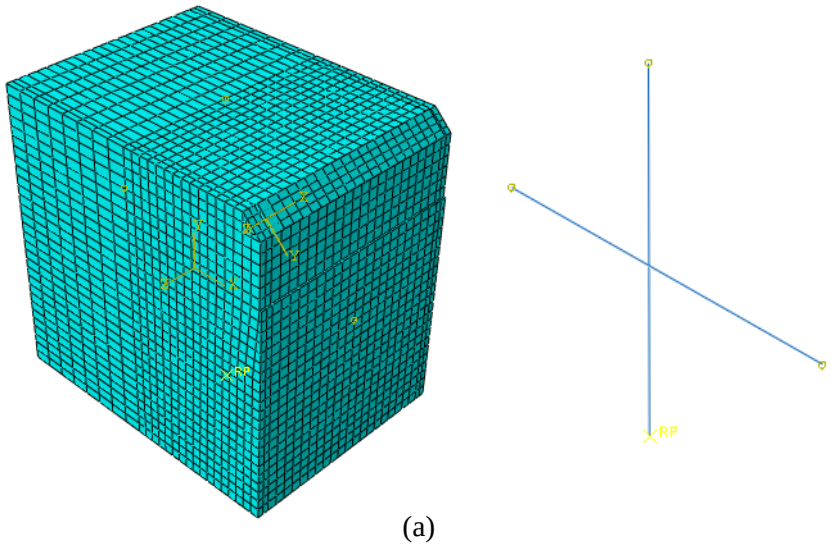

(a) (b)

Figure 5.7 : the model instances (a) Reinforced concrete, (b) Reinforcement bars

The load was applied linearly as displacement controlled exactly on the steel plate in a locally vertical direction (figure 5.8). And the displacements were prevented in horizontal and vertical surfaces where they should have been attached to the absent symmetric part. The model was meshed according to the tetrahedral meshing (figure 5.9).

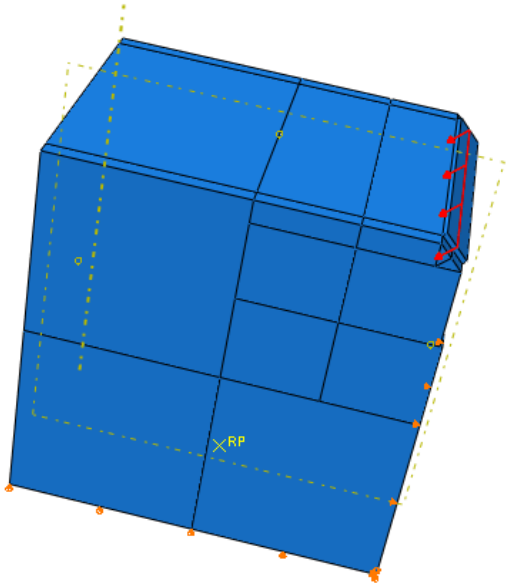

Figure 5.8: the applied load and the boundary conditions.

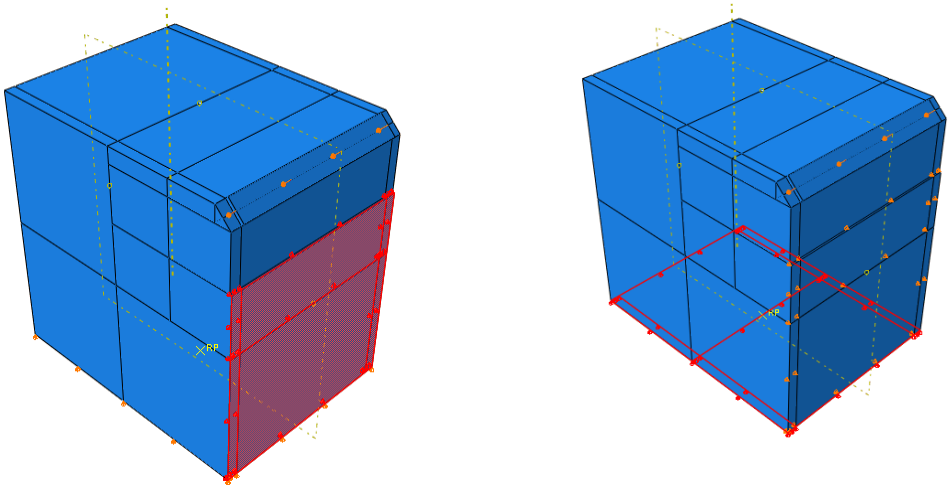

Figure 5.9: the boundary conditions (a) horizontally (b) vertically.

5.4. The results.

The results were presented in terms of horizontal force F_{sp} vs. Crack Opening Displacement COD. By referring to the experimental test carried out by A. Magri [magri 2012] many comparisons could be held between experimental and numerical results, as it will be further detailed. Figure 5.10 shows both results for the experimental test and the numerical model for the un-retrofitted specimen. The experimental test results are given for three specimens and the average is highlighted with a thick line. While because of the mean value of tensile strength and fracture energy, which were explained in section 5.2.1 according to model code [MC 2010], are not in good agreement with the experimental results other parameter - tensile strength and fracture energy- hence introduced in the tensile of the concrete. Also, another model was developed with a hexahedral element meshes in seek of find the most agreeable curve to the experimental one. Table 5.5 explains the number of modeled specimens.

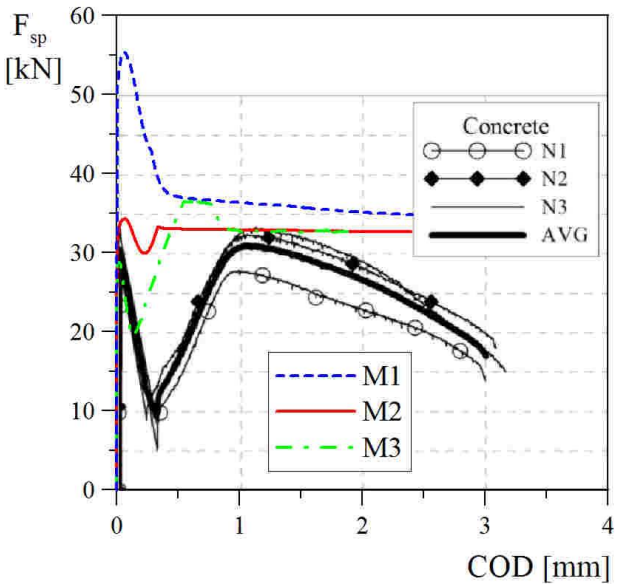

Figure 5.10: comparison between the results of numerical and experimental analysis in terms of horizontal force F_{sp} vs. crack opening displacement COD relationship.

Model	Tensile strength (Fctm) MPa	Fracture energy (Gf)	Element meshes
M1	2.56	0.086	Tetrahedral
M2	1.5	0.05	Tetrahedral
M3	1.5	0.05	Hexahedral

Table 5.5: the different types of modeled specimens.

Apparently, the first model M1 doesn't correspond to the experimental one with a very high load for the first crack. While, the curves obtained from model M2 and M3 don't correspond to experimental one completely, but the first crack load and the plateau are equal to those obtained from the experimental test. Predominantly the reason of the difference of the plateau goes to the hypothesis of the perfect bond between the reinforcement bars and concrete where the relative sliding can not occur.

5.4.1.Retrofitted specimen's model.

The model of the retrofitted specimen was developed from the model M3 that gives much closer results in the un-retrofitted model. So M3_R1 refers to the retrofitted model with 1.50 tensile strength and 0.05 fracture energy.

5.4.1.1. Using plain TRC .

The results of the retrofitted model are given in figure 5.11 in terms of contours distribution for the stress, displacement and plastic strain. The horizontal force F_{sp} vs. crack opening displacement COD relationship is plotted in figure 5.12.

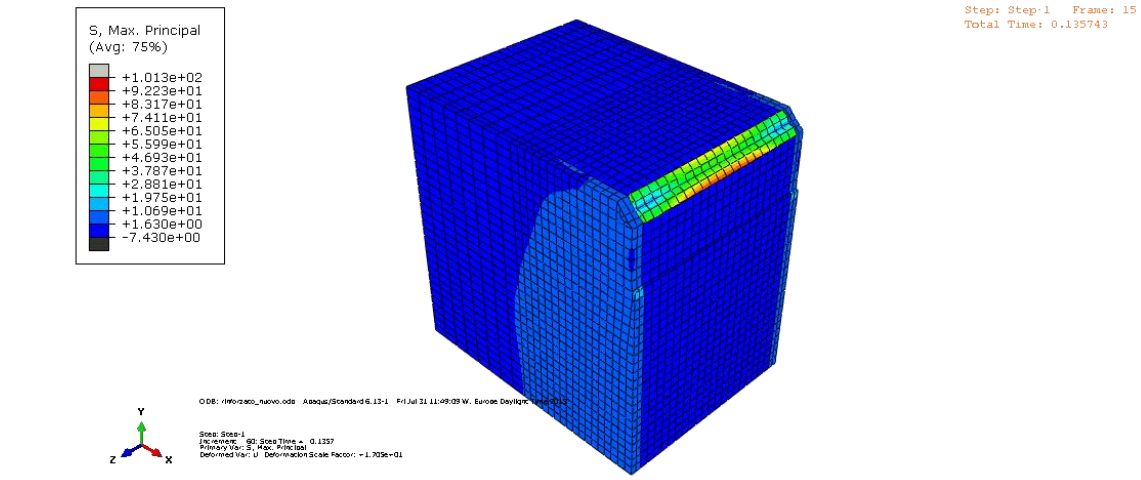
S, Max. Principal
(Avg: 75%)
+1.013e+02
+9.223e+01
+8.317e+01
+7.411e+01
+6.505e+01
+5.599e+01
+4.693e+01
+3.787e+01
+2.881e+01
+1.975e+01
+1.069e+01
+1.630e+00
-7.430e+00
Step: Step-1 Frame: 15
Total Time: 0.135743

(a)

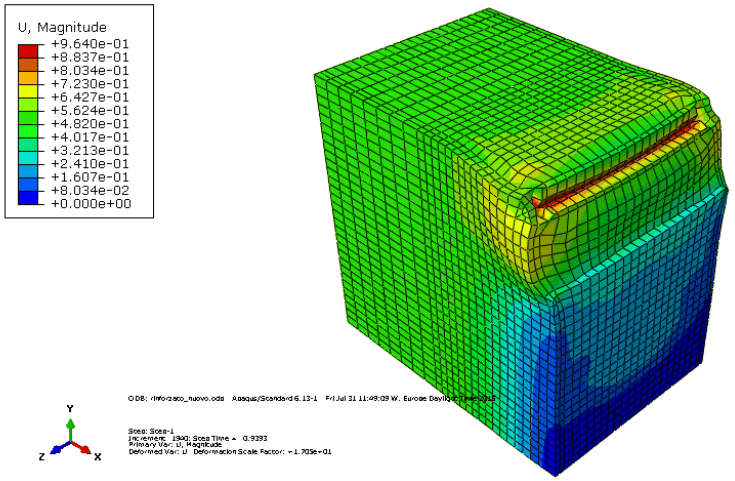
U, Magnitude
+9.640e-01
+8.837e-01
+8.034e-01
+7.230e-01
+6.427e-01
+5.624e-01
+4.820e-01
+4.017e-01
+3.213e-01
+2.410e-01
+1.607e-01
+8.034e-02
+0.000e+00

(b)

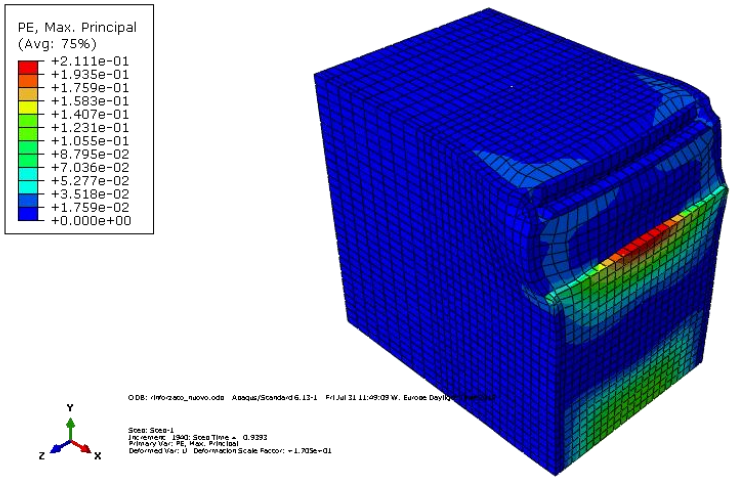

(c)

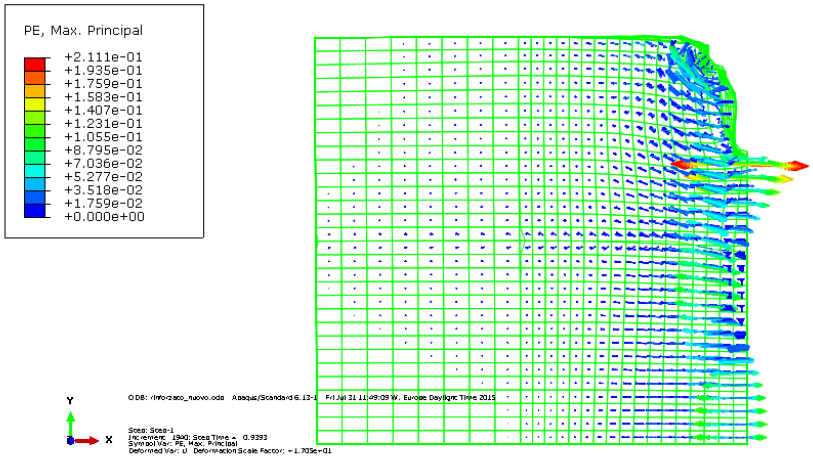

(d)

Figure 5.11: (a) stress-maximum principal, (b) The displacement magnitude, (c) Plastic strain- maximum principal (d) Plastic strain-maximum principal –symbols.

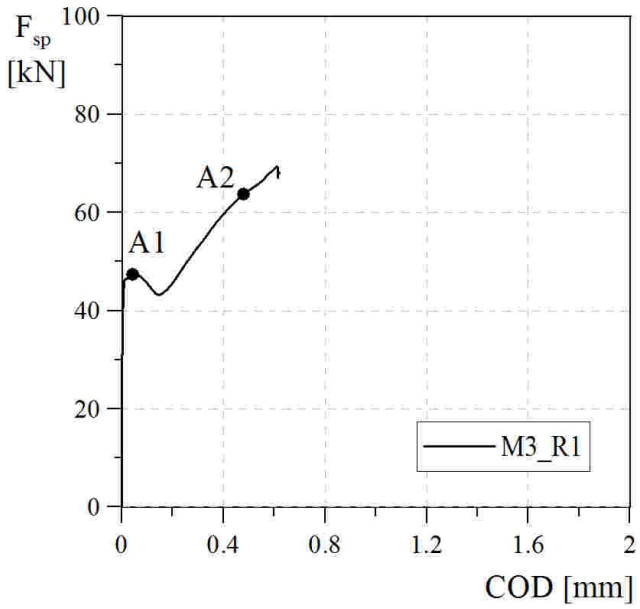

Figure 5.12: The horizontal force F_{sp} vs. crack opening displacement COD relationship.

Point A1 was highlighted as it refers to the point where all the height of ligament involved into plasticization (figure5.13). While A2 refers to the point where the reinforcement bars started to yield (figure 5.14).

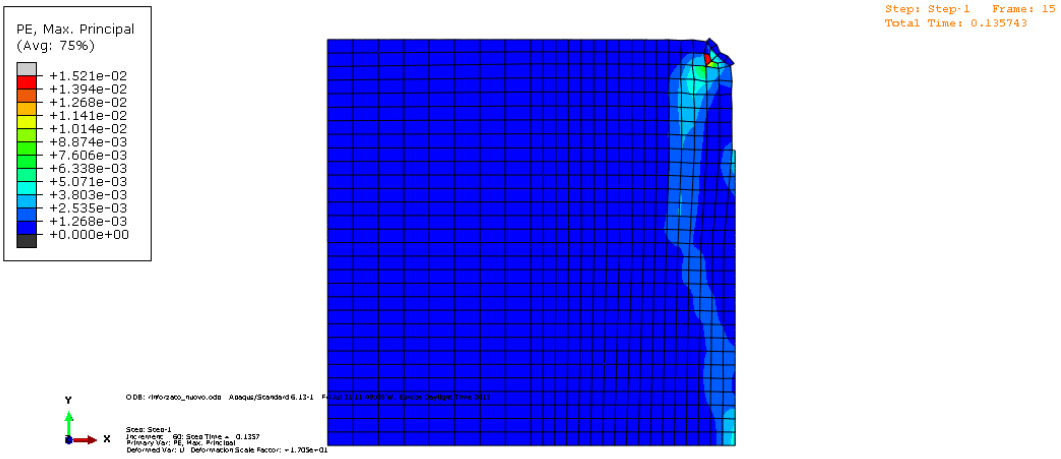

Figure 5.13: Plastic strain in concrete at point A1

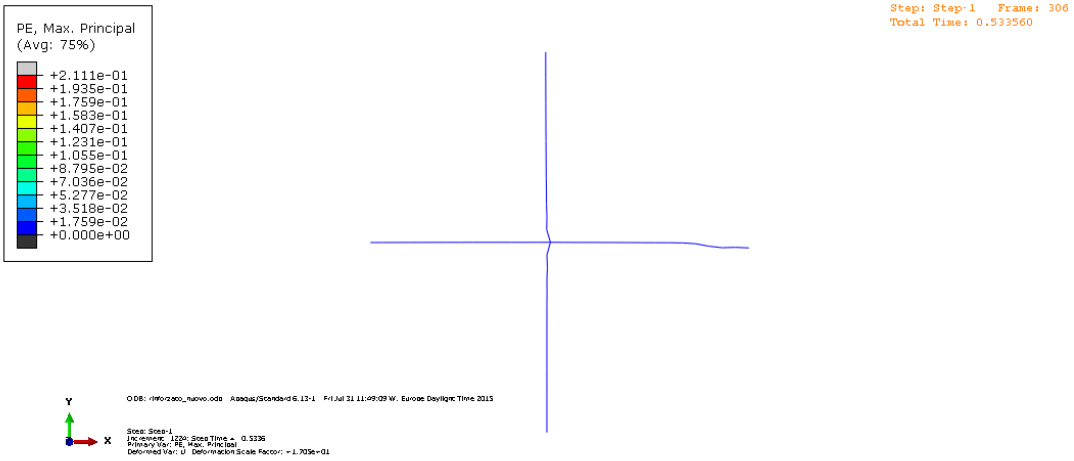

Figure 5.14: Plastic strain in reinforcing bars at point A2

Comparison between the results obtained from the retrofitted with plain TRC (M3_R1) and un-retrofitted (M3) specimen's model is presented in figure 5.15. Another comparison between the results obtained from the experimental and the numerical model of retrofitted specimen with plain TRC is shown in figure 5.16 the comparisons were given in terms of horizontal force F_{sp} vs. crack opening displacement COD relationship.

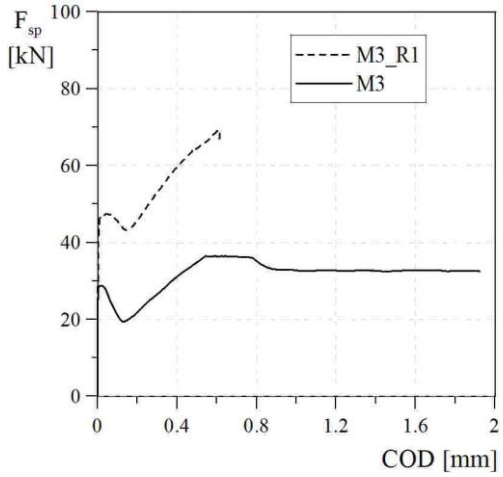

Figure 5.15: comparison between retrofitted with plain TRC and un-retrofitted DEWS specimens

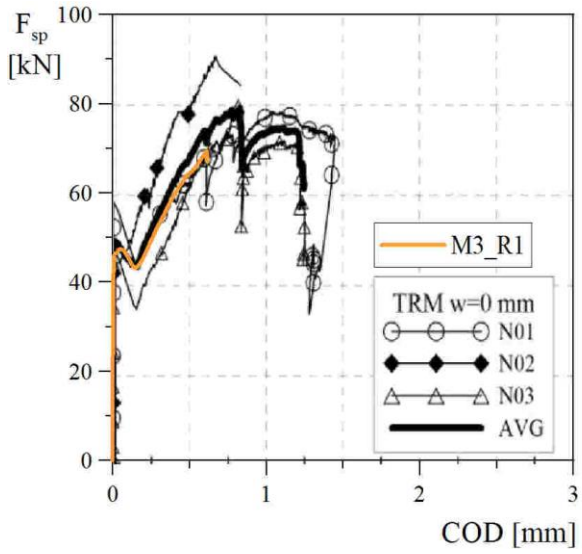

Figure 5.16: comparison between plain TRC retrofitted specimen's results for numerical and experimental.

5.4.1.2. Using TRC with Polypropylene.

Addressing the tensile strength of the TRC by introducing the constitutive curve obtained from the experimental direct tension test carried out on TRC matrix with Polypropylene addition. The results of the retrofitted model M1_R2 are given in figure 5.17 in terms of contours distribution for the stress, displacement and plastic strain. The horizontal force F_{sp} vs. crack opening displacement COD relationship is plotted in figure 5.18.

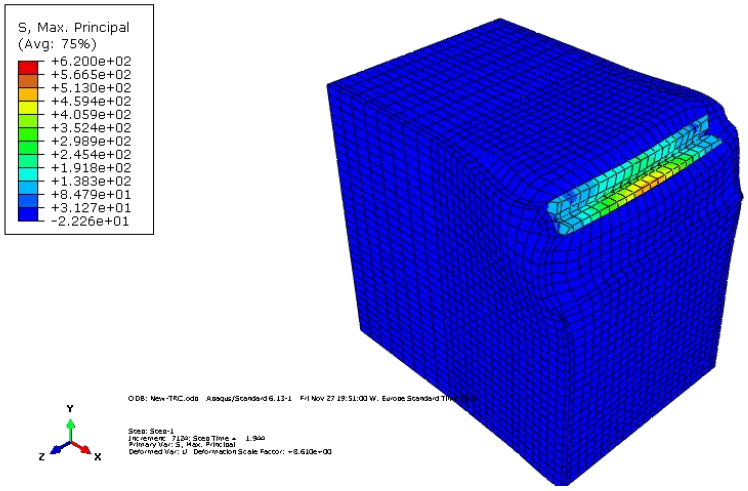
S, Max. Principal
(Avg: 75%)
+6.200e+02
+5.665e+02
+5.130e+02
+4.594e+02
+4.059e+02
+3.524e+02
+2.989e+02
+2.454e+02
+1.918e+02
+1.383e+02
+8.479e+01
+3.127e+01
-2.226e+01
Y
Z
X

(a)

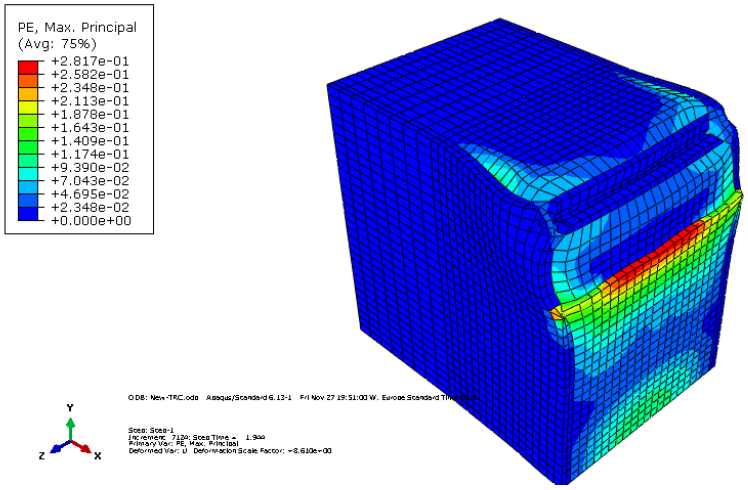
PE, Max. Principal
(Avg: 75%)
+2.817e-01
+2.582e-01
+2.348e-01
+2.113e-01
+1.878e-01
+1.643e-01
+1.409e-01
+1.174e-01
+9.390e-02
+7.043e-02
+4.695e-02
+2.348e-02
+0.000e+00
Y
Z
X

(b)

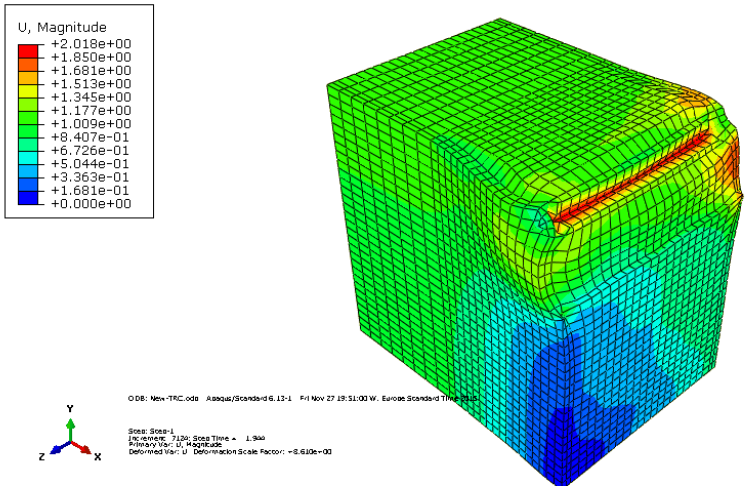

(c)

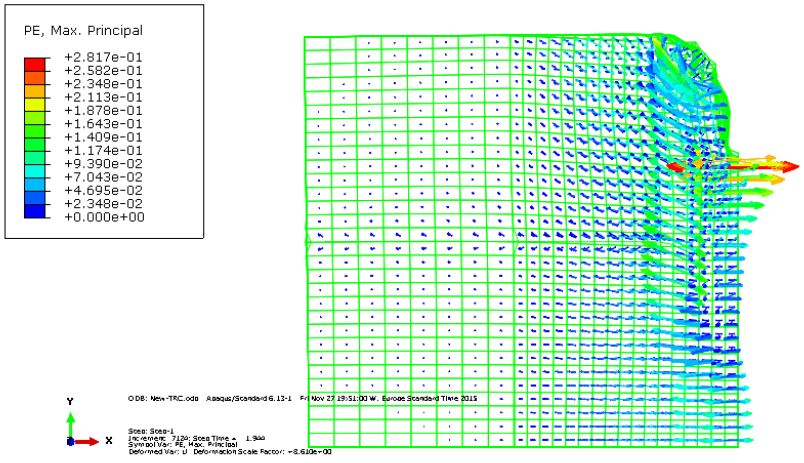

(d)

Figure 5.17: (a) stress-maximum principal, (b) The displacement magnitude, (c) Plastic strain- maximum principal (d) Plastic strain-maximum principal –symbols.

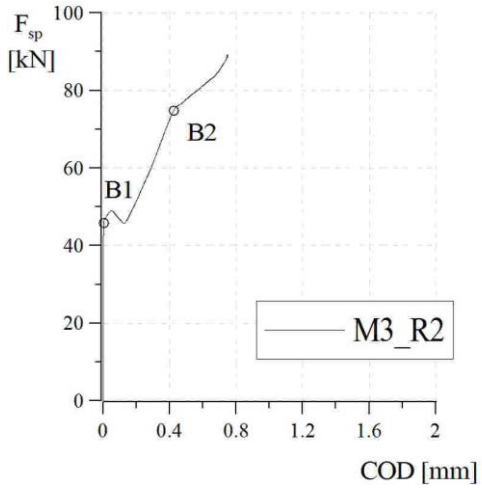

Figure 5.18: The horizontal force F_{sp} vs. crack opening displacement COD relationship.

Point B1 was highlighted as it refers to the point where all the height of ligament involved into plasticization (figure5.13). While B2 refers to the point where the reinforcement bars started to yield (figure 5.14).

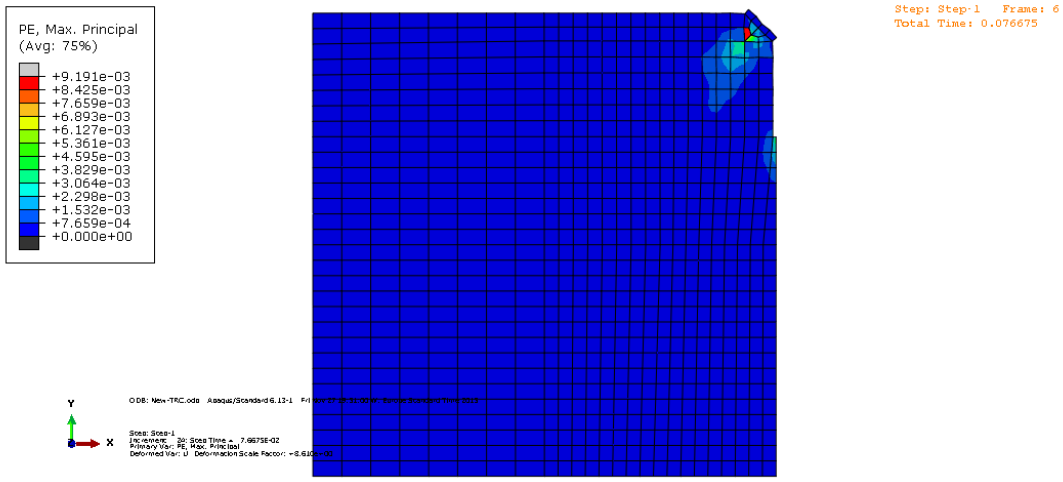

Figure 5.19: Plastic strain in concrete at point B1

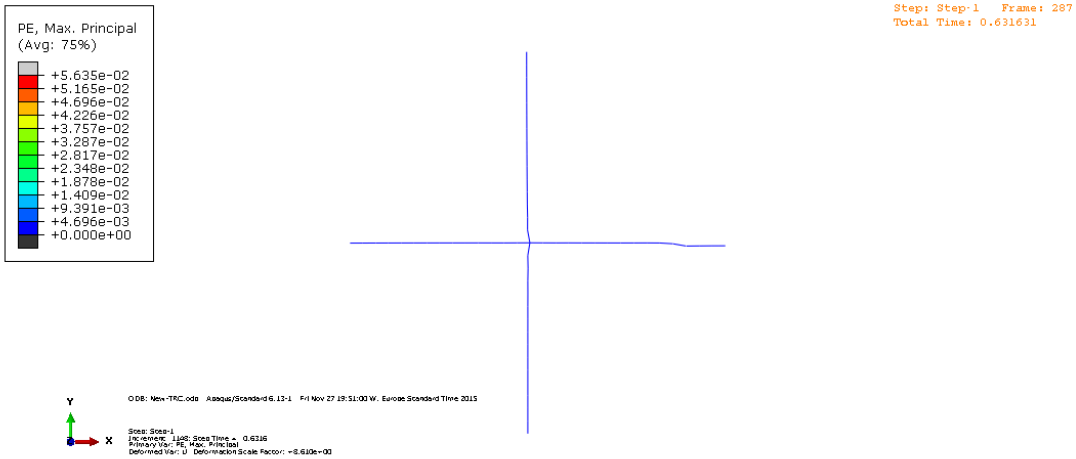

Figure 5.20: Plastic strain in reinforcing bars at point B2

Comparison between the results obtained from the retrofitted M1_R2 and un-retrofitted M3 specimen's model is presented in figure 5.21. Another comparison between the results obtained from the experimental and the numerical model of retrofitted specimen with TRC with polypropylene addition is shown in figure 5.22 the comparisons were given in terms of horizontal force F_{sp} vs. crack opening displacement COD relationship

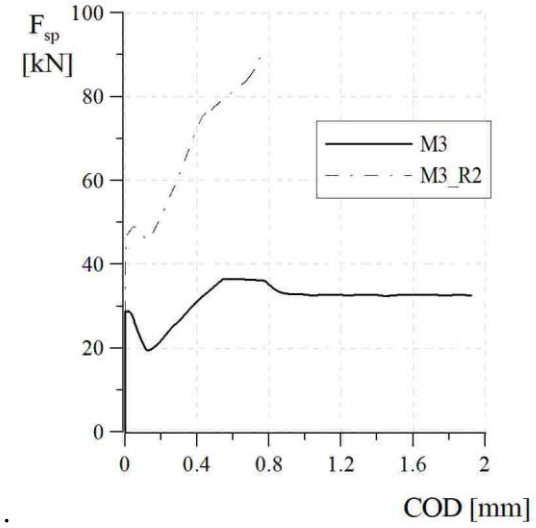

Figure 5.21: comparison between retrofitted and un-retrofitted specimens

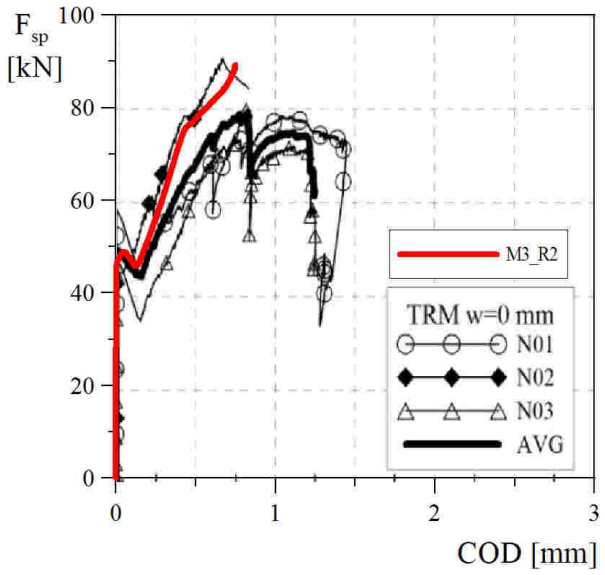

Figure 5.16: comparison between retrofitted specimen's M3_R2 results for numerical and experimental.

5.4.1.3. Comparison between the two proposals (M3_R1 and M3_R2).

The two models proposals gives almost the same response. However, the concrete plasticization involves all the height of ligament in model M3_R2 earlier than M3_R1, while the reinforcing bars yields in M3_R1 earlier than M1_R2. This was due to the higher concrete tensile yield strength that was defined in M3_R1 (7 MPa) comparing to the yield strength used in M3_R2 (5.16 MPa). Comparison between both results are given in figure 5.23 in terms of horizontal force F_{sp} vs. crack opening displacement COD relationship

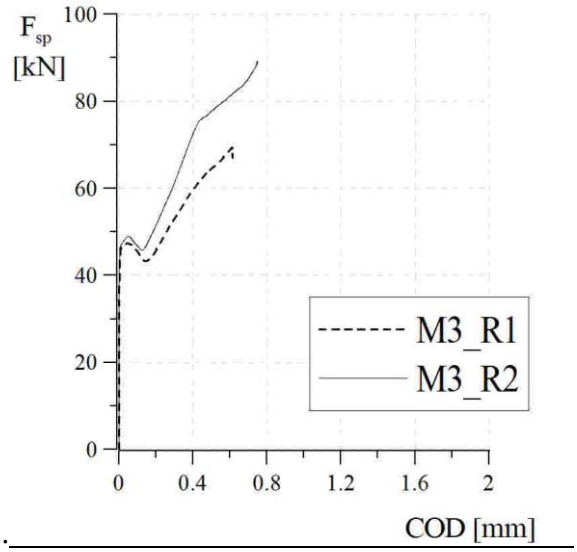

Figure 5.15: comparison between the two models proposals M3_R1 and M3_R2.

The two curves shows a distinct superiority to model M3_R2. This could be explained by referring to the constitutive curves used to define both the plain TRC and the TRC with polypropylene material and in model M3_R1 and M3_R2 (figure 5.5), evidently the first branch represent the crack pattern of the two materials where the first branch of the constitutive curve is shorter in M3_R2 than the first branch of M3_R1. This is due to the fact that the polypropylene fibres reduced the crack width of the TRC matrix therefore better stiffness was obtained with compare to plain concrete.

Chapter 6

Conclusion and remarks for further development

Since the most crucial aspects that must be taken in the account when choosing the strengthening material are the mechanical properties, environmental effect, needed volumetric size, easiness of application and durability. In this sense textile reinforced concrete (TRC) was introduced as a competent retrofitting solution. Principally, this thesis studies the possibility of using textile reinforced concrete for strengthening of concrete structures. The research aims to analyze the mechanical characterization of textile reinforced concrete and its coupling with traditional reinforced concrete. Two chapters of state of arts have explained in details most of the textile reinforced concrete features by referring to the mix design, reinforcing fibres, tensile strength, durability and fields of applications. Moreover, the bond between textile reinforced concrete and traditional concrete was presented as well with mentioning examples to tests done on a strengthened RC beams with TRC layers.

A comprehensive experimental program had been carried out in order to provide a better understanding to the mechanical properties of TRC. Direct tensile test was performed to different mix design to study the effect of the amount of Polypropylene on the tensile behavior of the matrix. The test aims to determine the workability of each mix by applying the slump test for the different mix design.

Figure 6.1 shows the comparison between the three different matrices design mix. Apparently, The graphs show, that adding the poly propylene fibres to the matrix raise the tensile strength of the matrix in general and precisely the position where the first crack branch start from. Regarding to the cracking pattern, the first matrix (without PP fibres) shows some spalling failure in the cracked specimen. In the other side the other two specimens (with PP fibres) have a smaller crack width. The second matrix (fibre amount equal to 0.007125Kg) had proven better workability during the casting process comparing with the third matrix (fibre amount equal to 0.0142Kg) which has very low workability influenced the bond between the mortar and the fabric.

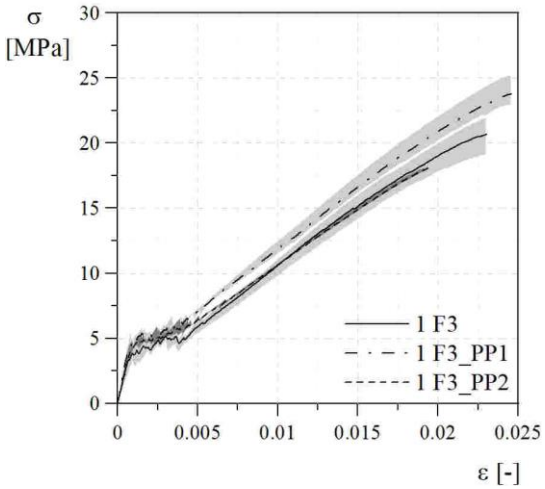

Figure 4.2: TRC stress strain curves (a) F3+ no fibre, (b) F3+ 4.75 kg/ m3 fibre, (c) F3+ 9.5 kg/ m3 fibre, (d) comparison between the three mix designs.

Introducing Double edge wedge splitting test as an innovative technique developed from wedge splitting test, gives many advantages in principal the possibility of carrying out tensile test by applying compressive load only. This option facilitates to avoid the common problems associated to the known tensile test such as, bending and Brazilian test.

The test was performed on three type of specimens; un-cracked, pre-cracked (w=0.30 mm)and pre-cracked (w=3mm). The test set up description, preparation and used materials are explained in details I chapter 4. While, the results for the test on the retrofitted specimens are given by referring to the average behavior for each crack opening considered. The crack opening displacements were measured by the transducers placed in the middle of the section and the results were reported in terms of load vs. vertical displacement and splitting force vs. the crack opening width.

Figure 6.2 shows that the linear branch of elastic behavior stopped when the cracking strength of concrete was reached where the splitting force is equal to 30 KN. After the first linear branch the steel bars starts to be loaded until they yield and fails. An average curve for the three curves was plotted in thicker font where it stopped at the first end of the three curves. Reference specimen was casted without strengthening layer and tested.

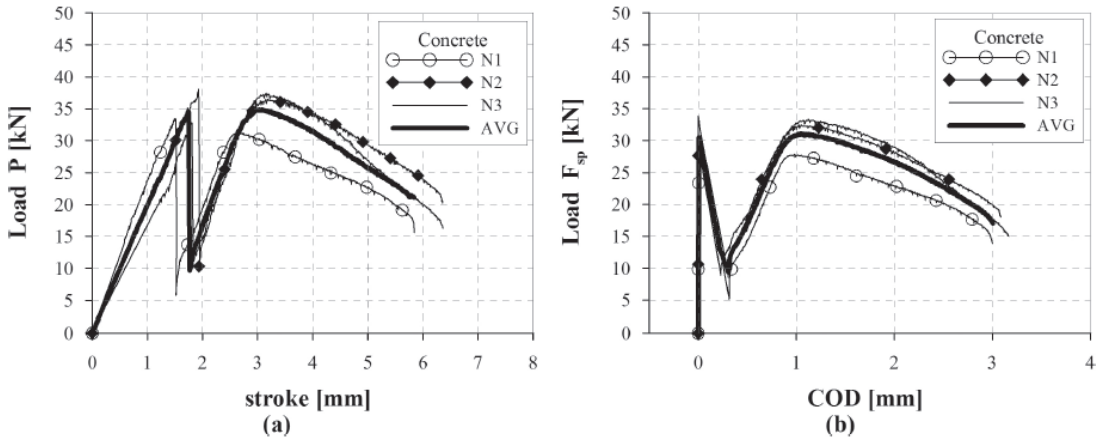

Figure 6.2: (a) vertical load Vs. vertical displacement (b) splitting force Vs. COD average [Magri 2012].

Moreover, the crack opening development with respect to vertical displacement in both specimens' sides and the development of the rotation in both specimens' sides had been calculated and presented in chapter 4.

Evidently, the strengthening layers have experienced a delamination in the central section for a length of 50 to 70 mm and sequentially multi-cracking starts. Moreover, the tangential stresses acting on the interface plane takes place in conjunction with the transferred tensile force in the middle plane of TRC layer

Compression test also had been carried out to the same specimens. The test was carried out by a hydraulic press Controls Advantest with maximum load of 3000 KN by imposing constant stroke rate 0.05 mm/sec on specimens with and without strengthening layers for all damage levels. Three LVDT transducers were fixed on both sides perpendicular to specimen plane to measure the detachment of the strengthening layer. In addition, another two transducers were placed in the lower plane to measure the stroke vertical displacement

The compressive strength of plain concrete was determined according to test carried out for ten cubic specimens [150 mm edge length] and the obtained average compressive strength was 34 Mpa. Thus, the maximum compressive load could be estimated as $P_{max}^{exp} = 748\ KN$. which is less than the obtained average of the peak load of two completed tests (901 KN). The author explains the reason behind this which might be due to the confinement effect favored by friction on the longest bases. This was due to the absence of stearic acid between steel plates and specimen during the test. The load was increased by 17% due to the confinement effect offered by the friction.

The numerical design prediction was given in chapter 5 of this thesis, many proposals were modeled in order to study the impact of adding TRC materials to retrofit the existing RC structures. Many factors were manipulated to study the correspondence between the numerical and experimental approaches. Apparently using the mean value of tensile strength and fracture energy which were suggested according to model code [MC 2010], are not in good agreement with the experimental results other parameter - tensile strength and fracture energy- hence introduced in the tensile of the concrete. And better results were obtained.

From the other side , detailed study has been explained numerically in order to determine the influence of adding polypropylene to TRC matrix. the results were presented in terms of horizontal force F_{sp} vs. crack opening displacement COD relationship and it show that the polypropylene fibres reduces the crack width of the TRC matrix therefore better stiffness was obtained with compare to plain concrete.

Remarks for further developments.

- the experimental investigation of the retrofitted specimen with textile reinforced concrete are more meaningful when they are compared with the new advanced cementitious materials. Moreover, the surface treatment condition influence on the result could be very important remarks that should be always taken in consideration.

- During modeling numerically DEWS test; the most challenging point was the definition of the relationship between the textile reinforced concrete and the traditional one model. Many proposals have been done during the working times in this research in order to obtain the best modeling. With the capabilities of Abaqus in modeling, this model can be developed to obtain the exact behavior of the real applications.

References

[Ald2005] Aldea C., Mobasher, B., Singla, N., "Cement-Based Matrix-Grid System For Masonry Rehabilitation," ACI Spring Convention, New York, April 20, (2005).

[Banholzer2006] Banholzer, B., Brockmann, T., Brameshuber, W. Material and bonding characteristics for dimensioning and modeling of textile reinforced concrete elements. Material and structures, 39:749-763, 2006. 10.1617/s11527-006-9140-x. (2006).

[Brahwiler 1990] E., Wittmann, F.H. "The Wedge Splitting test, a new method of performing stable fracture mechanics tests." *Engineering Fracture Mechanics*, 35:117 125, (1990).

[Brameshuber2001] Brameshuber W., Brockmann T. Calcium aluminate cement binder for textile reinforced concrete. In ROYAUME-UNI (2001) (Monographie) Institute of Ceramics, Stoke-on-Trent, editor, *Proc. International conference on calcium aluminate cement, Edinburgh ROYAUME-UNI 16-07-2001*, pages 5659-666, (2001).

[Brameshuber2003] Brameshuber W., Brockmann T., Size effect on mechanical properties of fine grained concrete matrices. Textile Reinforced structures, Proceeding of 2nd Colloquium, Dresden (CTRS2), Pages 161-172, (2003).

[Brameshuber2006] Mobasher, B., Peled, A., and Pahilajani, J. (2006). "Distributed cracking and stiffness degradation in fabric-cement composites". Materials and Structures, 39:317-331. (2006).

[Brockmann 2001] Brockmann, T. Requirements on and properties of mineral based fine grained concrete matrices. In *Textilbeton. 1. Fachkolloquium der* (2001) *sonderforschungsbereiche*, pages 528-532, 2001.

[Bla1998] Blaschko, M, Niedermeier, R., Zilch, K., 'Bond failure modes of flexural members strengthened with FRP', in

Proceedings of the Second International Conference on Composites in Infrastructures, Tucson, 1998 (Saadatmanesh, H. and Ehsani, M. R., (1998), pp. 315–327.

[Butler et al. 2010] Butler, M., Mechtcherine, V., and Hempel, S. "Durability of Textile Re-inforced Concrete made with AR glass Fibre": Effect of the matrix composition. Materials and Structures/Materiaux et Constructions, 43(10):1351-1368 (2010).

[Cavdar 2014] Cavdar, A. "Investigation of freeze-thaw effects on mechanical properties of Fiber Reinforced Cement mortars". Composites Part B: Engineering, 58:463-472. (2014).

[Colombo 2013] Isabella G. Colombo, A. Magri, G. Zani, M. Colombo, M. di Prisco. "Textile Reinforced Concrete: Experimental investigation on design parameters. Materials and Structures (2013) 46:1953–1971, DOI 10.1617/s11527-013-0023-7. (2013)

[Cohen&Peled2010] Cohen, Z. and Peled, A. "Controlled telescopic reinforcement system of Fabric-Cement Composites - Durability concerns". Cement and Concrete Re-search, 40:1495-1506. (2010).

[Curbach and Sheerer 2011] Curbach, M. and Sheerer, S. "Concrete light - Possibilities and Visions". In Proceedings of the fib Symposium Prague 2011 - Concrete Engineering for Excellence and Efficiency, pages 29-44. (2011).

[Di prisco 2010] Di Prisco, M., Lamperti, M.G.L., Lapola, S. " Double edge wedge splitting test: Preliminary results. In *Proceedings of conference FRAMCOS 7, Seogwipo, Jeju*, KOREA, (2010).

[Di prisco et. 2013] di Prisco, M., Cadoni, E., Colombo, M., Bonalumi, P., Caverzan, A., and Mar-tinelli, P. "On the Mitigation of the Risk of prefabricated Tunnel Linings": the ACCIDENT Project. In Proceedings of "Protect 2013 - Performance, Protection and Strengthening of Structures under Extreme Loading - Mysore,India". (2013).

[Graybeal and Tanesi 2007] Graybeal, B. and Tanesi, J. "Durability of an Ultrahigh-Performance Concrete". Journal of Materials in Civil Engineering, 19(10):848-854 (2007).

[Gri2004] Gries, T., "New developments on manufacturing fibers and textile structures for technical textiles",

Departamento de ingeniería textil y papelera, Universitat politècnica de Catalunya (Hrsg.): 2004 International Textile Congress: technical textiles; world market and future prospects, Terrassa, Spanien, 18.-20.10.2004, pp. 15-24. (2004).

[Han1996] Hankers, C., Zum Verbundtragverhalten laschenverstärkter Betonbauteile unter nicht vorwiegend ruhender Beanspruchung. (Bond of strengthened concrete elements under dynamic loading.) Braunschweig, Technische Universität, FakultätBauingenieurwesen, iBMB, Diss., (1996).

[Hegger et al 2004] Hegger, J., Will, N., Curbach, M., and Jesse, F. Tragverhalten von textilbewehrtem Beton. Beton-und Stahlbetonbau, 99:452-455. (2004)

[Hegger and Voss2008] Hegger, J. and Voss, S. "Investigations on the bearing behaviour and application potential of Textile Reinforced Concrete". Engineering Structures, 30:2050-2056. (2008).

[Hol1994] Holzenkämpfer, P., Ingenieurmodelle des Verbunds geklebter Bewehrung für Beton-bauteile. (Bond model for bond of glued reinforcement for concrete elements.) Braunschweig, Technische Universität, Fakultät Bauingenieurwesen, iBMB, Diss., (1994).

[Lomboy and Wang 2009]. Lomboy, G. and Wang, K. "Effects of strength, permeability, and air void parameters on freezing-thawing resistance of concrete with and without air entrainment". Journal of ASTM International, 6(10) (2009).

[Magri2012] Anna Magri, Advanced Cementitious Composites for Structural Retroftting. PhD dissertation, Doctoral School in Structural, Seismic and Geotechnical Engineering. Politecnico di Milano. 09 November (2012)

[MC 2010] Model Code (2010) final draft volume 1 *March 2012*.

[Mechtcherine2011] Mechtcherine, V. and Leboldt, M. "Permeation of water and gase through cracked Textile Reinforced Concrete". Cement and Concrete Com-posites, 33:725-734 (2011).

[Mechtcherine2013] Mechtcherine, V. Novel "Cement-based composites for the strengthening and repair of concrete structures". Construction and Building Materials, 41:365-373. (2013).

[Mobasher 2005] Mobasher, B., Peled, A., Pahilajani, J. Pultrusion of fabric high flyash blended cement composites. *In proceeding, world of coal April 11-15, 2005, Lexington KY, USA Pultrusion*, (2005).

[Muhaxheri2014] Muhaxheri, M. "Behaviour of coupling beams retrofitted with advanced cementitious composites" : experiments and modelling. PhD thesis, Doctoral School in Structural, Seismic and Geotechnical Engineering. (2014).

[Neu2000] Neubauer, U., Verbundtragverhalten geklebter Lamellen aus Kohlenstoffaser Verbund-werkstoff zur Verstärkung von Betonbauteilen. (Bond behaviour of strengthening structures with carbon and concrete elements.) Braunschweig, Technische Universität, Fakultät Bauingenieurwesen, iBMB, Diss., (2000).

[Neville 1996] Neville, A. Properties of Concrete. Wiley, New York. 3.3, 4.1.3 ODYSSEE_MURE (2012). Report: Energy Efficiency Trends in Buildings in EU- Lessons from the ODYSSEE MURE project (www.odyssee-indicators.org) (1996).

[Off2003] Offermann, P., Köckritz, U., Abdkader, A., Engler, T., Waldmann, M., Anforderungsgerechte Bewehrungsstrukturen für den Einsatz im Betonbau "Application oriented textile reinforcements for the use in concrete building". In: Curbach, M. (Edt.): Textile Reinforced Structures. Proceedings of the 2nd Colloqium on Textile Reinforced Structures (CTRS2), Dresden: Sonderforschungsbereich 528, Technische Universität Dresden, (2003).

[Orlowsky and Raulpach 2008] Orlowsky, J. and Raupach, M. "Durability model for AR-glass fibres in Textile Reinforced Concrete". Materials and Structures/Materiaux et Constructions, 41(7):1225-1233. (2008).

[Ort2003] Ortlepp, R., Curbach, M., 'Bonding Behaviour of Textile Reinforced Concrete Strengthening', in 'High Performance Fiber Reinforced Cement Composites – HPFRCC 4', Proceedings of the Fourth International RILEM Workshop, Ann Arbor, June 2003 (Naaman, A. E. and Reinhardt, H.-W., RILEM Proceedings PRO 30, Bagneux, (2003), pp. 517–527.

[Ort2004] Ortlepp, R., Ortlepp, S., Curbach, M., 'Stress Transfer in the Bond Joint of Subsequently Applied Textile

Reinforced Concrete Strengthening', in 'Sixth RILEM-Symposium on Fibre Reinforced Concrete (FRC) – BEFIB 2004', Proceedings of the Sixth RILEM-Symposium on Fibre Reinforced Concrete (FRC), Varenna-Lecco, September 2004 (Editor, N1. and Editor, N2., RILEM Proceedings PRO, Verlag, (2005)).

[Peled et al 2006] Peled, A., Sueki, S., and Mobasher, B. "Bonding in fabric-cement systems: Effects of fabrication methods". Cement and Concrete Research, 36:1661-1671. (2006).

[Peled et al 2008] Peled, A., Zaguri, E., and Marom, G. (2008). "Bonding characteristics of multipl-ament polymer yarns and cement matrices". Composites: Part A, 39:930-939. (2008)

[Purnell and Beddows2005] Purnell, P. and Beddows, J. "Durability and simulated ageing of new Matrix Glass Fibre Reinforced Concrete". Cement and Concrete Composites, 27(9-10):875-884. (2005).

1.1. [Santos and Júlio 2010] Petrina Santos, Eduardo.N.B.S.Julio. "Assessment of the Shear Strength between Concrete Layers." Research Gate. Conference paper.June (2010).

[Simulia 2011]. ABAQUS 6.11., Analysis analysis User's Manual, Simulia (2011).

[Sun et al 1999] Sun, W., Zhang, Y., Yan, H., and Mu, R. (1999). "Damage and damage resistance Of High Strength Concrete under the action of load and freeze-thaw cycles".Cement and Concrete Research, 29(9):1519-1523.

[Tri2006a] Triantafillou, T. C., Papanicolaou, C. G., Zissimopoulos, P., Laourdekis, T., "Concrete Confinement with Textile Reinforced Mortar (TRM) Jackets", 2005, ACI Structural Journal, 103(4), (2006).

[Tri2006b] Triantafillou, T. C., Papanicolaou, C. G., "Shear Strengthening of Reinforced Concrete Members with Textile Reinforced Mortar (TRM) Jackets, (2005), RILEM Materials and Structures, accepted for publication.

[Ula2003] Ulaga, T., Betonbauteile mit Stab- und Lamellenbewehrung: Verbund- und Zuggliedmodellierung. (Strengthened concrete elements – Modeling of bond and tesnion elements.)

Zürich, ETH, Institut für Baustatik und Konstruktion, Diss., (2003).

[Verbruggen2014] Seltana Verbruggen, Tine Tysmans, Jan Wastiels, "TRC or CFRP Strengthening for Reinforced Concrete Beams: An Experimental Study of the Cracking Behavior, Engineering Structures 28 July 2014.

[Wang et al 2009]. Wang, K., Lomboy, G., and Steffes, R. "Investigation into Freezing-Thawing Durability of Low-Permeability Concrete with and without Air En-training Agent". Technical report, National Concrete Pavement Technology Center - Institute for Transportation - Iowa State University. (2009).